

**SPACE AND TIME FREQUENCY-DEPENDENT
INTERACTIONS IN SUBTHALAMIC NUCLEUS LOCAL
FIELD POTENTIALS IN PARKINSON'S DISEASE**

A Thesis
Presented to
the Faculty of the Department of Computer Science
University of Houston

In Partial Fulfillment
of the Requirements for the Degree
Master of Science

By
Gianluca Meloni
August 2015

**SPACE AND TIME FREQUENCY-DEPENDENT
INTERACTIONS IN SUBTHALAMIC NUCLEUS LOCAL
FIELD POTENTIALS IN PARKINSON'S DISEASE**

Gianluca Meloni

APPROVED:

**Dr. Marc Garbey, Chairman
Dept. of Computer Science**

**Dr. Nuri F. Ince
Dept. of Biomedical Engineering**

**Dr. Nikolaos V. Tsekos
Dept. of Computer Science**

Dean, College of Natural Sciences and Mathematics

Acknowledgment

I would like to thank the Atlantis CRISP international double degree program for providing me financial support during my MSc studies. I would also like to thank my thesis advisor, Dr. Nuri F. Ince, who solely supervised my work in this thesis. I conducted all the experiments and analyses in this thesis under Dr. Nuri F. Ince's supervision with the resources provided in his laboratory in the Biomedical Engineering Department.

I wish to thank Dr. Aviva Abosch, Dr. Ibrahim Onaran and the recording team for their work, that made the valuable dataset I analyzed in the work available. I would like to thank also Ilknur Telkes and Anish Sen for their precious help provided during the whole year, together with all the Clinical Neural Engineering (CNEL) lab students.

**SPACE AND TIME FREQUENCY-DEPENDENT
INTERACTIONS IN SUBTHALAMIC NUCLEUS LOCAL
FIELD POTENTIALS IN PARKINSON'S DISEASE**

An Abstract of a Thesis
Presented to
the Faculty of the Department of Computer Science
University of Houston

In Partial Fulfillment
of the Requirements for the Degree
Master of Science

By
Gianluca Meloni
August 2015

Abstract

Parkinson's disease (PD) is the second most common neurodegenerative disorder in the US, with a prevalence of 1% in the population over 60 years old and an annual economic impact estimated in 23 billion dollars in direct costs only. Deep Brain Stimulation (DBS) is an effective surgical treatment for advanced PD in patients who developed a resistance to the pharmacological medication. DBS procedure allows the recording of electrophysiological signals known as Local Field Potentials (LFP) from deep brain structures such as the Subthalamic Nucleus (STN). LFP represent the synchronized activity of a relatively large population of neurons and have been shown to correlate with many PD symptoms and contribute with their use to the success of DBS practice. However, the pathophysiology of PD remains unclear.

In this work, long-term STN LFP recordings of ten PD patients were analyzed using classical as well as recently developed methods to investigate: (i) the spatial distribution of spectral activity and nonlinear cross-frequency coupling in the STN in medicated and unmedicated conditions, (ii) the pattern of spectral changes following medication intake, and (iii) the correlation of features extracted from LFP with clinical scores and sensory data during resting state and movement execution. The main findings showed that cross-frequency coupling is stronger in the superior part of STN and that the timings of changes in LFP spectral power after pharmacological

treatment are frequency-dependent. The results support and integrate existing evidence that LFP analysis may assist in the target localization during DBS surgery and contribute to the development of smarter algorithms for next generation closed-loop DBS applications.

Contents

1	Introduction	1
1.1	Organization	1
1.2	Aim of the Work and Motivation	2
2	Background	4
2.1	Parkinson's Disease	4
2.1.1	Symptoms	5
2.1.2	Etiology and Pathology	7
2.1.3	Diagnosis	9
2.1.4	Treatment	12
2.2	Deep Brain Stimulation	15
2.2.1	Origin	15
2.2.2	Surgical Protocol	16
2.2.3	Results and Limitations	18

2.3	Local Field Potentials	21
2.3.1	Subthalamic Nucleus Local Field Potentials in Parkinson's Dis- ease	21
3	Methods	29
3.1	Mathematical Methods	29
3.1.1	Filtering	29
3.1.1.1	FIR and IIR filters	29
3.1.1.2	Zero Phase Filtering	31
3.1.2	Power Spectral Density Estimation	33
3.1.2.1	Parametric methods	33
3.1.2.2	Non-parametric Methods	35
3.1.3	Time-varying Spectral Estimation	38
3.1.4	Phase-Amplitude Coupling Estimation	39
3.1.4.1	Mean Vector Length	40
3.1.4.2	Coherence Value	44
3.1.4.3	Phase-Locking Value	47
3.1.4.4	Significance Analysis	49
3.1.5	Statistical Analysis	51
3.1.5.1	Hypothesis Testing	53
3.1.5.2	Correlation	55

3.2	Dataset and Experimental Protocol	57
3.3	Data analysis	59
3.3.1	Definitions, Common Parameters, and Measures	59
3.3.2	Pre-processing	64
3.3.2.1	Re-referencing	64
3.3.2.2	Filtering	64
3.3.3	Rest Analysis	67
3.3.3.1	Spatial Distribution of Spectral Activity	67
3.3.3.2	Phase-Amplitude Coupling Analysis	69
3.3.3.3	Correlation of Power Spectral Changes with Clinical Scores	71
3.3.4	Off-to-On Transition Analysis	74
3.3.5	Movement Analysis	76
3.3.5.1	Correlation of Power Spectral Changes with Sensory Data	77
3.3.5.2	Phase-Amplitude Coupling Analysis	78
4	Results	79
4.1	Rest Analysis	79
4.1.1	Spatial Distribution of Spectral Activity	79
4.1.2	Phase-Amplitude Coupling Analysis	81

4.1.2.1	Mean Vector Length	81
4.1.2.2	Coherence Value	82
4.1.3	Phase-Locking Value	84
4.1.4	Correlation of Power Spectral Changes with Clinical Scores . .	86
4.2	Off-to-On Transition Analysis	86
4.3	Movement Analysis	89
4.3.1	Correlation of Power Spectral Changes with Sensory Data . .	89
4.3.2	Phase-Amplitude Coupling Analysis	93
5	Discussion and Future Developments	96
	Bibliography	105

List of Figures

2.1	Semi-quantitative assessment of pigmented neurons in the SNpc. Left images show templates of the distribution of pigmented neurons in healthy controls (A) and in patients with PD with mild (B), moderate (C), or severe (D) loss of pigmented neurons. Abbreviations: 3n, exiting 3rd nerve fibres; cp, cerebral peduncle; R, red nucleus. Reproduced from Dickson et al. [2009].	10
-----	---	----

2.2	Detailed description of the basal ganglia circuit in normal and parkinsonian states. Red arrows represent excitatory outputs and blue arrows indicate inhibitory projections. The thickness of the arrows is proportional to the firing rate activity of the connection. Dashed arrows indicate the lesion of the subsystem. Abbreviations: CM, centromedian nucleus; CMA, cingulate motor area; GPe, globus pallidus, external segment; GPi, globus pallidus, internal segment; M1, primary motor cortex; PMC, pre-motor cortex; PPN, pedunculopontine nucleus; SMA, supplementary motor area; SNc, substantia nigra pars compacta; SNr, substantia nigra pars reticulata; STN, subthalamic nucleus; VA/VL, ventral anterior/ventral lateral nucleus. Reproduced from Smith et al. [2012], who modified from Galvan and Wichmann [2008].	11
2.3	Figure A shows two four-contacts leads with different inter-contact spacing. Model #3387 on the left and #3389 on the right, both manufactured by Medtronic, Inc. Figure B shows the Active SC implanted pulse generator, by Medtronic, Inc. Image reproduced from http://cabellhuntington.org/	18

2.4	Stereotactic frame by Leksell (Leksell Stereotactic System). It includes a three-dimensional reference system and a center-of-arc instrument positioning system, used to as a guide for the insertion of exploratory microelectrodes and final macroelectrodes leads. Reproduced from http://www.elekta.com/	19
2.5	An example of local field potentials recorded in STN.	22
2.6	A) and B) show two LFP signals in “OFF” and “ON” medication respectively. The different oscillatory nature of the signals is clear and corroborated by the power spectral density in C) and D). Reproduced from Brown and Williams [2005].	23
2.7	Correlation between UPDRS sub-scale scores and beta band modulation. Adapted from [Kuhn et al., 2006].	24
2.8	Spectral characteristics of LFP in unmedicated (OFF) and medicated (ON) states, during rest condition. Reproduced from Lopez-Azcarate et al. [2010].	25

2.9	Comparison of bispectra obtained from LFP recorded in STN in untreated (A) and medicated (B) PD states, along with the power spectral densities of the signals in both conditions. The bispectrum is the 2-D Fourier transform of the third-order cumulant (the skewness) of a time series. A peak at the frequency pair (f_1, f_2) in the bispectrum means that the peak at the frequency $f_1 + f_2$ in the power spectral density of the time signal is produced by the phase coupled rhythms at f_1 and f_2 . Reproduced from Marceglia et al. [2006].	26
2.10	Phase-amplitude coupling between beta and HFO in untreated (“OFF”) and medicated (“ON”) states, computed in three different bipolar configurations from a four-contacts electrode placed in the STN. Bipolar pair 0-1 is at the bottom of the STN, pair 1-2 in the middle and 2-3 at the top. Reproduced from Lopez-Azcarate et al. [2010].	27
3.1	Example of PAC in LFP recorded at the STN level. At the top, the fast oscillation (around 250 Hz) is represented together with the slow one (around 15 Hz). It is possible to notice how the amplitude of the fast wave is modulated depending on the phase of the slow oscillation (in this example, higher amplitude is associates with the crests of the slow wave). In the bottom, the same oscillations are filtered and shown superimposed, where the effect of the modulation is even clearer. . . .	41

3.2	Algorithm for the detection of PAC in a signal using the MVL. From top to bottom: extraction of phase and amplitude frequency components from the original signal with adequate bandpass filters, estimation of the phase of the slow wave and amplitude envelope of fast wave and generation of the composite signal $g(n)$, represented in the complex plane. The points of $g(n)$ with amplitude smaller than 2 have been removed for sake of clarity. The thick red arrow represent the magnitude of the phase-amplitude strength between the two frequencies considered.	45
3.3	Algorithm for the detection of PAC using the Coherence Value. From top to bottom: the raw signal is filtered in the amplitude frequency range and its envelope is estimated. Then the magnitude squared coherence is computed between the envelope sequence and the raw signal. The measure of coupling strength is obtained integrating coherence value in small bins.	48
3.4	Overall processing flow to estimate PAC using the MVL method. HF are the high (amplitude) frequencies whereas LF are the low (phase) frequencies.	51

3.5	Overall processing flow to estimate PAC using the CV method. HF are the high (amplitude) frequencies whereas LF are the low (phase) frequencies.	52
3.6	Overall processing flow to estimate PAC using the PLV method. HF are the high (amplitude) frequencies whereas LF are the low (phase) frequencies.	52
3.7	Schematic representation of DBS lead model #3389 by Medtronic, Inc. The four platinum-iridium contacts are indicated with numbers from 0 (the most caudal) to 3 (the most rostral). Distances and size of the components are expressed in millimeters. Reproduced from Darvas and Hebb [2014].	59
3.8	Experimental protocol (motor part). The thick arrow represents the flow of time. The recordings start before the first “OFF” state and end after the last “ON” state. A 120 s long resting period is included in each state.	60
3.9	Room setup for the long-term recordings. In this screenshot, the patient is engaged in the keyboard tapping task, assisted by a nurse.	61

3.10	Magnitude and phase responses of the high pass filter applied to the data. The phase response is shown just for clarity, since the nonlinear behavior represented is not maintained when using zero phase filtering techniques.	65
3.11	Example of notch filter applied to the data stopping the oscillations at 60 Hz. The considerations on the phase are the same as Fig. 3.10.	65
3.12	Pre-processing of the LFP data. Raw monopolar derivations (A) were transformed in bipolar references (B) that were sequentially filtered using eight notch filters and a high pass filter (C). Note that signals in different plots have different amplitude scales.	66
3.13	The set of nine comodulograms computed in each condition was obtained combining the provenience of phase and amplitude frequencies across the three bipolar derivations. Every comodulogram has axis as shown in the middle one.	70

3.14	Work flow for the generation of PAC maps. The legend of symbols is shown in Fig. 3.8. In each state, a set of nine comodulograms was computed from the combination of phase and amplitude frequencies of the three bipolar derivations LFP 0-1, LFP 1-2, LFP 2-3. Then, the comodulograms corresponding to the same combination are averaged to create a single set of comodulograms describing a condition for each patient (“OFF” or “ON” state). In the figure, only the mechanism for “OFF” state is shown, but the same work flow applies for the “ON” state as well.	72
4.1	Spatial distribution of low beta peak activity (left) and “OFF” state HFO activity (right) across the subthalamic nucleus. The bottom STN is corresponding to the bipolar derivation LFP 0-1, intermediate STN to LFP 1-2 and top STN to LFP 2-3. Asterisks represent significant statistical differences in the distribution of spectral power.	80
4.2	Spatial distribution of gamma and “ON” state HFO activity across STN.	81
4.3	Spatial distribution of phase-amplitude coupling in STN in untreated (A) and medicated condition (B) using <i>MVL</i> . Hotter color is associated with stronger coupling.	83

4.4	Example of spatial distribution of phase-amplitude coupling in “OFF” state for a representative patient. The ranges of phase and amplitude frequencies where PAC occur are more localized compared to the average maps.	84
4.5	Spatial distribution of phase-amplitude coupling in STN in unmedicated (A) and treated condition (B) using <i>CV</i> method. Hotter color is associated with stronger coupling.	85
4.6	Spatial distribution of phase-amplitude coupling in STN in unmedicated (A) and treated condition (B) using <i>PLV</i> method. Hotter color is associated with stronger coupling.	87
4.7	Scatter plot showing the correlation of low beta peak power change in LFP 2-3 (top STN) with mUPDRS score change between unmedicated and medicated conditions. The thick line represents the regression line.	88

4.8 A) Timing of significant changes in the low beta, gamma and “ON” HFO peak powers after medication intake (corresponding to time 0). Asterisks represent significant differences in the time of changes between the power band considered. B) Percent power change in the three bands compared to the baseline (average of the power in the corresponding band in the thirty minutes prior to the medication intake) in a representative off-to-on transition obtained extracting LFP data for 210 minutes to show also the wash-out effect of medication in terms of power changes. 90

4.9	<p>A) Representative time-frequency map of a off-to-on transition (medication intake at time 0). At the top, the raw map. At the bottom, the spectra have been computed has percent change compared to the average spectrum of the thirty minutes preceding the levodopa intake. Accordingly to the pattern shown in Fig. 4.8, the power in the low beta range decreases tens of minutes before the gamma power increases.</p> <p>B) Representative time-frequency map of a off-to-on transition (different from the one in A). At the top, the raw map. At the bottom, the spectra have normalized with respect to the period preceding the drug medication intake (time 0). Two distinct HFO activities are shown: “OFF” state HFO at around 250 Hz and “ON” state HFO spread around 350 Hz.</p>	91
4.10	<p>Top: scatter plot showing the correlation between the percent low beta peak power change and the percent change in number of keyboard presses during task execution for LFP 1-2. Bottom: scatter plot showing the correlation with percent power change in the “ON” state HFO range for LFP 1-2.</p>	92

4.11	Comodulograms showing the strength of PAC before the task initiation and during task execution. The comodulogram relative to the pre-task period is noisier probably because estimated with a shorter data segment (10 s) than the comodulogram computed on the signals recorded during task execution (30 s). A) Untreated condition. B) Medicated condition.	94
4.12	Average spectrograms of bipolar derivations showing stronger phase-amplitude coupling in resting condition. The interval from -10 to 0 s is resting prior to task execution, which starts at time 0 for 30 s.	95
5.1	Hypothesis for the presence of abnormal phase-amplitude coupling in the parkinsonian state. The cortical beta input to the basal ganglia circuit is filtered in the physiological state while remains present in parkinsonian condition. This may lead to a loss of independence between neuronal discharges at different rates. Reproduced from de Hemptinne et al. [2013].	102

List of Tables

3.1	Definition of frequency bands.	59
4.1	Correlations of low beta peak power changes with mUPDRS score changes between unmedicated and medicated states. In bold the significant correlations.	86
4.2	P-values of tests comparing the timings of changes between low beta, gamma and “ON” state HFO peak powers.	88
4.3	Correlations of low beta peak power changes with mUPDRS score changes between unmedicated and medicated states. In bold the significant correlations.	89

Chapter 1

Introduction

1.1 Organization

The present manuscript is structured in five chapters. The first serves as introduction and explains the purpose of the work and its presentation. The second chapter describes the background and includes a review of Parkinson's disease, deep brain stimulation and local field potentials. The third chapter depicts the experimental protocol and the mathematical methods used in the work, including data collection, pre-processing and analysis in the time and frequency domains using linear as well as nonlinear methods. The fourth chapter illustrates the results obtained. Finally, the fifth chapter contains the discussion and conclusive remarks with future developments.

1.2 Aim of the Work and Motivation

Parkinson's disease (PD) is the second most common neurodegenerative disorder affecting older American adults. Pathophysiologically resulting from the loss or degeneration of dopaminergic neurons in the substantia nigra pars compacta and the development of neuronal Lewi bodies, it is associated with both motor and non-motor symptoms such as tremor at rest, rigidity, bradykinesia, postural instability, and depression, anxiety, and dementia respectively.

The etiology of PD is still unknown, with the majority of patients presenting an idiopathic condition and a minority where it is possible to relate with known genetic factors. In the past decades several pharmacological therapies have been developed to address the motor symptoms of Parkinson's disease, with important but increasingly insufficient results and collateral effects when the symptoms worsen. More recently a surgical treatment, the deep brain stimulation (DBS), has been introduced as alternative and complementary therapy in advanced PD cases. The treatment consists of the unilateral or bilateral placement of multi-contact macroelectrode leads in deep brain structures - usually the subthalamic nucleus (STN) - and consequent chronic voltage stimulation provided by a device placed in a subcutaneous chest pocket. Since the leads insertion and neurostimulator placement are performed in different surgical operations, researchers are offered the unique opportunity of recording neurosignals coming from the deep brain, known as local field potentials (LFP), while the contacts

are still externalized. LFP represent the synchronized activity of a relatively large ensemble of neurons and have been extensively analyzed in the last two decades to achieve a better comprehension of the abnormal neural dynamics caused by PD and other motor disorders, for example, Essential Tremor and Tourette's syndrome, for which DBS is also used.

The data analyzed in this work originate from an investigator-initiated project lead by Dr. Aviva Abosh and Dr. Nuri F. Ince and funded by Medtronic, Inc. Usually, the LFP data collection in untreated and medicated PD conditions is performed soon after the surgery in separate time periods before and after the drug administration or DBS therapy, making it possible to investigate the modulation patterns of LFP in different clinical conditions, but not allowing to detect time-depending LFP modulations. In this scheme, the experimental protocol of the study required 10 PD patients to be hospitalized; data collection was performed continuously for 24 hours.

Therefore, the aim of the present work is to analyze the space and time and frequency-dependent interactions and modulations of LFP recorded in the context of the aforementioned study, in order to contribute to understanding the pathophysiology of PD and correlate the extracted information with clinical scores as well as sensory data.

Chapter 2

Background

2.1 Parkinson's Disease

In his 1817 work “An essay on the shaking palsy”, James Parkinson was the first to provide a detailed description of the clinical syndrome named after him [Parkinson, 2002]. More than 100 years passed before it was recognized that patients suffer from a loss of cells in the substantia nigra (1919) and more than 140 before the research team of Carlsson - who won the Nobel Prize in Medicine in 2000 - discovered dopamine as a putative neurotransmitter in 1957 [Bjorklund and Dunnett, 2007]. Parkinson's disease is the second most common neurodegenerative disorder after Alzheimer's disease and, in developed countries, its prevalence is approximately 0.3% with an increase to 1% in individuals above the age of 60 and a peak of 4% in the population

older than 80 [de Lau and Breteler, 2006]. The incidence is between 8 and 18 new cases every 100,000 inhabitants per year [de Lau and Breteler, 2006]. The economic impact of PD results in direct costs estimated to be around \$ 10,000 per patient per year, for a total of 23 billion dollars in the US alone [Findley, 2007]. The indirect costs, although not quantified, could be high as well due to the loss of productivity of the patients and the need for assistance, resulting in a reduction of the quality of life caused by the debilitating symptoms of the disease [Findley, 2007].

The term *parkinsonism* refers in general to a number of disorders and medical condition that give rise to symptoms similar to the ones of Parkinson's disease, but are different in etiology and pathophysiology.

2.1.1 Symptoms

Usually classified as a motor disorder, the four cardinal features of PD are: tremor at rest, rigidity, bradykinesia (or akinesia), and postural instability. Tremor is apparently the most well-known symptom, though around 30% of the patients do not show it at the disease onset. It is usually present at rest, with a frequency in the range 4-6 Hz, disappearing during the execution of voluntary movement and sleep [Jankovic, 2008]. Bradykinesia, the slowness of movement, is characterized by difficulties along the whole motor process starting from the planning to the initiation and final execution of the movement. Rigidity is the stiffness and resistance to limb

movement resulting from an increase of the muscle tone, and is frequently associated with joints pain, that represents an initial manifestation of PD in most cases [Jankovic, 2008]. Postural instability, finally, leads to impaired balance and causes frequent falls, with 40% of the patients experiencing at least one fall and 10% once a week [Yao et al., 2013]. Other motor features including postural deformities (flexed neck and elbows and trunk posture) and freezing, i.e. motor blocks frequently occur. However, Parkinson's disease also causes a number of equally impairing cognitive disorders and neuropsychiatric disturbances, such as disorders of mood and sleep, anxiety, apathy, depression and hallucinations [Ondo et al., 2001, Aarsland et al., 2007, Jankovic, 2008].

To clinically assess the severity of the symptoms, the unified Parkinson's disease rating scale (UPDRS) is used. The scores range from 0 to 4, with higher scores representing worse symptoms. It is based on six criteria:

- I. evaluation of mentation, behavior and mood;
- II. self-evaluation by the patients of activities of daily life (speech, swallowing, handwriting, dressing, hygiene, falling, salivating, turning in bed, walking, and cutting food);
- III. clinician-scored evaluation of motor state (tremor, rigidity and bradykinesia, evaluated in the upper and lower limbs);

IV. complications of therapy;

V. prognostic evaluation using the Hoehn and Yahr scale;

VI. disability evaluation using the Schwab and England scale.

2.1.2 Etiology and Pathology

Parkinson's disease is represented for the majority of the cases as an idiopathic condition, meaning that there are no known causes. Factors such as pesticide exposure and head injuries have been associated with an increased risk of developing PD, but no causal relationships were demonstrated [Noyce et al., 2012, Van Maele-Fabry et al., 2012]. However, with 15% of the patients having a first-degree relative who developed the disease, genetic studies conclusively showed that mutations in specific genes cause PD, such as the ones that code for alpha-synuclein, parkin, dardarin, PINK1, DJ-1, and ATP13A2 [Davie, 2008, Lesage and Brice, 2009].

In terms of pathophysiology, PD is characterized by the death of dopamine-secreting cells caused by abnormal intraneuronal accumulation of alpha-synuclein protein in the brain in the form of Lewis bodies [Dickson et al., 2009]. This loss of neurons takes place in the substantia nigra pars compacta (SNpc, Fig. 2.1). The dopamine (3,4-dihydroxyphenethylamine) is a neurotransmitter of the catecholamine and phenethylamine families that plays an important modulatory effect especially in

the circuit of the basal ganglia (BG, Fig. 2.2), which is a group of subcortical brain structures in the central nervous system. It comprises the striatum, the pallidum, the substantia nigra, and the subthalamic nucleus (STN).

The striatum is the largest structure in the group, and is composed by 96% of GABAergic cells, meaning that the great majority of its neurons use γ -Aminobutyric acid (GABA) as neurotransmitter, which has an inhibitory effect on the target [Stocco et al., 2010]. The sector of the striatum that is most important for the BG system is called the putamen. It receives inputs principally from the cortex and the thalamus and has projections to the pallidum and the substantia nigra.

The pallidum is also a large structure that can be divided in globus pallidus and ventral pallidum; the globus pallidus has two parts with distinct functionality called internal (GPi) and external (GPe) globus pallidus. The external segment receives signals from the striatum and projects to the STN, while the GPi also receives inputs from the putamen but with two different pathways, direct and indirect. GPi represents one of the two outputs of the basal ganglia, and has efferent connections to the dorsal thalamus, the centromedian complex, and the pedunculopontine.

The substantia nigra is divided in the pars compacta, where, as mentioned, the death of dopamine-secreting neurons occur, and the pars reticulata (SNpr). The main input of SNpr comes from the putamen and projects to the thalamus and caudal nuclei, it being the other output of BG system.

The subthalamic nucleus, whose small size is estimated to be 3x5x12 mm [Yelnik, 2002], has afferent connections mainly from the GPe, but receives neuromodulatory inputs via dopaminergic axons from the SNpc and additional inputs from the peduncolopontine. Most of the neurons have multi-targeted, excitatory outputs - that use glutamate as neurotransmitter - projecting to the pallidum and the SNpr. The STN is anatomically divided in three areas with different functionality, namely, the sensorymotor part (dorsolateral position), the associative area (venteromedial localization), and the limbic part (in medial position).

Overall, the basal ganglia system is connected through five major pathways to the motor, oculo-motor, associative, limbic, and orbitofrontal circuits. The loss of dopaminergic input to the BG system determines alterations in these pathways, explaining the symptoms of PD [Obeso et al., 2008].

2.1.3 Diagnosis

There is no specific clinical test able to diagnose early Parkinson's disease with sufficient accuracy . Physicians state their conclusions after a number of observations including medical images, clinical records, and medication trials. This process is mainly used to rule out disorders that exhibit similar symptoms to PD: atypical and secondary parkinsonian syndromes (caused for example by cerebral infarction, hydrocephalus, or traumatic and toxic injuries) and non-dopamine deficient syndromes

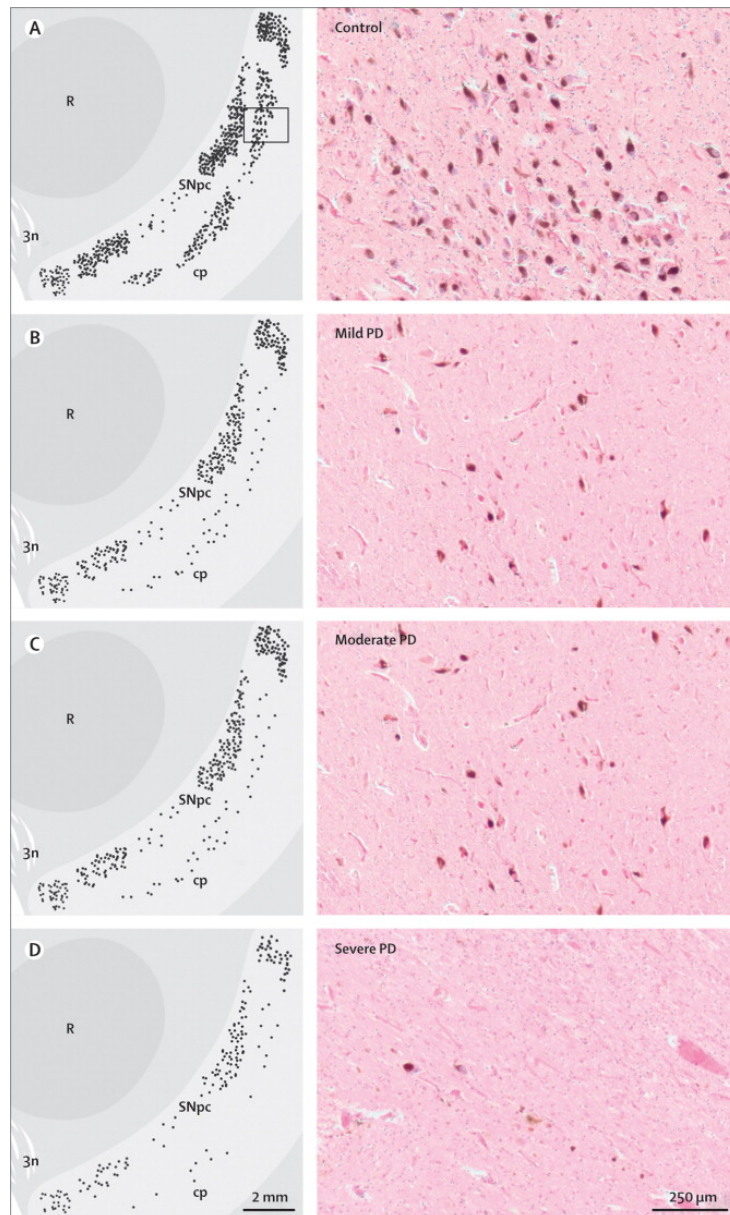


Figure 2.1: Semi-quantitative assessment of pigmented neurons in the SNpc. Left images show templates of the distribution of pigmented neurons in healthy controls (A) and in patients with PD with mild (B), moderate (C), or severe (D) loss of pigmented neurons. Abbreviations: 3n, exiting 3rd nerve fibres; cp, cerebral peduncle; R, red nucleus. Reproduced from Dickson et al. [2009].

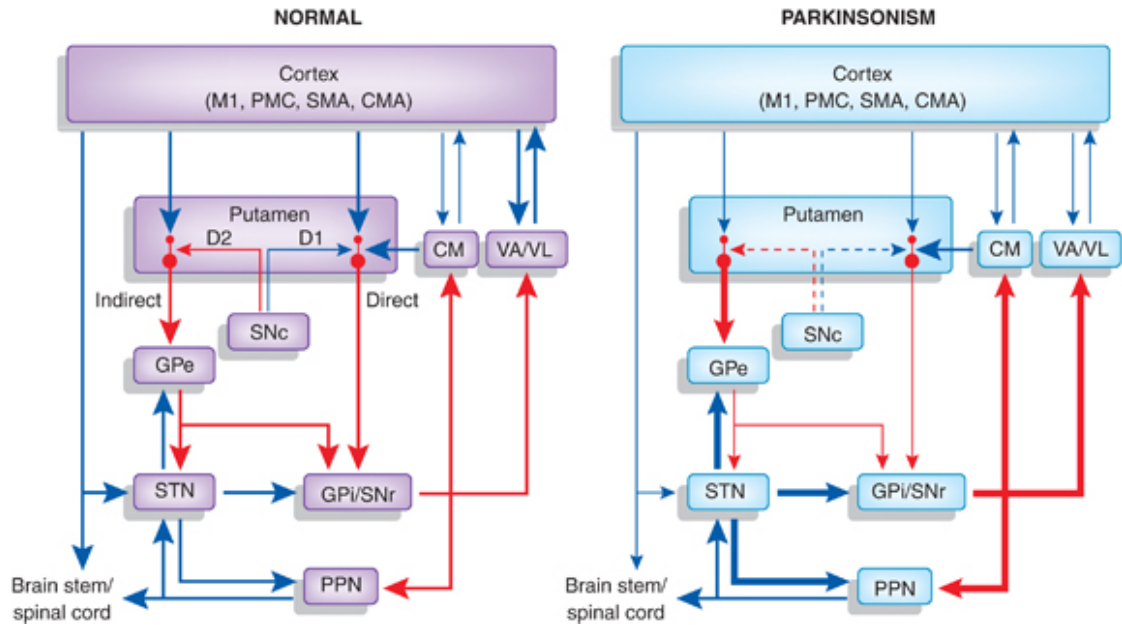


Figure 2.2: Detailed description of the basal ganglia circuit in normal and parkinsonian states. Red arrows represent excitatory outputs and blue arrows indicate inhibitory projections. The thickness of the arrows is proportional to the firing rate activity of the connection. Dashed arrows indicate the lesion of the subsystem. Abbreviations: CM, centromedian nucleus; CMA, cingulate motor area; GPe, globus pallidus, external segment; GPi, globus pallidus, internal segment; M1, primary motor cortex; PMC, pre-motor cortex; PPN, pedunculopontine nucleus; SMA, supplementary motor area; SNc, substantia nigra pars compacta; SNr, substantia nigra pars reticulata; STN, subthalamic nucleus; VA/VL, ventral anterior/ventral lateral nucleus. Reproduced from Smith et al. [2012], who modified from Galvan and Wichmann [2008].

(benign tremor and drug-induced PD). The main step in the diagnosis consists in showing evidence of striatal lesions (using magnetic resonance imaging, MRI) and sequentially dopamine deficiency in the same structures, since it receives inputs from the SNpc, where the dopamine cells death occur. After this, a trial with dopaminergic medication is attempted, and depending on its result, PD is diagnosed [Brooks, 2010]. Generally, the diagnosis is so difficult that some authorities suggest to review it periodically, when the tracked progress of the disease may provide useful information on the nature of the symptoms [Jankovic, 2008].

2.1.4 Treatment

Although there is no cure for Parkinson's disease, enormous progress has been made in its treatment over the last 50 years. Drug-based medication relies mainly on the use of L-DOPA (L-3,4-dihydroxyphenylalanine, or levodopa), which is a chemical that is converted in dopamine by dopa decarboxylase in dopaminergic neurons. Since in PD a striatal lack of dopamine is observed, the external input of L-DOPA diminishes the symptoms. However, only 5% to 10% of the administered levodopa crosses the blood-brain barrier, and the remaining part has to be metabolized elsewhere. To overcome this issue, the medication contains carbidopa or Benserazide, chemicals able to inhibit the peripheral dopa decarboxylase, thus decreasing dopamine availability in peripheral neurons.

Despite this precaution, long-term L-DOPA administration gives rise to a number of collateral effects that become equally impairing as the disease's symptoms. The main side effects are dyskinesia, i.e. involuntary movements that range from slight tremor to uncontrollable upper limb or lower extremities movements, and severe fluctuations in the symptoms relief after medication intake. For this reason, levodopa doses are kept to a minimum while still effective, and the treatment of early PD is initiated with other drugs based on dopamine agonists and MAO-B inhibitors. Dopamine agonists (such as pramipexole, ropinirole, apomorphine, and lisuride) bind to dopaminergic post-synaptic receptors in the brain and have similar effects to levodopa, although not being as effective in the control of the motor symptoms and generating significant side effects including hallucinations, insomnia, nausea, and constipation, that may occur even with the minimal dose. MAO-B inhibitors increase the level of dopamine in the basal ganglia by blocking its metabolism and have the same characteristics as the dopamine agonists in terms of efficacy in the treatment of PD [National Collaborating Centre for Chronic Conditions, UK, 2006; Jankovic and Aguilar 2008].

In advanced PD, a surgical treatment known as deep brain stimulation (DBS) has been developed and performed on patients after that collateral effects of prolonged sole drug treatment compromised its efficacy. To maximize its benefits, DBS is usually used in conjunction with drug medication, although in greatly reduced dosages

compared to drug treatment alone.

2.2 Deep Brain Stimulation

Deep brain stimulation is an effective surgical treatment used in patients who developed a resistance to the pharmacological medication. It consists of the unilateral or bilateral implantation of multi-contact macroelectrode leads in deep brain structures and consequent chronic voltage stimulation provided by a device placed in a subcutaneous chest pocket. It is performed not only in patients with Parkinson's disease but also Essential Tremor and Tourette's syndrome. In particular, it was approved by the Food and Drug Administration (FDA) in 2003 for PD patients in STN and Gpi as anatomical targets.

2.2.1 Origin

Deep brain stimulation is an evolution of functional stereotactic neurosurgery techniques, initially used to produce selective lesions of specific deep brain structures (thalamic and cerebellar nuclei) [Sironi, 2011]. In fact, ablation of the Gpi (pallidotomy) and regions of the thalamus (thalamotomy) using radio frequencies has been performed since the 1940s, before the discovery and availability of levodopa [Starr et al., 1998]. Such procedures were found to improve motor symptoms related to tremor and rigidity, although generating side effects affecting the speech, muscular tone, and visual-spatial defects [Starr et al., 1998]. Of course, the main drawback of ablative procedures was their irreversibility.

The turning point arrived with the work of the neurosurgeon Alim-Louis Benabid and colleagues in Grenoble, France. He was using electrical stimulation in PD subjects for both target localization and prediction of lesioning effects after ablation of the target. Since the stimulation seemed to reduce tremor and other symptoms itself, he tested various frequencies of stimulation - from 1 Hz to more than 100 Hz - and concluded that, in the upper part of the frequency range, the result of the stimulation would mimic the ablation without having to perform it [Williams, 2010]. Since then, the DBS procedure has been developed and eventually approved by the Food and Drug Administration (FDA) in different years and for different pathologies.

2.2.2 Surgical Protocol

The surgical procedure of DBS allows implanting macroelectrode leads precisely in certain brain areas through a combination of stereotactic and neuroimaging techniques. A subcutaneous external pacemaker lets the electrodes send electrical impulses to the brain. The components of the surgery are therefore three: the leads, their extensions, and the implanted pulse generator (IPG).

The leads consist on a coiled wire insulated in polyurethane, and generally have 4 platinum-iridium low impedance macroelectrodes or contacts (Fig. 2.3). The extensions are insulated wires that connect the leads to the IPG, which is a battery powered voltage stimulator encased in a titanium housing (Fig. 2.3).

There are two predominant technical approaches to placing DBS leads: frame-based stereotaxy (Fig. 2.4) and frameless neuronavigation-guided implantation using a skull-mounted aiming device, in conjunction with bone-implanted fiducial markers. In both techniques, brain images used for targeting (CT and/or MRI) are obtained preoperatively. Surgical planning software is used to register brain targets (STN or Gpi in PD) in an image space (stereotactic space) defined by the frame geometry or by bone-implanted fiducial markers. Placement of the DBS leads subsequently takes place in a standard operating room by navigation in stereotactic space, which is assumed to remain immobile with respect to the brain target.

Frequently, the initial anatomical target is refined by intraoperative microelectrode recordings (MER), that are inserted in multiple location (from 3 to 5) to explore the neural activity around the target area. Single-unit activity (relative to a small number of neurons) as well as local field potentials (regarding the ensemble activity of thousands of neurons), are recorded and visually inspected to retrieve useful information for the targeting [Starr et al., 2010].

Implantation may occur bilaterally (in both the cerebral hemispheres) or unilaterally (just one), depending on the clinical case. The implantation of the IPG takes place from a few days to a few weeks after the lead implantation, and consists in the placement of the device into a subcutaneous pocket, usually in the chest, which is eventually connected with the lead extensions. After the installation, the IPG



Figure 2.3: Figure A shows two four-contacts leads with different inter-contact spacing. Model #3387 on the left and #3389 on the right, both manufactured by Medtronic, Inc. Figure B shows the Active SC implanted pulse generator, by Medtronic, Inc. Image reproduced from <http://cabellhuntington.org/>.

is calibrated by a neurologist to optimize symptoms suppression and control side-effects [Volkman et al., 2002]. The stimulation parameters are voltage (range 0-5 V), frequency (range 130-200 Hz), and pulse width (60-90 μ s).

2.2.3 Results and Limitations

Results from a plethora of studies showed that DBS, in addition to drug treatment, is superior to drug medication alone [Deuschl et al., 2006, Williams et al., 2010, Bronstein et al., 2011]. Improvement in motor function, as assessed by motor diaries and UPDRS sub-scales, was significantly greater in patients undergoing DBS. Of particular importance is the improvement in mobility by 7.6-9.6 hours per day [Deuschl et al., 2006, Weaver et al., 2009]. However, the limitations of DBS - cost,



Figure 2.4: Stereotactic frame by Leksell (Leksell Stereotactic System). It includes a three-dimensional reference system and a center-of-arc instrument positioning system, used to as a guide for the insertion of exploratory microelectrodes and final macroelectrodes leads. Reproduced from <http://www.elekt.com/>.

long-term benefit, and risk of serious adverse effects - must be taken into account before DBS can be recommended to PD patients.

Since DBS is expensive [McClelland, 2011], cost must be considered when determining risk versus benefit. Significant reduction in the use of drug medication is an advantage provided to patients undergoing DBS, which leads to a reduction of both collateral effects and cost of treatment. The long-term benefit is also to be considered, since it has been shown that DBS does not alter the progression of the disease [Bronstein et al., 2011], and that UPDRS III (motor) scores are significantly higher 10 years after the surgery compared to 5 years [Castritto et al., 2011]. Serious adverse effects consist in surgical complications due to DBS, including intracranial

hemorrhage (0-10% of the cases), stroke (0-2%), infection (0-15%), lead erosion (1-2.5%), lead fracture (0-15%), lead migration (0-19%), and death (0-0.4%) [Bronstein et al., 2011].

2.3 Local Field Potentials

Since the lead insertion and the IPG placement occur in surgical operations that may be separated by a few days to a few weeks, it is possible during this time interval to use the lead extension to record neurosignals coming from the area where the electrodes have been implanted. As the impedance of the electrodes is low, it is possible to record the activity of a relatively large tissue volume (thousands of neurons). Net ionic currents generated by neuronal activity cause changes of the electric potential of extracellular medium; the recorded signal, the local field potentials measured in Volts or sub-multiples (Fig. 2.5), is the effect on the surface of the electrode of the sum of all these local currents.

LFP represent the synchronized activity of the population of neurons nearby the electrodes, and are classified as stochastic signals recorded in the time domain.

2.3.1 Subthalamic Nucleus Local Field Potentials in Parkinson's Disease

Following DBS approval by the FDA, researchers started to record LFP activity in the STN and analyze it using the standard signal processing tools. In particular, given the oscillatory nature of local field potentials, they were first analyzed in the frequency domain by means of power spectral density. Early studies reported

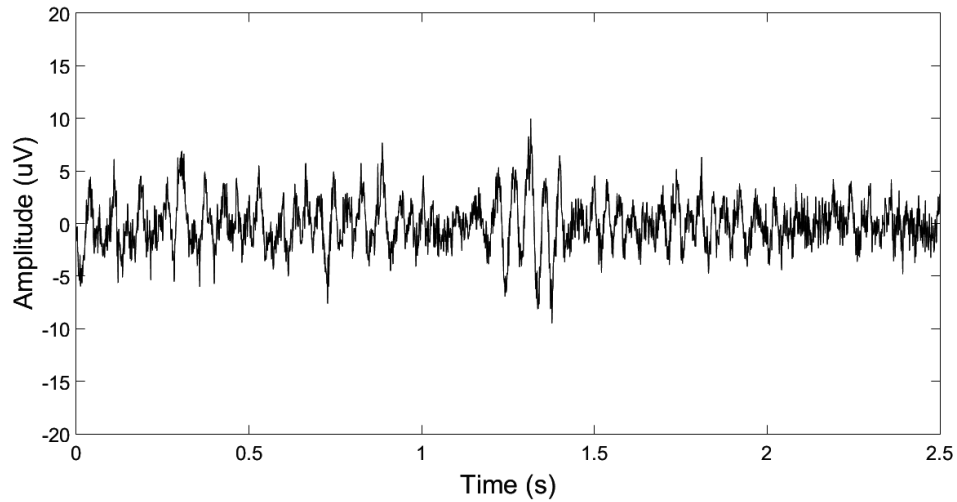


Figure 2.5: An example of local field potentials recorded in STN.

excessively synchronized activity in the beta frequency range (8-35 Hz) while patients were off the medication, to be reduced significantly after levodopa-based drug administration; conversely, gamma oscillations (60-90 Hz) were found to increase in power after medication, while being absent in pathological condition (Fig. 2.6) [Brown et al., 2001, Brown, 2003, Brown and Williams, 2005]. The power of the beta band was also found to be suppressed during the movement planning and execution (mechanism known as event related desynchronization, ERD) and the level of modulation correlated with motor performances and clinical scores (Fig. 2.7) [Kuhn et al., 2004]. Moreover, gamma activity was found to synchronize during movement execution [Brown, 2003] and correlate with clinical scores [Kuhn et al., 2004].

Subsequent studies pointed out that the activity in the beta region can be divided in two further ranges, namely low beta (13-20 Hz) and high beta (21-35 Hz), that

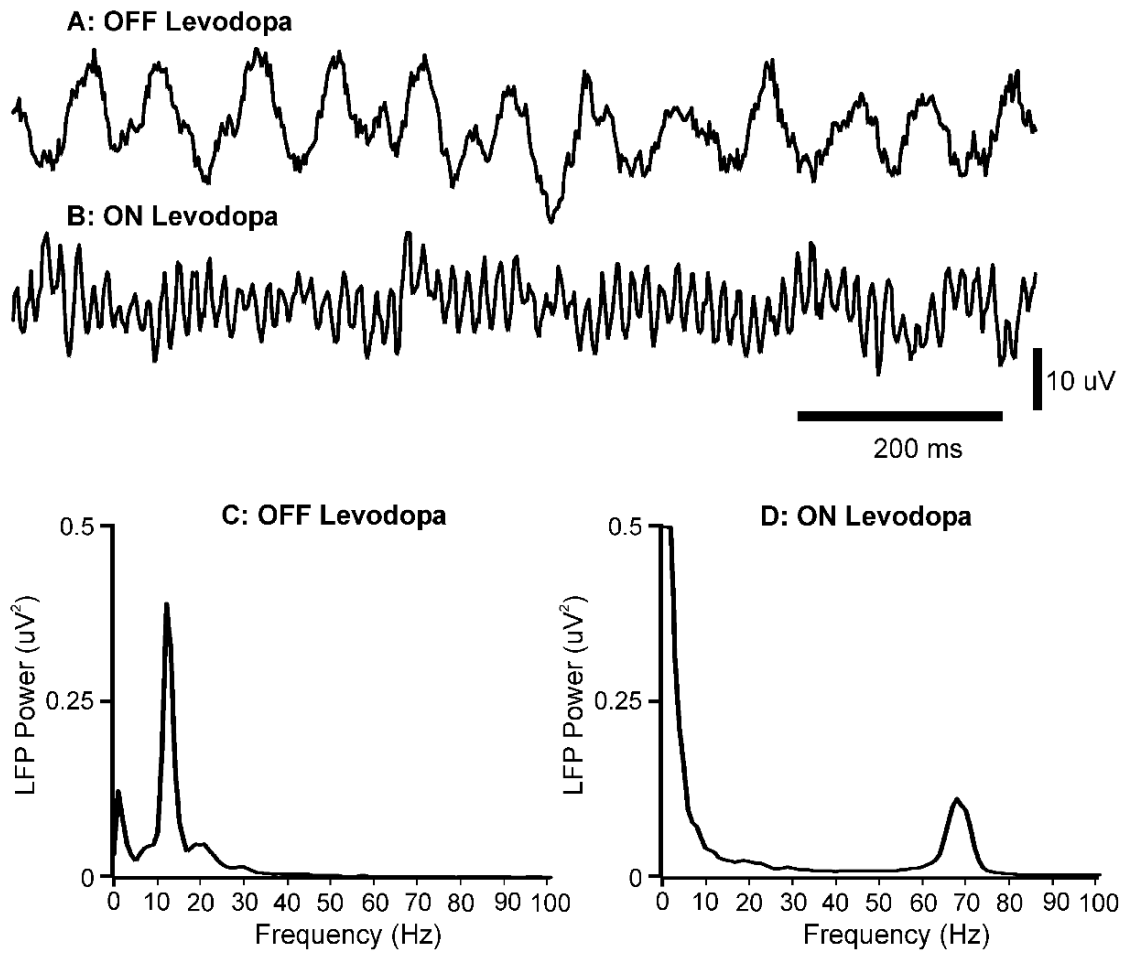


Figure 2.6: A) and B) show two LFP signals in “OFF” and “ON” medication respectively. The different oscillatory nature of the signals is clear and corroborated by the power spectral density in C) and D). Reproduced from Brown and Williams [2005].

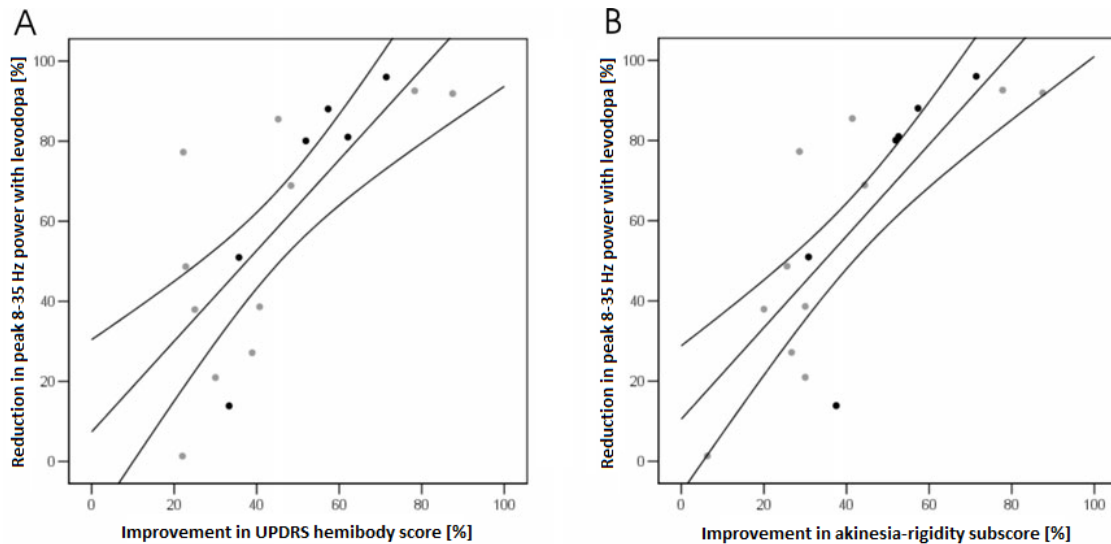


Figure 2.7: Correlation between UPDRS sub-scale scores and beta band modulation. Adapted from [Kuhn et al., 2006].

exhibited rhythms that are believed to be substantially different in nature [Marceglia et al., 2006, Lopez-Azcarate et al., 2010]. In fact, while low beta power decreased after medication intake, the activity of high beta wasn't significantly modulated. This observation lead to the hypothesis that the low beta rhythm is pathological (i.e. generated as the consequence of lack of dopamine in the basal ganglia network) while the high beta is physiological. More recently, other groups of oscillations, the high frequencies (150-450 Hz, also called HFO), have been studied in both medicated and unmedicated states.

High frequency oscillations were first discovered in the medicated state as broad 300 Hz activity [Foffani et al., 2003], but were also recently found in the unmedicated PD condition [Lopez-Azcarate et al., 2010, Ozkurt et al., 2011], although in a different

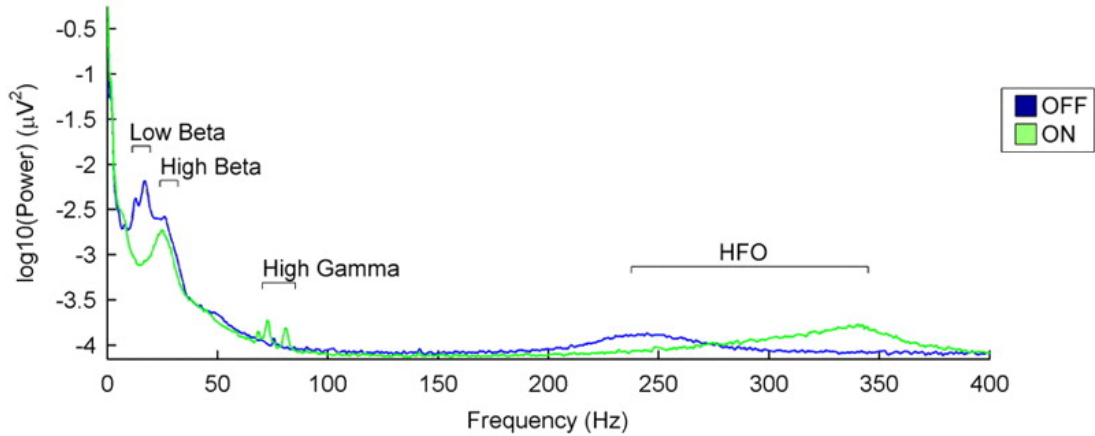


Figure 2.8: Spectral characteristics of LFP in unmedicated (OFF) and medicated (ON) states, during rest condition. Reproduced from Lopez-Azcarate et al. [2010].

frequency range (around 250 Hz). The power of the high frequencies present in the medicated condition, was found to increase during motor execution [Foffani et al., 2003]. High frequency activity in the unmedicated state is commonly referred to as sHFO (slow HFO), whereas in the medicated condition as fHFO (fast HFO). A visual comparison of the LFP spectral characteristics in medicated and unmedicated states, during rest condition, is shown in Fig. 2.8.

In addition to classical analysis by means of power spectral density and event related synchronization/desynchronization, LFP recorded in the basal ganglia have been studied with more sophisticated tools. Analysis performed using bispectrum and bicoherence (Fig. 2.9) showed that in the unmedicated state, different rhythms, especially low and high beta, are non-linearly correlated through phase coupling; this

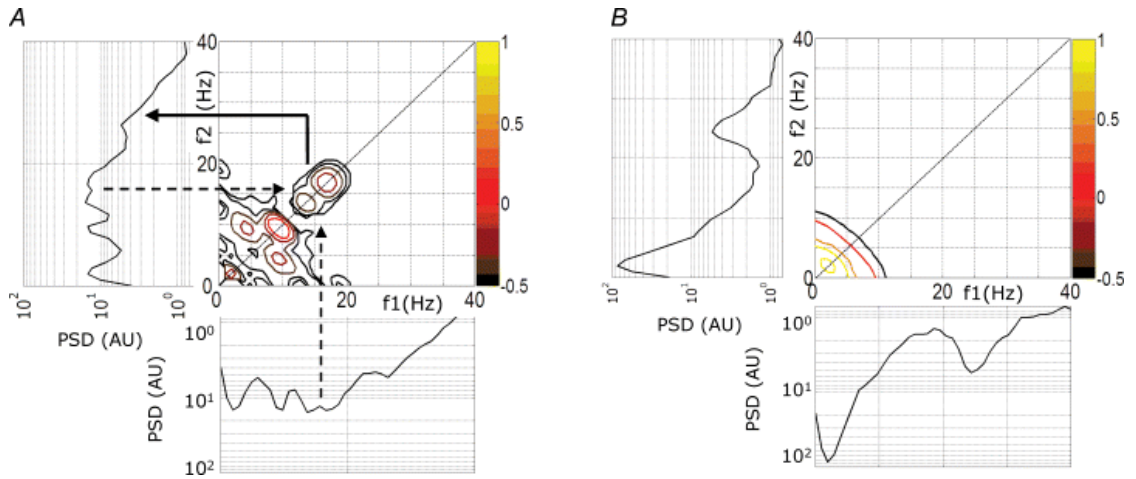


Figure 2.9: Comparison of bispectra obtained from LFP recorded in STN in untreated (A) and medicated (B) PD states, along with the power spectral densities of the signals in both conditions. The bispectrum is the 2-D Fourier transform of the third-order cumulant (the skewness) of a time series. A peak at the frequency pair (f_1, f_2) in the bispectrum means that the peak at the frequency $f_1 + f_2$ in the power spectral density of the time signal is produced by the phase coupled rhythms at f_1 and f_2 . Reproduced from Marceglia et al. [2006].

interaction was lost after levodopa administration [Marceglia et al., 2006].

A similar result was achieved through the analysis of phase-amplitude coupling (PAC) between frequencies in the beta range and HFO, which is a type of nonlinear interaction that was found to play a role in physiological processes such as memory and behavioral tasks, especially at the cortical level [Mormann et al., 2005, Voytek et al., 2010]. Phase-amplitude coupling is believed to be a mechanism for the information transfer between neuronal populations of different scales with different firing patterns. Phase-amplitude coupling was revealed at the STN level during untreated pathological condition in PD, and was highly reduced after medication (Fig. 2.10),

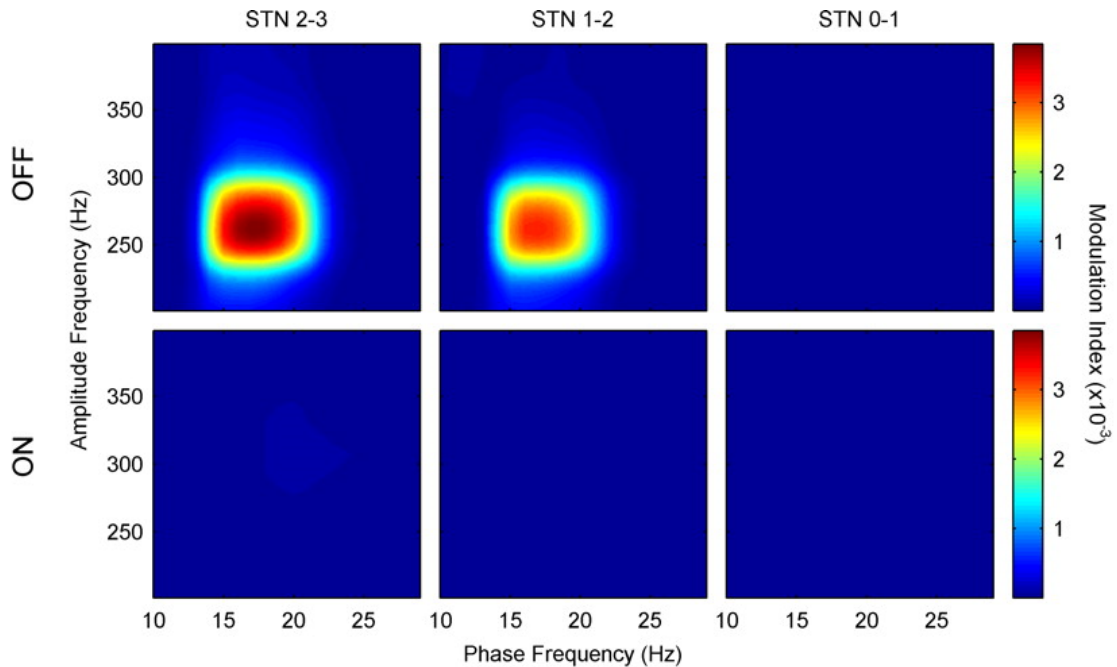


Figure 2.10: Phase-amplitude coupling between beta and HFO in untreated (“OFF”) and medicated (“ON”) states, computed in three different bipolar configurations from a four-contacts electrode placed in the STN. Bipolar pair 0-1 is at the bottom of the STN, pair 1-2 in the middle and 2-3 at the top. Reproduced from Lopez-Azcarate et al. [2010].

showing again that in the clinical “ON” state rhythms are more segregated and independent [Lopez-Azcarate et al., 2010]. It was also found in invasive motor cortex recordings [de Hemptinne et al., 2013] in untreated PD state, while it disappeared after medication and DBS therapy. However, another study showed the consistent presence of PAC in medicated state, although in a different frequency range [Ozkurt et al., 2011].

Taken together, all these evidence shows the reliability of the use of LFP to assess the clinical condition of the patients. Nonetheless, the analysis of local field potentials

not only aims to improve the understanding of the neurophysiopathological mechanisms underlying PD, but also to contribute and support the decision-making process regarding the DBS therapy. Intraoperative recording of LFP may be used during the leads placement to help surgeons navigate through the basal ganglia structures and identify the anatomical target borders [Chen et al., 2006, Telkes et al., 2014] and, after the implantation, postoperative LFP recording can be used to assist the IPG device programming, since evidence demonstrated that the anatomical location of beta and higher frequencies activity can predict the optimal stimulation contacts [Ince et al., 2010].

In most of the studies the collection of LFP data takes place intraoperatively or in the days right after the lead insertion; importantly, there's evidence supporting the fact that LFP analysis provide reliable results even after years from the lead implantation. Long-term recordings happening up to 7 years after the DBS surgery showed that, although smaller in amplitude, LFP activity had the same modulation patterns in response to movement as early recordings [Abosch et al., 2012]. This feature supports the idea that LFP may be used in next generation closed-loop DBS applications.

Chapter 3

Methods

3.1 Mathematical Methods

3.1.1 Filtering

3.1.1.1 FIR and IIR filters

Raw signals are commonly filtered in order to remove oscillations that are solely attributable to noise or are not of interest in the analysis. There are two filter implementations widely used for this purpose: Finite Impulse Response filters (FIR) and Infinite Impulse Response filters (IIR) [Oppenheim et al., 1999].

Let $x_n, n = 0, \dots, N - 1$ be a real valued discrete sequence obtained sampling a continuous process $x(t)$ such that $x_n = x(n\Delta t), n = 0, \dots, N - 1$ with Δt being the

sampling period (the inverse of the sampling frequency). Digital filters are commonly described with a difference equation in the time domain that relates the filter output y_n with the input x_n in the following way:

$$y_n = \frac{1}{a_0} \left(\sum_{i=0}^P b_i x_{n-i} + \sum_{j=1}^Q a_j y_{n-j} \right) \quad (3.1)$$

or, equivalently using the transfer function formulation:

$$H(z) = \frac{Y(z)}{X(z)} = \frac{\sum_{i=0}^P b_i z^{-i}}{\sum_{j=0}^Q a_j z^{-i}}, \quad (3.2)$$

where P is the feed forward filter order, Q the backward filter order, $b_i, i = 0, \dots, P$ are the feed forward filter coefficients and $a_j, j = 1, \dots, Q$ are the backward filter coefficients. X_z and Y_z are the Z-transform of x_n and y_n respectively, obtained as:

$$X(z) = \sum_{n=-\infty}^{\infty} x_n z^{-n} \quad (3.3)$$

z being, in general, a complex number. In the frequency domain the parameters of interest are represented by the magnitude response of the filter and its phase response, computed as the frequency varies. In particular, if the transfer function of a filter is $H(z)$, its magnitude response is:

$$|H(e^{j\omega})| = \sqrt{\text{Re}\{H(e^{j\omega})\}^2 + \text{Im}\{H(e^{j\omega})\}^2}, \quad (3.4)$$

and its phase response:

$$\angle H(e^{j\omega}) = \text{atan}(\text{Im}\{H(e^{j\omega})\}/\text{Re}\{H(e^{j\omega})\}), \quad (3.5)$$

where $z = e^{j\omega}$. If $a_j = 0 \forall j \neq 0$, then the filter is a FIR filter. Otherwise, there's a recursive component in the output of the filter and it represents a IIR filter. The advantages associated with the use of FIR filters are that they are always stable and that it's easy to design them in a way that the phase response is linear. However, to meet desired specifications such as stop-band attenuation and pass-band ripple attenuation, the filter order and consequently its length has to be high. On the other hand, IIR filters, when stable, offer better performances even with low filter orders, which allows faster computation since the number of total operations in the filtering process is lower. The important drawback of their use is that the phase response is not linear, meaning that oscillations at different frequencies in the output are not delayed of the same amount of time samples. This is a serious issue, especially when they are applied to electrophysiological signals, where the morphology of the signal itself is fundamental.

3.1.1.2 Zero Phase Filtering

The non-linearity of the phase response of IIR filters can be corrected if the signal processing is done completely offline, which means that all the samples of the time

sequence are available at the time of filtering. In fact, a forward-backward filtering technique can be implemented in order to get a IIR filtering stage whose phase response is uniformly zero, avoiding therefore any type of distortion [Gustafsson, 1996]. Let $Y'(e^{j\omega})$ be the output, in the frequency domain, of the first filtering stage such that:

$$Y'(e^{j\omega}) = X(e^{j\omega})H(e^{j\omega}) \quad (3.6)$$

Applying now time-reversal in the frequency domain (an operation that brings to a loss of causality and therefore is not suitable in online applications), which is represented by replacing ω with $-\omega$, and applying again the filter, the result is:

$$Y''(e^{j\omega}) = Y'(e^{-j\omega})H(e^{j\omega}) = X(e^{-j\omega})H(e^{-j\omega})H(e^{j\omega}) = X(e^{-j\omega}) |H(e^{j\omega})|^2. \quad (3.7)$$

Re-applying time-reversal the final expression of the filtering stage is:

$$Y(e^{j\omega}) = X(e^{j\omega}) |H(e^{j\omega})|^2, \quad (3.8)$$

since $|H(e^{j\omega})|^2 = |H(e^{-j\omega})| \cdot |H(e^{j\omega})|$. $|H(e^{j\omega})|^2$ represents also the transfer function of the system that, being completely real valued, has therefore a null phase response.

3.1.2 Power Spectral Density Estimation

Neuroelectrophysiological signals in the time domain, such as LFP, are well suited to be represented in the frequency domain, since they present oscillatory-like activity. The main idea behind the frequency domain representation of a time domain signal lies in the consideration that, by means of harmonic analysis, a time series (real or complex valued, continuous or discrete) can be decomposed into a linear combination of individual sinusoidal components, each consisting of amplitude, frequency, and phase. A common way to display the frequency information hidden in the time signal of interest is computing the power spectral density (PSD, or power spectrum), that shows the power associated with an oscillation as the frequency changes. There are two main families of methods used to compute the PSD: the parametric methods and the non-parametric methods. Parametric methods will be briefly described since they haven't been used in this work, while a more detailed treatment of non-parametric methods will follow [Oppenheim et al., 1999].

3.1.2.1 Parametric methods

Parametric methods assume that the signal can be considered as the output of a system whose parameters (order and coefficients) are unknown and have to be estimated using model identification techniques. Three steps are needed in order to estimate the power spectral density of a signal using a parametric approach:

- i. choice of the family of models;
- ii. estimate the model parameters using the available data;
- iii. compute the PSD from the theoretical expression associated with the particular model chosen at the beginning.

Families of models usually used in this context are autoregressive models (AR), mobile average models (MA), and autoregressive mobile average models (ARMA). Once the family is chosen, the order of the model can be estimated using algorithms such as Final Prediction Error (FPE), Akaike Information Criterion (AIC), and Minimum Descriptive Length (MDL). The estimation of model coefficients results from the minimization of the expected squared prediction error; the set of model coefficients can be finally plugged in the theoretical expression of the PSD for the chosen model to obtain an estimation of the power spectral density of the signal. The main advantage of a parametric approach in the PSD estimation is that the frequency resolution is high and does not depend on the length of the available data; the drawbacks are high computational cost and uncertain results when a high level of noise is present in the data. For these reasons, the spectral analysis of LFP is usually carried out using non-parametric methods.

3.1.2.2 Non-parametric Methods

Non-parametric methods require no a priori knowledge about the system that generated the signal of interest, and use the Fourier transform to estimate the PSD. This can be obtained using a direct or indirect method.

Direct Method Let $x_n, n = 0, \dots, N-1$ be a real valued discrete sequence obtained sampling a continuous process $x(t)$ such that $x_n = x(n\Delta t), n = 0, \dots, N-1$ with Δt being the sampling period. The Discrete Fourier Transform of x_n is a N -periodic sequence X_k of complex numbers in the form:

$$X_k = \sum_{n=0}^{N-1} x_n e^{-\frac{2\pi jnk}{N}}, k \in \mathbb{Z} \quad (3.9)$$

Each X_k encodes both amplitude and phase information of a sinusoidal component of x_n with frequency $\omega = \frac{k}{N}$ cycles per sample. The DFT is usually computed using the Fast Fourier Transform algorithm, that speeds up a computation that by definition would need $O(n^2)$ operations to only $O(N \log_2 N)$. The periodogram S_f can then be computed as the squared modulus of the DFT of x_n :

$$\hat{S}(f) = \frac{\Delta t}{N} \left| \sum_{n=0}^{N-1} x_n e^{-2\pi jnf} \right|^2, -f_n < f \leq f_n \quad (3.10)$$

where f is now the frequency in cycles/second, $f_n = 1/2\Delta t$ is the Nyquist frequency, and the frequency resolution $\Delta f = 1/N\Delta t$. The periodogram as described in this simple formulation has two main problems: the first one is that it is not consistent estimator, meaning that the $\hat{S}(f)$ does not converge to the real PSD $S(f)$ as $N \rightarrow \infty$, and the second one is that it suffers from very high spectral leakage, since x_n can be thought as a rectangular windowed segment of an infinite signal. Moreover, the variance of the PSD estimated with this method is high and it requires x_n to be stationary and ergodic; this is often not the case when dealing with electrophysiological signals. To address these problems, various solutions have been adopted: the most famous and widely used is Welch's modified periodogram. It consists of the division of the signal x_n into M segments of length L , overlapping each other of D samples. If D is 0, the overlap is said to be 0%, if $D = L/2$ is 50% and so on. After the segmentation, each segment $x_l^m, l = 0, \dots, L - 1$ is then multiplied with a window function in order to mitigate the spectral leakage. Finally, a periodogram $\hat{S}^m(f)$ is computed for every segment $m = 1, \dots, M$ and the final estimation of the PSD of x_n is given by:

$$\bar{S}(f) = \frac{1}{M} \sum_{m=1}^M \hat{S}^m(f) \quad (3.11)$$

The modified periodogram method has several advantages, the first being that the variance of the estimation of the PSD reduces as M increases. Additionally, if L is

chosen to be much smaller than N , the requirements of stationarity and ergodicity for x_n are more easily satisfied. However, since the computation of $\hat{S}^m(f)$, $m = 1, \dots, M$ is done on segments of length L , the frequency resolution of $\bar{S}(f)$ is $\Delta f = 1/L\Delta t$, which means that the shorter are the M segments, the poorer will be the frequency resolution. The choice of L is therefore determined by a trade-off between the reduction of the variance of the PSD estimation and the resulting frequency resolution.

Indirect Method The indirect method estimates the PSD of x_n as the DFT of its autocorrelation function \hat{R} , and is therefore usually referred to as autocorrelogram. This equivalence is guaranteed by the Wiener-Khinchin theorem. An unbiased estimation of \hat{R} is:

$$\hat{R}_p = \frac{1}{Np} \sum_{n=0}^{N-p-1} x_{n+p}x_n, \quad (3.12)$$

where p is the sample (time) lag and $p < N$. The estimation of the PSD is then:

$$\hat{S}_f = \frac{\Delta t}{N} \sum_{p=0}^{N-1} \hat{R}_p e^{-2\pi jpf} \quad (3.13)$$

Since a higher amount of variance is associated with higher order lags, windowing is used. This leads to the same observation made for the Welch's modified periodogram in terms of frequency resolution. When using a non-parametric approach to estimate

the PSD of a signal, the direct method is most widely used.

3.1.3 Time-varying Spectral Estimation

When, during the processing, not only the frequency content of a signal is of interest but also how it varies with time, the methods previously described for the PSD estimation have to be modified. One of the most widely used techniques to generate time-varying spectral maps (also called time-frequency maps) implements the use of the short-time Fourier transform STFT [Mitra, 2001].

Let $x_n, n = 0, \dots, N - 1$ be a real valued discrete sequence obtained sampling a continuous process $x(t)$ such that $x_n = x(n\Delta t), n = 0, \dots, N - 1$ with Δt being the sampling period. The STFT $X(m, \omega)$ of x_n is defined as:

$$X(m, \omega) = \sum_{n=0}^{N-1} x_n w_{n-m} e^{-j\omega n}, \quad (3.14)$$

where $w(n)$ is a window function and m is a shift in samples. The spectrogram of x_n , which is the representation of its time-frequency map, is computed by simply squaring the STFT of the signal:

$$\text{spectrogram}(m, \omega) = |X(m, \omega)|^2 \quad (3.15)$$

The size of the window function is crucial since the time and frequency resolutions

of the spectrogram depends on it. In fact, the higher the window size, the higher the frequency resolution, since more samples are available to compute the DTF. However, the time localization is poorer, so it's not possible to discriminate with accuracy when a change in the frequency content occurs. On the other hand, small window length allows a better time localization with the drawback of having a poor frequency resolution, meaning that close spectral peaks cannot be distinguished. The relationship between time resolution Δt and frequency resolution Δf of the estimate spectrogram is indirectly related with the Heisenberg uncertainty principle and it follows the law:

$$\Delta t \Delta f \leq \frac{1}{4\pi}. \quad (3.16)$$

3.1.4 Phase-Amplitude Coupling Estimation

The phase-amplitude coupling (PAC) is a nonlinear interaction between oscillations occurring at different frequencies ranges, such that there exists a faster wave whose amplitude envelope is modulated by the phase of a slower one (Fig. 3.1). There is actually no golden standard for the estimation of the strength of this type of interactions; however, several methods have been proposed. Three of them (Mean Vector Length [Canolty et al., 2006], Coherence Value [Colgin et al., 2009], and Phase-Locking Value [Penny et al., 2008, Cohen, 2008]) will be described in detail and a

comparison of their performances will be discussed once both applied to neuroelectrophysiological signals.

3.1.4.1 Mean Vector Length

Let $z_n, n = 0, \dots, N - 1$ be a real valued discrete sequence obtained sampling a continuous process $z(t)$ such that $z_n = z(n\Delta t), n = 0, \dots, N - 1$ with Δt being the sampling period (the inverse of the sampling frequency). Suppose that the slow, modulating (or phase) frequency is f_ϕ , and the fast, modulated (or amplitude) frequency is f_A . Let x_n be the output of a band pass filter (with linear phase response, or used forward and backward) applied to z_n , such that x_n contains only a narrow range of frequencies around f_ϕ that are believed to modulate, with their phase, the amplitude envelope of y_n . Similarly, y_n is the output of a band pass filter (with linear phase response, or used forward and backward) applied to z_n , such that y_n contains only a range of frequencies around f_ϕ . By means of Hilbert transformation, it is possible to obtain the analytic representation of x_n and y_n . Generally, the analytic representation t'_n of a signal $t_n, n = 0, \dots, N - 1$ is defined as:

$$t'_n = t_n + j\hat{t}_n \tag{3.17}$$

where \hat{t}_n is the result of the convolution between t_n and the impulse response h_n of the Hilbert transformer [Johansson, 1999]:

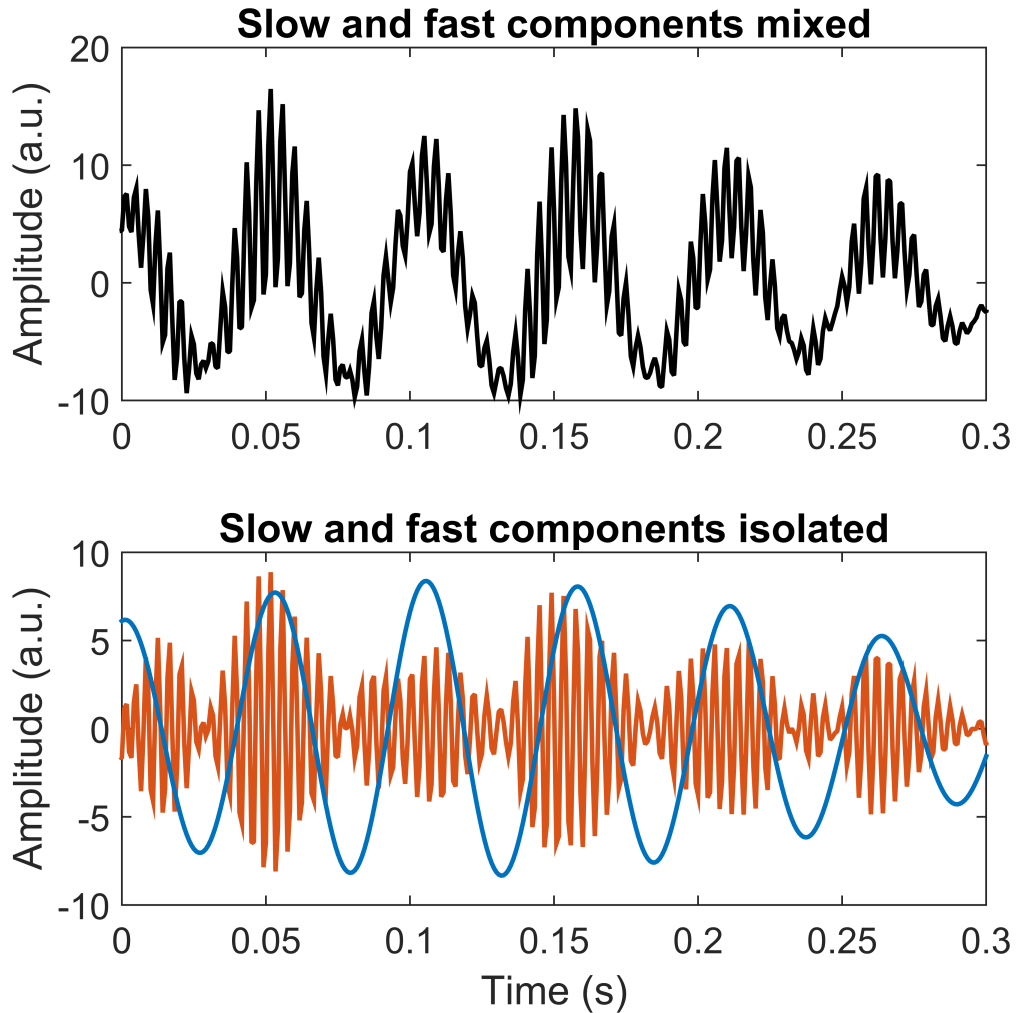


Figure 3.1: Example of PAC in LFP recorded at the STN level. At the top, the fast oscillation (around 250 Hz) is represented together with the slow one (around 15 Hz). It is possible to notice how the amplitude of the fast wave is modulated depending on the phase of the slow oscillation (in this example, higher amplitude is associated with the crests of the slow wave). In the bottom, the same oscillations are filtered and shown superimposed, where the effect of the modulation is even clearer.

$$\hat{t}_n = \sum_{m=0}^{N-1} h_{n-m} t_m \quad (3.18)$$

with

$$h(n) = \begin{cases} \frac{2}{N} \sin^2\left(\frac{\pi n}{2}\right) \cot\left(\frac{\pi n}{2}\right) & \text{for } N \text{ even} \\ \frac{1}{N} \left(\cot\left(\frac{\pi n}{N}\right) - \frac{\cos\left(\frac{\pi n}{N}\right)}{\sin\left(\frac{\pi n}{N}\right)} \right) & \text{for } N \text{ odd} \end{cases} \quad (3.19)$$

From its analytic representation, the instantaneous phase and the instantaneous amplitude (envelope) of a signal can be extracted. In particular, let $\Phi_x(n)$ be the instantaneous phase of x_n computed as:

$$\Phi_x(n) = \arg(x'_n) \quad (3.20)$$

and $A_y(n)$ the instantaneous amplitude of y_n , computed as:

$$A_y(n) = \left| y'_n \right| \quad (3.21)$$

Now, a composite signal $g(n)$ can be created as follows:

$$g(n) = A_y(n) e^{j\Phi_x(n)} \quad (3.22)$$

The sequence $g(n)$ consists in a complex sinusoidal function modulated, in amplitude, by the envelope of the fast oscillations at the frequency f_A and, in phase, by the instantaneous phase of the slow oscillation at the frequency f_Φ . Every value of $g(n)$ is, then, a point in the complex plane. It's reasonable to assume that, if no phase-amplitude coupling occurs, $g(n)$ for N large enough is distributed symmetrically around the center of the plane, since $A_y(n)$ and $\Phi_x(n)$ are independent. On the contrary, if a PAC occurs, it means that $A_y(n)$ is higher for some phases $\Phi_x(n)$ than others. This leads to a loss of circular symmetry around the zero of the complex plane, since some points of $g(n)$ will be concentrated in a specific region. A natural way to quantify this observation is to take the absolute value of the mean of $g(n)$, creating then a function $MVL(f_\Phi, f_A)$ that measures the strength of phase-amplitude coupling between f_Φ and f_A :

$$MVL(f_\Phi, f_A) = |\langle g(n) \rangle|, \quad (3.23)$$

where $\langle \cdot \rangle$ denotes the mean over all samples $n = 0, \dots, N - 1$. $MVL(f_\Phi, f_A)$ is a real number that tends to zero when no PAC occurs at the considered pair of frequencies, whereas the existence of coupling leads to larger mean vector lengths. Of course, it's difficult to know a priori the pair of frequencies where the coupling occurs, so a common practice is to iterate the process described (Fig. 3.2) varying f_Φ and/or f_A . To be more precise, although the MVL measure is able to investigate only

two frequency ranges at a time (i.e. an (f_Φ, f_A) pair), it can be used to build the a phase-amplitude comodulogram plot, a visual tool that reports the strength of coupling among multiple bands simultaneously. The comodulogram is constructed scanning multiple frequency band pairs and computing the PAC measure for each one. The final result is a color coded plot where the horizontal axis represents the frequencies analyzed as f_Φ whereas f_A is represented in the vertical axis. Hotter colors are associated with stronger PAC.

3.1.4.2 Coherence Value

The coherence value CV is computed based on the consideration that, if $A_y(n)$ is modulated by $\Phi_x(n)$, then the power spectral density of $A_y(n)$ should present a peak at f_Φ . Moreover, the phase of $A_y(n)$ at f_Φ should have some relationship with $\Phi_x(n)$ if the phase-amplitude coupling phenomenon is consistent. A function that is able to take into consideration both requirements is the magnitude squared coherence, computed, in particular, between $A_y(n)$ and z_n . The magnitude squared coherence [Carter et al., 1973] is a function of frequency f that quantifies the linear transfer in the frequency domain between two time sequences, and is defined as:

$$C_{\alpha\beta}(f) = \frac{|S_{\alpha\beta}(f)|^2}{S_{\alpha\alpha}(f)S_{\beta\beta}(f)}, \quad (3.24)$$

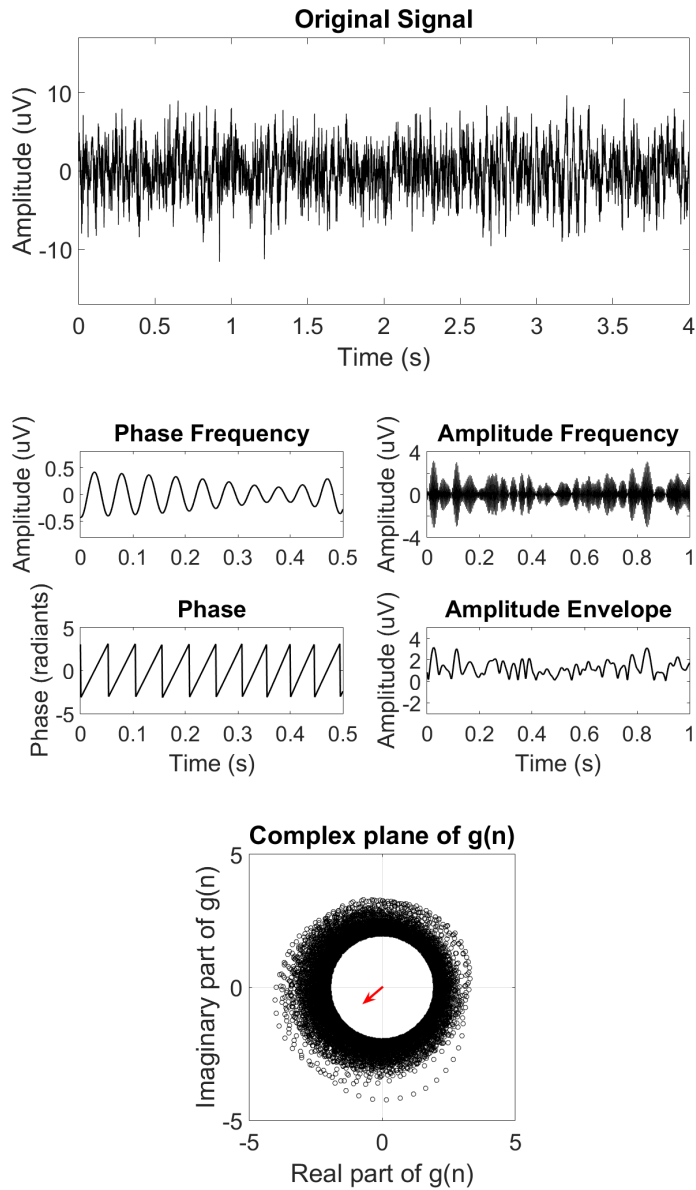


Figure 3.2: Algorithm for the detection of PAC in a signal using the MVL. From top to bottom: extraction of phase and amplitude frequency components from the original signal with adequate bandpass filters, estimation of the phase of the slow wave and amplitude envelope of fast wave and generation of the composite signal $g(n)$, represented in the complex plane. The points of $g(n)$ with amplitude smaller than 2 have been removed for sake of clarity. The thick red arrow represent the magnitude of the phase-amplitude strength between the two frequencies considered.

where α_n and β_n are two real valued discrete time sequences, $S_{\alpha\alpha}$ and $S_{\beta\beta}$ are the respective autospectra, and $S_{\alpha\beta}$ is the cross-spectrum which is obtain from the DFT of the cross-correlation of the two sequences. For the proper estimation of $C_{\alpha\beta}(f)$, the signals α_n and β_n should be segmented in several windows (whose length will define the frequency resolution of the estimation), then compute and average the autospectra and the cross-spectra over the windows, and finally apply the definition given. The magnitude squared coherence ranges from 0 (no linear relationship between the two signals at the chosen frequency) and 1 (perfect linear relationship). The use of the magnitude squared coherence between $A_y(n)$ and z_n , referred as $C_{A_y z}(f)$, to quantify phase-amplitude couplings is interesting since it allows the visualization of all the possible modulating frequencies for a certain f_A in a single plot; whereas in the *MVL* method previously described, it is necessary to first choose the candidate f_Φ since the computation of that PAC measure requires the filtering of z_n , also in the phase frequency range. To obtain a measure of the influence of the phase at the frequency f_Φ in the modulation of the amplitude at f_A , a function known as coherence value $CV(f_\Phi, f_A)$ can be derived averaging $C_{A_y z}(f)$ over a narrow range centered in f_Φ :

$$CV(f_\Phi, f_A) = \frac{1}{K} \sum_{f=f_\Phi-s}^{f_\Phi+s} C_{A_y z}(f), \quad (3.25)$$

where $2s$ is the frequency resolution for the phase frequencies and K is the number of samples of $C_{A_yz}(f)$ contained in $2s$. The higher the CV values is, the stronger is the phase-amplitude coupling at the considered frequency pair. A visualization of the algorithm is shown in Fig. 3.3. By averaging the values of $C_{A_yz}(f)$ over different frequency bins and repeating this process for different f_A , it's possible to generate a comodulogram plot equivalent to the one described for the MVL measure.

3.1.4.3 Phase-Locking Value

The rationale behind the use of the phase-locking value PLV to estimate phase-amplitude coupling lies on the same consideration about the oscillatory properties of $A_y(n)$ described in section 3.1.4.2. This measure does not directly use $A_y(n)$; however, it's based on the relationship between the phase of the wave at frequency f_Φ extracted from $A_y(n)$ with $\Phi_x(n)$. Since no amplitude values are used in the computation of the PLV , it is said to be an amplitude-free measure. Given that the $\Phi_A(n)$ is the phase of the component of $A_y(n)$ at the frequency f_Φ (estimated with the methods previously described), a composite function $d(n)$ can be constructed as follows:

$$d(n) = e^{j[\Phi_x(n) - \Phi_A(n)]} \quad (3.26)$$

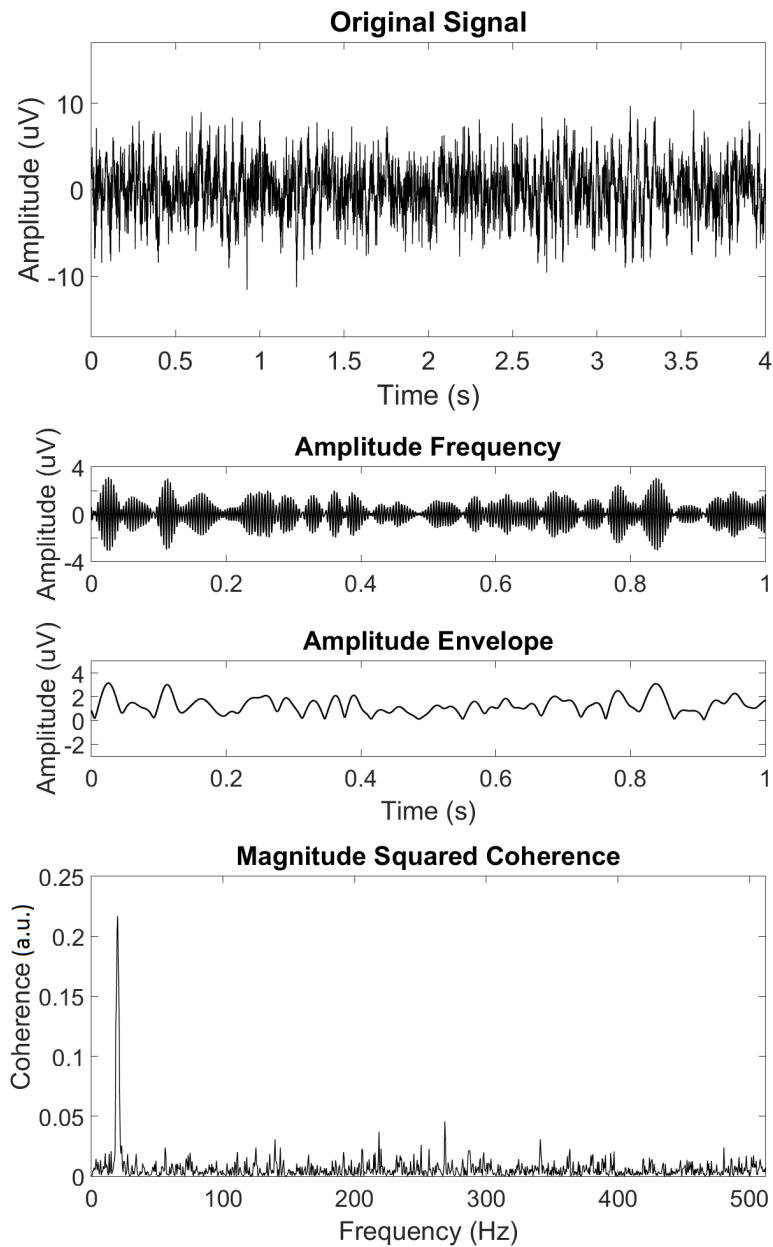


Figure 3.3: Algorithm for the detection of PAC using the Coherence Value. From top to bottom: the raw signal is filtered in the amplitude frequency range and its envelope is estimated. Then the magnitude squared coherence is computed between the envelope sequence and the raw signal. The measure of coupling strength is obtained integrating coherence value in small bins.

In the complex plane, $d(n)$ is represented by a cloud of points, all with unitary radius and phase dependent by the difference between $\Phi_x(n)$ and $\Phi_A(n)$. If they are independent and no coupling occurs, the points of $d(n)$ will be symmetrically distributed around the origin, while if it is present, the points distribution will be biased towards certain privileged directions, since the phase difference tends to be constant. A natural way to extrapolate a PAC measure is to average all points of $d(n)$ and then take the absolute value:

$$PLV(f_\Phi, f_A) = |\langle d(n) \rangle|, \quad (3.27)$$

where $\langle \cdot \rangle$ denotes the mean over all samples $n = 0, \dots, N - 1$. Similarly to the *MLV* measure, a comodulogram can be constructed scanning multiple frequency band pairs and computing the PAC measure for each of them.

3.1.4.4 Significance Analysis

For both the methods described to detect PAC, it's necessary to test if the value obtained as a measure of the strength of the coupling is different from what would be obtained by chance [Tort et al., 2010]. In order to do so, a surrogate analysis is performed. In particular, a certain number $R \geq 100$ of surrogates of $A_y(n)$ is generated by dividing the original sequence into 1000 equally long segments and randomly rearranging them for each surrogate. The PAC measure (*MVL* or *CV*) is

then calculated for all the surrogate series, leading to a distribution of surrogate PAC measures. Defining $\bar{\mu}$ as the experimental PAC value measured with the data and μ_s the mean of the PAC surrogate distribution, assuming normality for this distribution it's possible to perform a t -test with the following hypotheses:

$$\begin{aligned} H_0 : \mu_s &= \bar{\mu} \\ H_1 : \mu_s &\neq \bar{\mu} \end{aligned} \tag{3.28}$$

The common use of a significance level $\alpha = 0.05$ is not well suited for this application. In fact, to investigate the existence of PAC in a signal, a comodulogram plot (described earlier) is usually generated. If the phase frequencies range is divided in P narrow bands and the amplitude frequencies range in Q bands, the total number of (f_ϕ, f_A) combinations and therefore tests needed to generate the comodulogram is PQ , which is usually much greater than 50. It is clear that a correction for the number of comparisons is necessary, and it is usually performed by means of Bonferroni's correction, which lowers the significance level of each test to $\alpha = 0.05/PQ$. If the significance test is not passed for a certain pair (f_ϕ, f_A) , then the related PAC measure is arbitrarily set to zero; otherwise, it maintains its experimental value.

The main drawback of the significance testing performed through hypothesis testing is that the number PQ may be really big, making it nearly impossible to detect a significant phase-amplitude coupling when α becomes very small. A solution

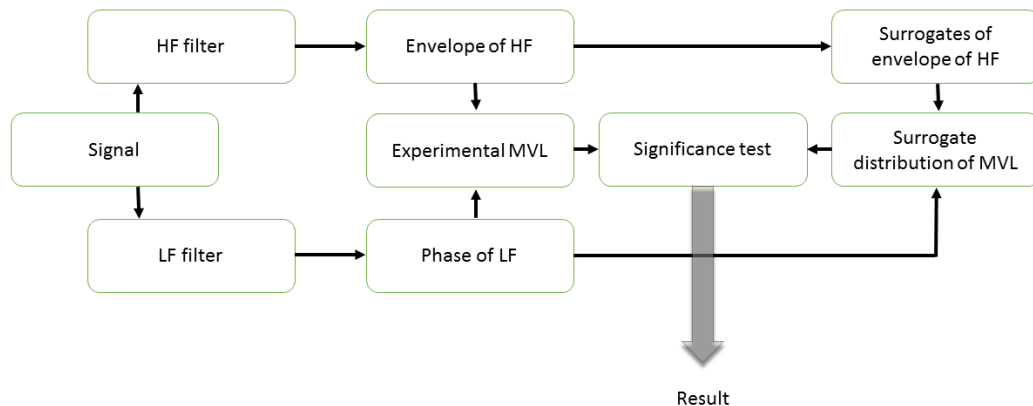


Figure 3.4: Overall processing flow to estimate PAC using the MVL method. HF are the high (amplitude) frequencies whereas LF are the low (phase) frequencies.

for this problem is to standardize the experimental PAC value obtained in (f_{ϕ}, f_A) subtracting the mean of the PAC measures obtained with surrogates and dividing by its standard deviation. This method also allows results to be compared among bipolar derivations and subjects.

The flow charts that describe the process to obtain PAC measures with significance testing are shown in Fig. 3.4, Fig. 3.5, and Fig. 3.6.

3.1.5 Statistical Analysis

Statistical analysis in this work was performed by means of hypothesis testing and correlation between variables [Stuart et al., 2008].

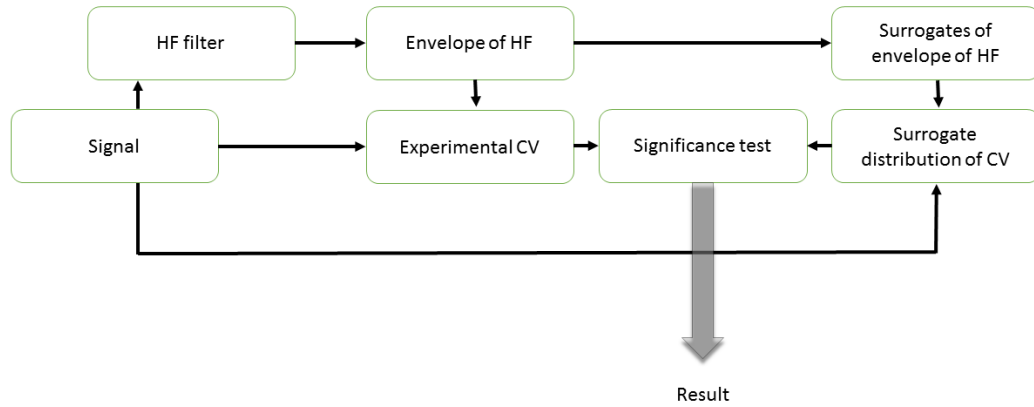


Figure 3.5: Overall processing flow to estimate PAC using the CV method. HF are the high (amplitude) frequencies whereas LF are the low (phase) frequencies.

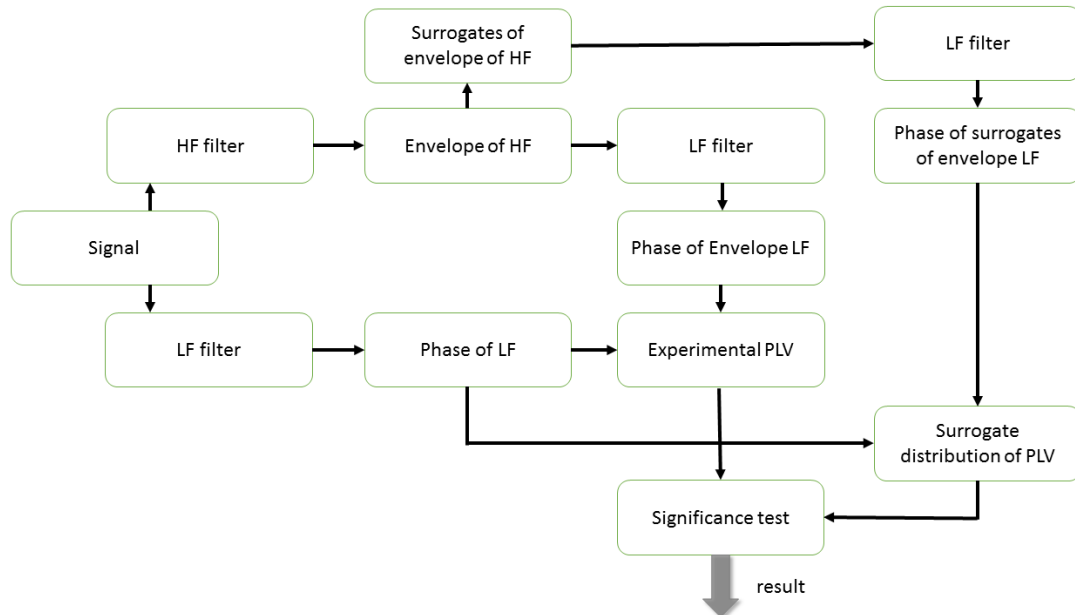


Figure 3.6: Overall processing flow to estimate PAC using the PLV method. HF are the high (amplitude) frequencies whereas LF are the low (phase) frequencies.

3.1.5.1 Hypothesis Testing

The process of statistical inference performed with hypothesis testing can be divided in three cases: one-sample testing, two-sample testing, and testing more than two samples. In any case, tests can be performed using parametric tests, meaning that some assumptions about the distribution of the variables considered is made, or non-parametric tests, where little or no assumptions are necessary. In general, basic assumptions like independence of observations, a sufficient sample size, and absence of extreme outliers are needed.

The hypothesis of tests are two: the first one is indicated as the null hypothesis H_0 , and usually states that a particular parameter of the population sample under exam (indicator of location or shape) is not significantly different from a fixed number (in the case of one-sample tests) or from the same parameter estimated from another sample (two-sample test or more). The other hypothesis, known as alternative hypothesis H_1 , is the complementary of H_0 .

Associated with hypothesis testing is the p-value, that quantifies the probability that the experimental outcome (that's being tested) results from the assumption that H_0 is true. When the p-value is smaller than a significance level α (usually 0.01 or 0.05 in case of single comparisons) than H_0 is rejected and H_1 is accepted, otherwise H_0 holds.

One-sample tests commonly used are:

- parametric t -test, to compare the sample mean with a fixed number, under the assumptions that the population follows the normal distribution and its standard deviation is unknown;
- parametric χ^2 test, to compare the sample variance with some value, under the assumption that the population is normal;
- Kolmogorov-Smirnov test to check if a sample is drawn from a normal distribution;
- non-parametric Wilcoxon Signed Rank test, to compare the sample median with a specified value.

Two-sample tests used are, among the others:

- parametric t -test, to compare two sample means, under the assumptions that the populations from which the samples are drawn are normal with equal but unknown variances;
- parametric Welch's t -test, to compare two sample means, under the assumptions that the populations from which the samples are drawn are normal with unequal and unknown variances;
- parametric F -test, to compare the variances of two samples under the assumption of normality;

- non-parametric Mann-Whitney U -test, to check if two samples come from the same population;
- non-parametric Squared Ranks test, to compare the variances of two samples.

Common tests for more than two samples are:

- parametric one-way ANOVA (analysis of variance), to compare sample means under the assumptions of normality and equality of variance between samples populations;
- non parametric one-way Kruskal-Wallis analysis of variance, to test if three or more samples originate from the same distribution.

Analysis of variance can be presented in terms of general linear modeling and can be enriched using, for example, blocking factors. It is important to notice that the output of a ANOVA or Kruskal-Wallis testing does only indicate if there's a difference in the test parameter between the groups, not where it occurs.

When used in this work, significance and p-value of the tests have been specified.

3.1.5.2 Correlation

To quantify the amount of linear dependence between two samples belonging to the random variables $X = \{x_1, \dots, x_N\}$ and $Y = \{y_1, \dots, y_N\}$, it is possible to use Pearson's correlation coefficient r_{xy} defined as:

$$r_{xy} = \frac{\sum_{i=1}^N (x_i - \bar{x})(y_i - \bar{y})}{\sqrt{\sum_{i=1}^N (x_i - \bar{x})^2} \sqrt{\sum_{i=1}^N (y_i - \bar{y})^2}}, \quad (3.29)$$

where \bar{x} is the sample mean of X : $\bar{x} = \frac{1}{N} \sum_{i=1}^N x_i$ and analogously for \bar{y} . The correlation coefficient ranges from -1 to 1. Values close to $|1|$ mean that in the scatter plot of (X, Y) the data points of X and Y lie on a line and are therefore linearly correlated. Negative values represent negative linear correlation, meaning that the more positive becomes a variable, the more negative becomes the other. Similarly, a positive correlation coefficient represent the tendency to grow with the same sign. Finally, values close to 0 represent the absence of linear relationship.

Associated with the correlation coefficient is a p-value which indicates the significance of the correlation; if smaller than a specified level (usually 0.05) then there is no significant correlation between the variables considered, whatever the correlation coefficient may be.

3.2 Dataset and Experimental Protocol

The data analyzed in this work were recorded at Fairview Hospital, University of Minnesota, in 2008 from 10 PD patients who provided informed consent and, with the approval of the University of Minnesota Institutional Review Board, were then enrolled in the study. The study was supported by a Medtronic, Inc. grant for an investigator-initiated project lead by Dr. Aviva Abosh and Dr. Nuri F. Ince. All the subjects carried a diagnosis of Parkinson’s Disease and underwent DBS surgery per routine protocol (see section 2.2.2) which allowed the unilateral implantation of macroelectrodes #3389 (manufactured by Medtronic Inc, Fridley, Minnesota, Fig. 3.7) in the STN. The surgery was performed in such a way that middle contacts of the electrode (“1” or “2”) were placed inside of the STN.

LFP recordings were made during an extended inpatient hospitalization taking place three weeks after the lead implantation, during which patients underwent 24 hours (over two solar days) of continuous LFP recording from the implanted DBS electrode with concurrent videotaping (Fig. 3.9) . In addition to LFP data, electroencephalographic, electromyographic, and tremor accelerometry recordings were obtained using the EMU40 system (XLTEK-Natus, San Carlos, California) at a sampling rate of 1024 Hz with 16 bit of Analog-to-Digital Converter resolution. All channels were analogically high-pass filtered at 0.1 Hz. LFP data were recorded from all four contacts of the macroelectrode. Data collection was performed by a team

including neurosurgeon, electrical engineers, a clinical nurse, and EEG technician. The recording period included periods of sleep and wakefulness in each patient. All patients underwent 3 “OFF” periods (unmedicated state) and 3 “ON” periods (medicated condition) during the 24-hour monitoring sessions. Each medication intake (L-DOPA-carbidopa based) occurred at late morning and late afternoon of the first day and early morning of the following. Patients were instructed to verbally inform the nurse when, after drug administration, they started to feel the effect of the medication; UPDRS III (motor) scoring by a nurse followed to confirm the clinical “ON” state. Patients were asked to stay in a resting condition for at least 120 s in each state. During the recording period, patients also performed a movement task that consisted in tapping alternatively two specific keys of a keyboard in a fixed amount of time (30 seconds) preceded by 10 s of rest. This task was repeated twice for every “OFF” and twice for every “ON” state. All the key presses as well as errors (i.e. wrong key press) were registered together with their timings. A scheme of the motor experimental protocol is shown in Fig. 3.8).

Model 3389

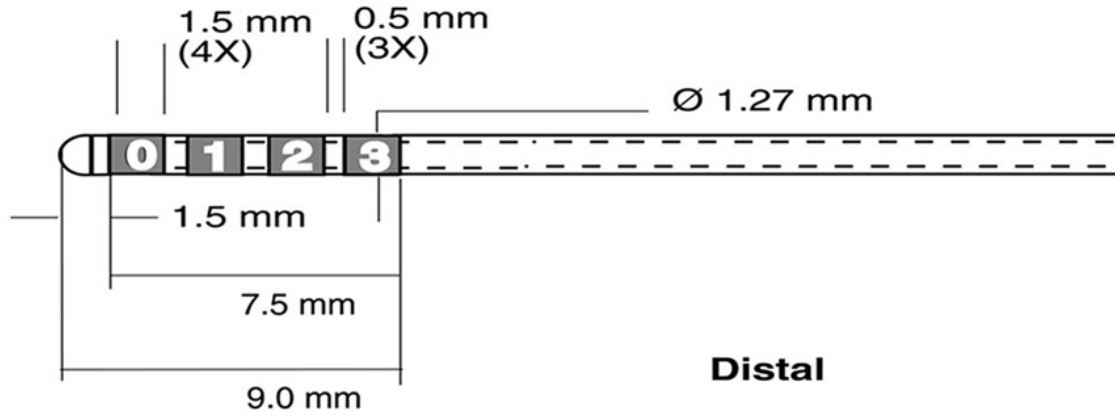


Figure 3.7: Schematic representation of DBS lead model #3389 by Medtronic, Inc. The four platinum-iridium contacts are indicated with numbers from 0 (the most caudal) to 3 (the most rostral). Distances and size of the components are expressed in millimeters. Reproduced from Darvas and Hebb [2014].

Low beta	High beta	Gamma	HFO
12-20 Hz	21-35 Hz	60-90 Hz	150-450 Hz

Table 3.1: Definition of frequency bands.

3.3 Data analysis

3.3.1 Definitions, Common Parameters, and Measures

The frequency bands of interest in the data analysis are defined in Table 3.1.

Other quantities are indicated as follows:

- f_{LB} is the frequency corresponding to the maximum of spectral power in the low beta range (low beta peak);

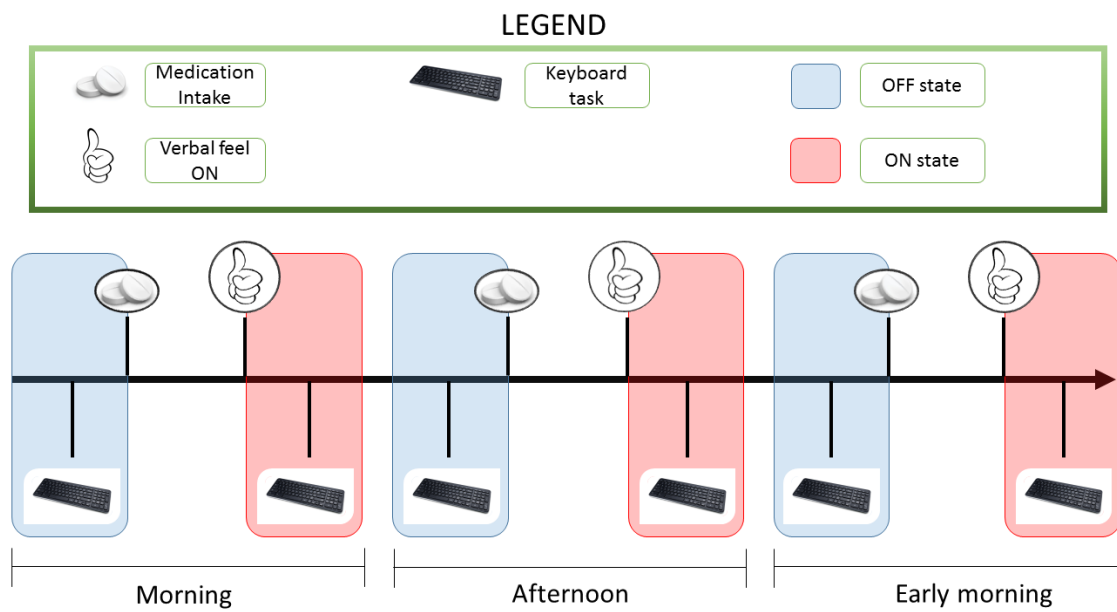


Figure 3.8: Experimental protocol (motor part). The thick arrow represents the flow of time. The recordings start before the first “OFF” state and end after the last “ON” state. A 120 s long resting period is included in each state.

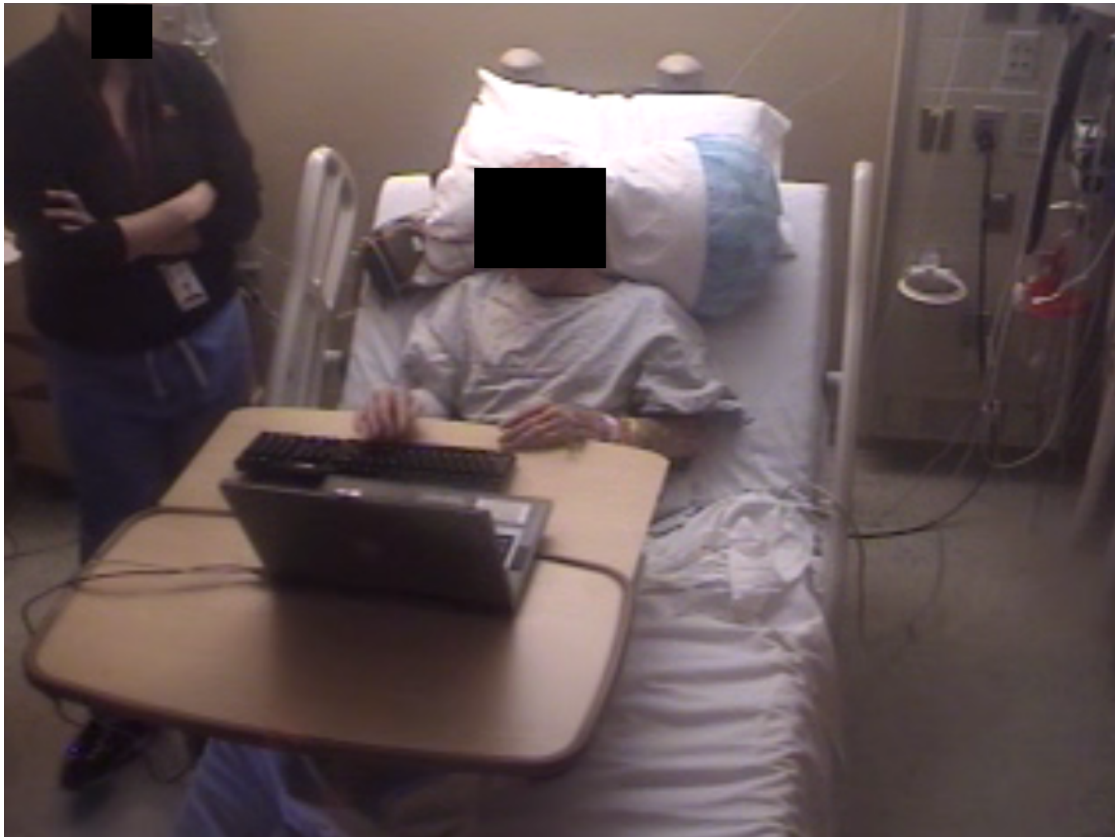


Figure 3.9: Room setup for the long-term recordings. In this screenshot, the patient is engaged in the keyboard tapping task, assisted by a nurse.

- f_γ is the frequency corresponding to the maximum of spectral power in the gamma range (gamma peak);
- HFO frequency region presents two different activities depending on the clinical condition, but it's difficult to clearly separate them since they overlap extensively (section 2.3.1). f_{HFO}^{off} indicates the frequency corresponding to the maximum of spectral power in the HFO range detected in the unmedicated state (“OFF” HFO peak), whereas f_{HFO}^{on} represent the same quantity but detected in the medicated state (“ON” HFO peak);
- indicated with \hat{S}_f the power spectral density of the signal, the low beta peak power was computed as:

$$P_{LB} = \sum_{f=f_{LB}-2}^{f_{LB}+2} \hat{S}_f(f) \quad (3.30)$$

- indicated with $P_{12:35}$ the sum of the power spectral density of the signal \hat{S}_f from 12 to 35 Hz (beta band), the low beta peak relative power was computed as:

$$P_{LB}^N = \frac{P_{LB}}{P_{12:35}} \quad (3.31)$$

- the gamma peak power was computed as:

$$P_\gamma = \sum_{f=f_\gamma-2}^{f_\gamma+2} \hat{S}_f(f) \quad (3.32)$$

- indicated with $P_{60:90}$ the sum of the power spectral density of the signal \hat{S}_f from 60 to 90 Hz (the gamma range), the gamma peak relative power was computed as:

$$P_{\gamma}^N = \frac{P_{\gamma}}{P_{60:90}} \quad (3.33)$$

- the HFO peak power was computed as:

$$P_{HFO} = \sum_{f=f_{HFO}-24}^{f_{HFO}+24} \hat{S}_f(f_{HFO}) \quad (3.34)$$

- indicated with $P_{150:450}$ the sum of the power spectral density of the signal \hat{S}_f from 150 to 450 Hz (the HFO range), the HFO peak relative power was computed as:

$$P_{HFO}^N = \frac{P_{HFO}}{P_{150:450}} \quad (3.35)$$

The power in the low beta and gamma peak bands was calculated in a frequency range of 5 Hz centered on the peak frequency because the relative peaks are narrow. On the other side, the HFO activity is broadband in both “OFF” and “ON” states so a frequency range of 50 Hz has been chosen.

The normalization of the peak powers was performed in order to decrease the inter-subject and intra-subject variability in terms of power associated to the signals.

3.3.2 Pre-processing

All the analysis performed on the LFP signals were done offline, using the software MATLAB version R2015a (Mathwork, Natick, Massachusetts), using custom scripts after pre-processing of the data. Pre-processing included a transformation of the reference and filtering.

3.3.2.1 Re-referencing

The four monopolar signals, indicated as LFP 0, LFP 1, LFP 2, and LFP 3, were re-referenced in three bipolar derivations by subtracting the activity of adjacent contact, indicated as LFP 0-1, LFP 1-2, and LFP 2-3. The re-referencing was performed in order to increase the spatial resolution and remove part of the correlated activity of the signals.

3.3.2.2 Filtering

After re-referencing, each of the three bipolar LFP were filtered with a high pass filter at 2 Hz using a second-order Butterworth IIR filter (Fig. 3.10) in conjunction with zero phase filtering technique. The same principle was applied while using eight fourth-order Butterworth IIR notch filters (Fig. 3.11) to remove power line artifacts at 60 Hz and harmonics up to 480 Hz. The whole pre-processing stage is shown in Fig. 3.12.

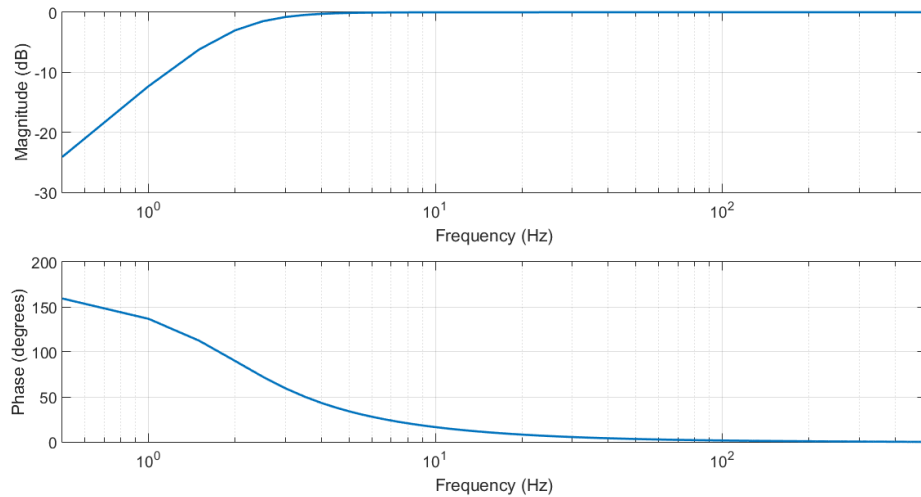


Figure 3.10: Magnitude and phase responses of the high pass filter applied to the data. The phase response is shown just for clarity, since the nonlinear behavior represented is not maintained when using zero phase filtering techniques.

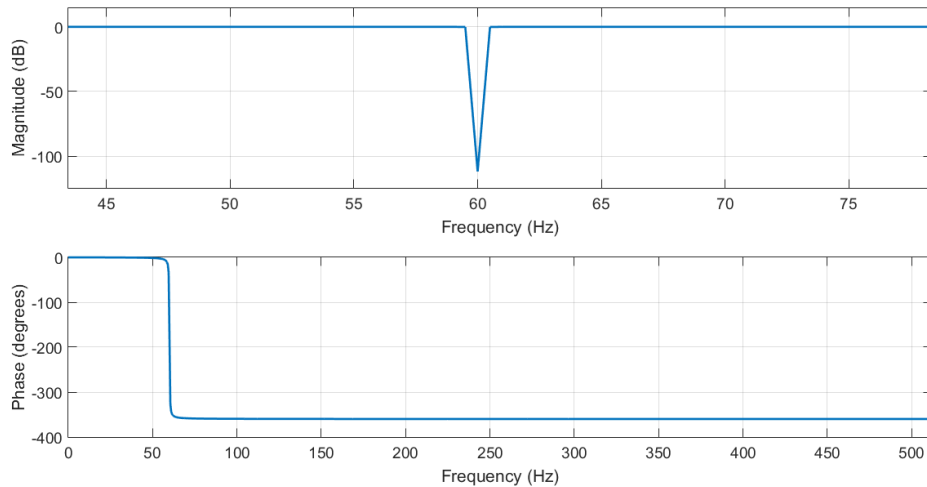


Figure 3.11: Example of notch filter applied to the data stopping the oscillations at 60 Hz. The considerations on the phase are the same as Fig. 3.10.

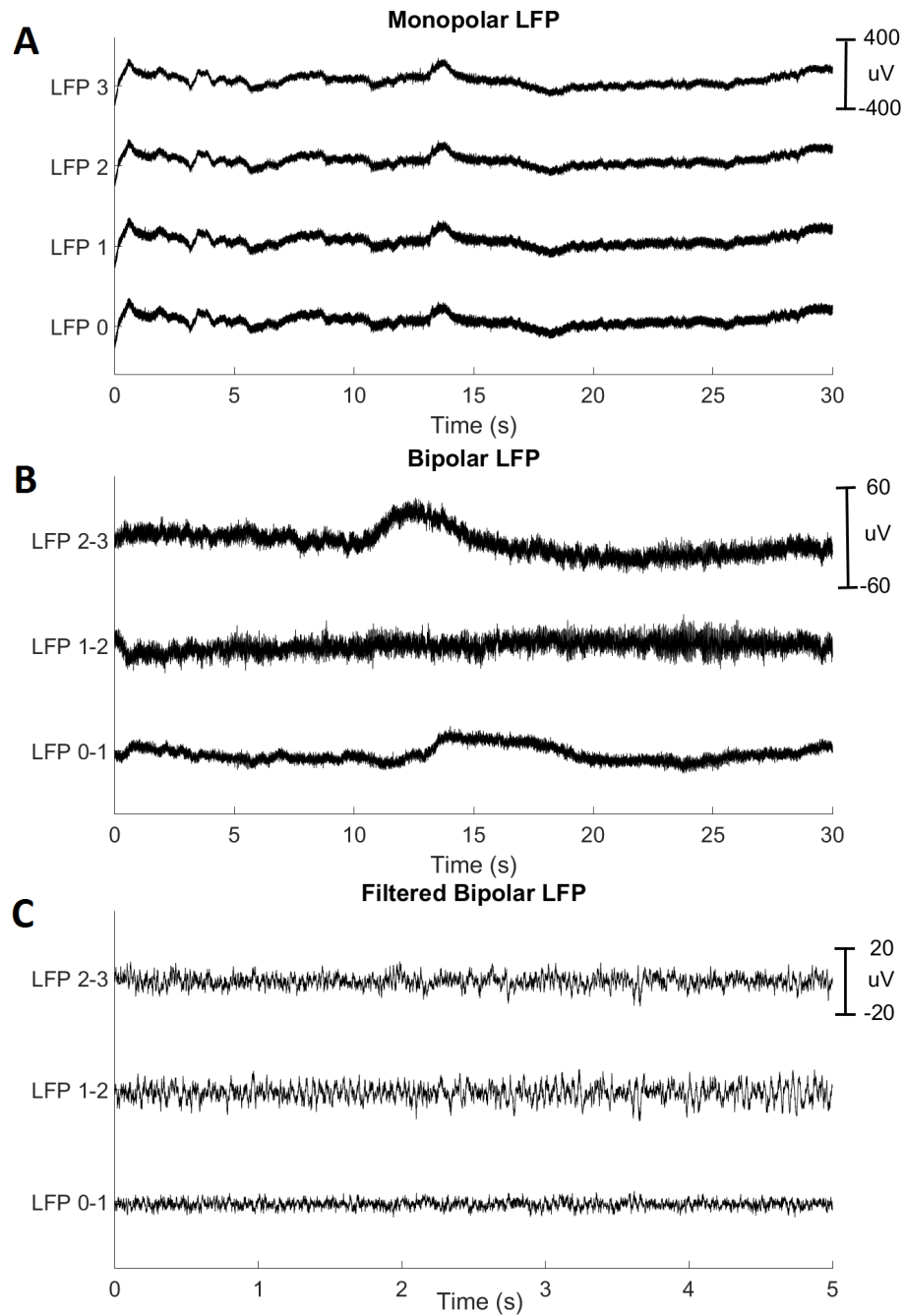


Figure 3.12: Pre-processing of the LFP data. Raw monopolar derivations (A) were transformed in bipolar references (B) that were sequentially filtered using eight notch filters and a high pass filter (C). Note that signals in different plots have different amplitude scales.

3.3.3 Rest Analysis

The rest analysis refers to the analysis of the signals recorded when the patients were in resting condition, meaning that no other tasks (motor or cognitive) were performed. Continuous LFP data 120 s long were extracted for each state (three “OFF” and three “ON”) for every patient and visually inspected to detect clear artifacts that, if present, were removed. The rest analysis focused on the characterization of the LFP activity in terms of spatial distribution of spectral power across the subthalamic nucleus, phase-amplitude coupling and its spatial distribution, and correlation with clinical scores.

3.3.3.1 Spatial Distribution of Spectral Activity

Spatial information about the localization of STN LFP sources of activity can be retrieved by analyzing the spectral power distribution across the three bipolar derivations LFP 0-1, LFP 1-2, and LFP 2-3. They are defined in such a way that they represent the localized activity in the bottom, intermediate, and top of the STN respectively. Since the STN is anatomically divided into three areas with different functionality, non-homogeneous distribution in spectral power in specific bands may provide clues about the role of certain rhythms expressed by the neuronal populations in the structure. The spatial characterization interested both the “OFF” and “ON” states but with different features.

“OFF” State The LFP data recorded during the “OFF” states were divided into three groups based on their spatial provenience: bottom, intermediate, or top STN. For each signal, the power spectrum was computed using the Welch’s modified periodogram with 1024 samples long Hanning windows and 50% overlap, to get a frequency resolution of 1 Hz. The frequencies f_{LB} and f_{HFO}^{off} were detected as the frequency corresponding to the maximum activity in low beta and HFO range. If present in at least one of the three bipolar LFP for each resting period considered, the low beta peak relative power P_{LB}^N and HFO peak relative power P_{HFO}^N were computed for all bipolar derivations. Group-wise statistical analysis followed to investigate the spatial distribution of low beta and HFO activity in the unmedicated state among patients.

“ON” State The LFP data recorded during the “ON” states were divided into three groups based on their spatial provenience: bottom, intermediate, or top STN. For each signal, the power spectrum was computed using the Welch’s modified periodogram with 1024 samples long Hanning windows and 50% overlap, to get a frequency resolution of 1 Hz. The frequencies f_{γ} and f_{HFO}^{on} were detected as the frequency corresponding to the maximum activity in low beta and HFO range. If present in at least one of the three bipolar derivations for each resting period considered, the gamma peak relative power P_{γ}^N and HFO peak relative power P_{HFO}^N were

computed for all bipolar LFPs. Group-wise statistical analysis followed to investigate the spatial distribution of gamma and HFO activity in the unmedicated state among patients.

3.3.3.2 Phase-Amplitude Coupling Analysis

This analysis aimed to investigate the presence and spatial distribution of nonlinear cross-frequency interactions in terms of phase-amplitude coupling in the unmedicated and medicated states. It has already been shown [Lopez-Azcarate et al., 2010] that phase-amplitude coupling may be a pathological mechanism for PD since it is present only in untreated condition; however another study also reported its presence in medicated state, although in different frequency regions [Ozkurt et al., 2011]. Also, little is known about its topological distribution across STN or about the localization of rhythms that produce the coupling.

The signals were first divided in two groups depending on whether they were recorded during the “OFF” or “ON” state. As described in section 3.2, for each patient, three “OFF” states and three “ON” states were available. For each of these states, the three bipolar derivation signals were processed together. In particular, a set of nine comodulograms was computed combining the phase frequencies and amplitude frequencies extracted from all bipolar LFPs. For example, one comodulogram was computed combining the phase frequencies of LFP 0-1 with the amplitude

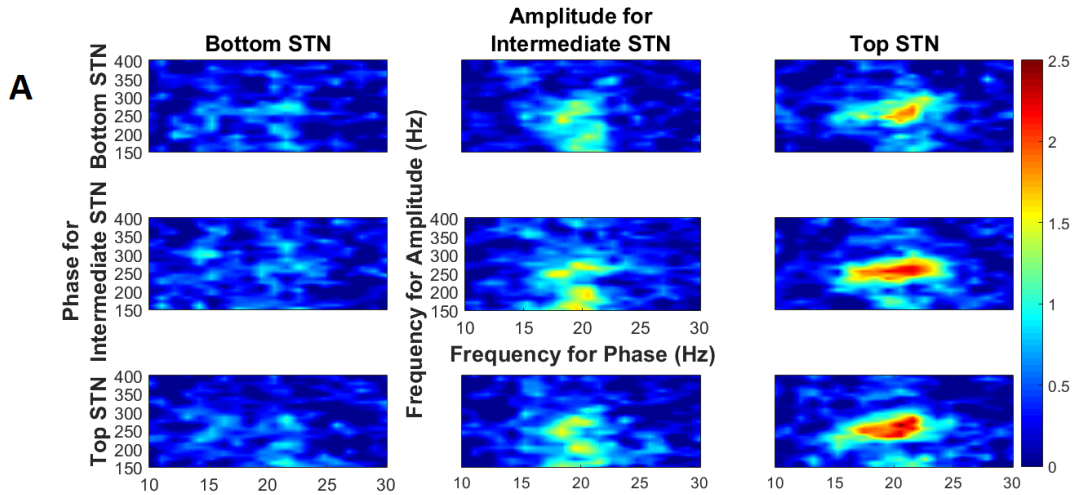


Figure 3.13: The set of nine comodulograms computed in each condition was obtained combining the provenience of phase and amplitude frequencies across the three bipolar derivations. Every comodulogram has axis as shown in the middle one.

frequencies of LFP 0-1, another comodulogram with the phase frequencies of LFP 0-1 again and the amplitude frequencies of LFP 1-2 and so on, for a total of nine combinations (Fig. 3.13).

It resulted that for each patient a triplet of nine comodulograms was available for the “OFF” as well as the “ON” states; the comodulograms belonging to the triplet were averaged for each combination of phase and amplitude frequencies locations. In total, for each patient two sets of nine comodulograms were obtained, one describing the “OFF” state and one the “ON” state (Fig. 3.14), that were then averaged across patients. The comodulograms were computed using the *MLV*, *CV* and *PLV* methods in parallel. In all cases, the phase frequencies ranged from 10 to 30 Hz divided into bins of 1 Hz each (filtering the signal forward-backward with Butterworth filters

of third order and 2 Hz bandwidth centered in the lower frequency of each bin), whereas the amplitude frequencies ranged from 150 to 400 Hz divided in intervals of 10 Hz (filtering forward-backward the signal with Butterworth filters of third order and 50 Hz bandwidth centered in the lower frequency of each bin). For the *CV* measure, the magnitude squared coherence was computed with Hanning windows 2048 samples long and 50% overlap. Experimental PAC measures were standardized with the mean and standard deviation of the 100 surrogates PAC values generated for each (f_ϕ, f_A) combination.

A visual comparison of the sets of comodulograms obtained was made to clarify the presence of phase-amplitude coupling and the difference in the quantification of the nonlinear interaction when three different measures are used.

3.3.3.3 Correlation of Power Spectral Changes with Clinical Scores

The correlation analysis served as control to check, accordingly to many works in the literature, that features extracted from STN LFP correlate with the severity of motor clinical symptoms. These are quantified by the UPDRS III (mUPDRS) as the sum of the scores in the categories bradykinesia and rigidity.

For each medication intake, LFP data and mUPDRS are available regarding the “OFF” period prior to medication and the “ON” period after the medication had effect on the symptoms of the patient. The LFP activity to correlate with the clinical scores

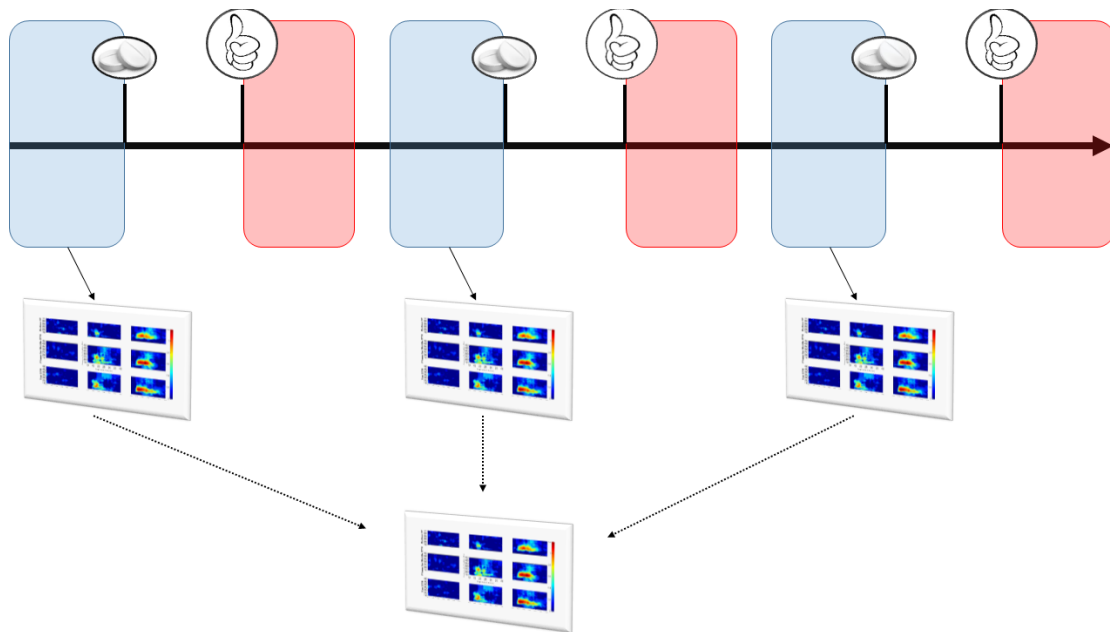


Figure 3.14: Work flow for the generation of PAC maps. The legend of symbols is shown in Fig. 3.8. In each state, a set of nine comodulograms was computed from the combination of phase and amplitude frequencies of the three bipolar derivations LFP 0-1, LFP 1-2, LFP 2-3. Then, the comodulograms corresponding to the same combination are averaged to create a single set of comodulograms describing a condition for each patient (“OFF” or “ON” state). In the figure, only the mechanism for “OFF” state is shown, but the same work flow applies for the “ON” state as well.

was measured in terms of band power, namely low beta and “ON” state HFO. The low beta and HFO peaks used in this analysis were previously detected in section 3.3.3.1. To correlate the spectral LFP activity and the clinical scores in the form of mUPDRS testing, percent power and scores changes compared to a baseline were used. In particular, given that P_{LB}^{off} is the power of low beta peak in the “OFF” condition and P_{LB}^{on} is the power of low beta peak in the “ON” state, the percent variation of low beta peak power is:

$$P_{LB}^{\%} = 100 \frac{P_{LB}^{on} - P_{LB}^{off}}{P_{LB}^{off}}, \quad (3.36)$$

where the baseline is P_{LB}^{off} . The same percent power variation was computed for the HFO peak around f_{HFO}^{on} . Similarly, if the mUPDRS score in “OFF” state is $mUPDRS^{off}$ and in “ON” state is $mUPDRS^{on}$, the percent variation of mUPDRS is:

$$mUPDRS^{\%} = 100 \frac{mUPDRS^{on} - mUPDRS^{off}}{mUPDRS^{off}} \quad (3.37)$$

It is clear that a negative percent variation of power or mUPDRS score means that the spectral power or mUPDRS score computed in the “OFF” state is higher than in the “ON” state, whereas a positive percent variation has the exact opposite meaning.

The values of $P_{LB}^{\%}, P_{HFO}^{\%}$ (where P_{HFO} is the power around f_{HFO}^{on}) and $mUPDRS^{\%}$

were used for the correlation analysis.

3.3.4 Off-to-On Transition Analysis

The off-to-on transition analysis refers to the quantitative description of the power spectral changes that take place from the medication intake to the clinical “ON” state.

Continuous LFP data were extracted starting from 30 minutes prior to the medication until 30 minutes after the verbal feel “ON”, for a total of 90 signals after pre-processing (three bipolar derivations for each of the three transitions per subject, which were ten). Each signal was divided in non-overlapping segments of 60 seconds. After segmentation, signals were visually inspected to detect clear artifacts that, if present, were removed. For each segment the power spectral density was computed using the Welch’s modified periodogram with 1024 samples long Hanning windows and 50% overlap, to get a frequency resolution of 1 Hz.

The choice of performing a segmentation of the entire off-to-on transition signal rested on the consideration that, in such a long interval, the parameter of interest is the slow variation of the spectral power in time due to the medication intake. Therefore, it is not necessary to compute a spectrogram of the entire signal, as is commonly used to visualize and quantify relatively fast variation of power among frequency components. Moreover, the choice of 60 second segments allowed a reliable

estimation of the power spectrum with the specifications aforementioned, even when part of the signal was removed due to noise that heavily afflicted the recordings, since in such a long recording period the patients were able to do a number of different activities that could give rise to artifacts in the signals.

The visual output of the processing is, for each transition and bipolar LFP, a time-frequency map where the time resolution Δt (in the horizontal axis) is 60 s and the frequency resolution Δf (vertical axis) is 1 Hz.

Timing of Spectral Changes The only parameter of interest in the off-to-on transition analysis is the time corresponding to significant spectral changes. Several studies (section 2.3.1) described the amount of variation in spectral components from the “OFF” to the “ON” state, but so far no studies attempted to quantify when, after the medication, they happen. Temporal changes were quantified for the low beta, gamma, and “ON” HFO bands. The frequencies f_{LB} , f_{γ} , and f_{HFO}^{on} were previously detected in section 3.3.3.1. For each segment of the off-to-on transition, the peak powers of low beta, gamma, and “ON” state HFO were computed and indicated with $P_{LB}(n)$, $P_{\gamma}(n)$, $P_{HFO}(n)$, with n the progressive number of segments. The average “OFF” state peak powers were calculated as the average of the peak powers for each band in the thirty minutes prior to the medication and indicated as P_{LB}^{off} , P_{γ}^{off} , and P_{HFO}^{off} . Then, three time series were constructed normalizing the peak powers in the

three bands in each segment of the transition with respect to the baseline “OFF” power values:

$$P\%(n) = 100 \frac{P(n) - P^{off}}{P^{off}} \quad (3.38)$$

for each of the three bands low beta, gamma, and “OFF” HFO, to get $P_{LB}\%(n)$, $P_{\gamma}\%(n)$, and $P_{HFO}\%(n)$. Finally, the time points n_{LB} , n_{γ} and n_{HFO} corresponding to significant changes in the spectral power of the three bands were calculated as the closest point whose value $P\%(n)$ was half of the maximum absolute value of $P\%(n)$ in the corresponding band. This process was performed in case that the power suppression or increase in the band was greater than 30% in absolute value; otherwise, no time points were computed for that particular band since it didn’t show any significant increase or decrease in power.

Statistical analysis followed to investigate differences in the time of significant spectral changes between power bands (low beta, gamma, and “ON” state HFO) and/or location in the STN (determined by the bipolar pairs).

3.3.5 Movement Analysis

The movement analysis was performed to investigate correlation of power spectral changes in specific bands with sensory data and changes of phase-amplitude coupling caused by the movement execution. Continuous LFP data were extracted from ten

seconds prior to task beginning until ten seconds after task end; signals were extracted for each bipolar LFP, clinical state (“OFF” and “ON”), and task repetition, for a total of 360 signals after pre-processing.

3.3.5.1 Correlation of Power Spectral Changes with Sensory Data

Using the peak frequencies f_{LB} and f_{HFO}^{on} , previously detected in section 3.3.3.1, the peak power of the corresponding bands was computed in the signals segments when the task is executed (using Welch’s modified periodogram with 1024 samples long Hanning windows and 50% overlap). The band powers were then averaged for the repetitions in the same state. The percent change of the power computed for the “ON” state was calculated with respect to the power in the “OFF” state relative to the task execution taking place before the particular medication intake. Similarly, the number of key presses was averaged within repetitions and the percent change of number of key presses in the “ON” state was computed with respect to the one obtained in the “OFF” state for each medication intake. Then, the correlation between the percent change of power in the two bands and percent change of number of key presses was computed. This process was done for every bipolar LFP.

3.3.5.2 Phase-Amplitude Coupling Analysis

The bipolar LFP pair with stronger coupling activity was detected from the analysis in section 3.3.3.2. The phase-amplitude coupling comodulograms were computed in the ten seconds prior to task beginning and in the thirty seconds of task execution. The comodulograms were computed using the *MLV* measure. The phase frequencies ranged from 10 to 40 Hz and were divided in bins of 1 Hz each (filtering the signal forward-backward with Butterworth filters of third-order and 2 Hz bandwidth centered in the lower frequency of each bin), whereas the amplitude frequencies ranged from 150 to 450 Hz divided in intervals of 5 Hz (filtering the signal forward-backward with Butterworth filters of third order and 25 Hz bandwidth centered in the lower frequency of each bin). Comodulograms were averaged within the “OFF” and “ON” conditions, and then compared to detect phase-amplitude coupling changes between rest state and movement execution in unmedicated or medicated conditions. Experimental PAC measures were standardized with mean and standard deviation of the 100 surrogates PAC values generated for each (f_{Φ}, f_A) combination.

Spectrograms were also computed for the bipolar derivations showing stronger coupling using 1024 samples long Hanning windows with 768 samples of overlap, to visualize the spectral activity during rest and movement execution. Spectrograms were then averaged within conditions (“OFF” and “ON”) across subjects and then visually compared to detect modulation patterns.

Chapter 4

Results

4.1 Rest Analysis

4.1.1 Spatial Distribution of Spectral Activity

“OFF” State Signals related to patient 7 were discarded after visual inspection of their power spectrum because of the high amount of artifacts. Low beta peaks at 17.4 ± 1.71 Hz were found in all the remaining 9 patients. The spatial distribution of low beta peak power across STN is shown in Fig. 4.1. Visually it’s possible to notice that there aren’t significant differences in the power spatial localization, a result confirmed by a Kruskal-Wallis test ($\alpha = 0.05$) which returned a p-value of 0.7794. Non-parametric analysis was performed because the groups showed distributions different from the Gaussian. Three Kolmogorov-Smirnov tests returned a

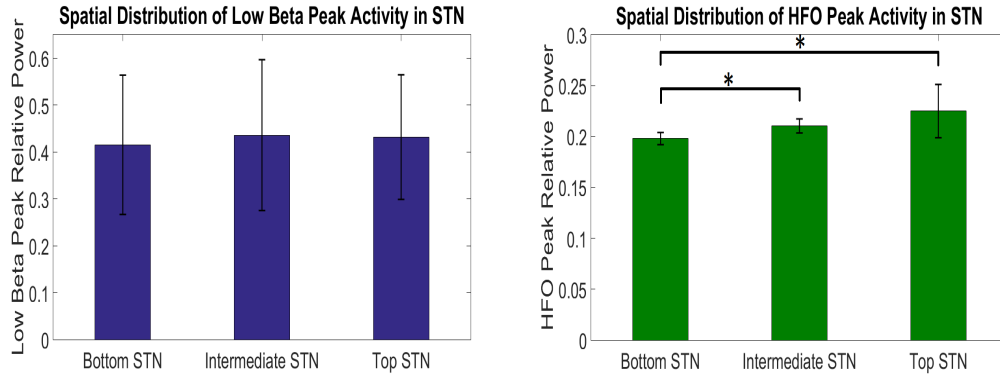


Figure 4.1: Spatial distribution of low beta peak activity (left) and “OFF” state HFO activity (right) across the subthalamic nucleus. The bottom STN is corresponding to the bipolar derivation LFP 0-1, intermediate STN to LFP 1-2 and top STN to LFP 2-3. Asterisks represent significant statistical differences in the distribution of spectral power.

p-value smaller than 0.05 in all cases.

“OFF” state HFO peaks at 238 ± 9.88 Hz were detected in at least one bipolar configuration in 8 patients out of 9. The spatial distribution of low beta peak power across STN is shown in Fig 4.1. The groups didn’t show normal distribution (Kolmogorov-Smirnov tests, p-value < 0.05), and the Kruskal-Wallis ($\alpha = 0.05$) test returned a p-value of $1.67 \cdot 10^{-7}$, meaning that there are significant differences in the spatial distribution of HFO power. Subsequent tests (Mann-Whitney U , with $\alpha = 0.05$), showed that the HFO relative power in middle and top STN is significantly different from the one in the bottom (p-values $1.47 \cdot 10^{-6}$ and $3.67 \cdot 10^{-6}$).

“ON” State Gamma peaks at 78.25 ± 2.63 Hz were found in 4 patients out of 9 in the “ON” state signals. Kruskal-Wallis test ($\alpha = 0.05$) returned a p-value of

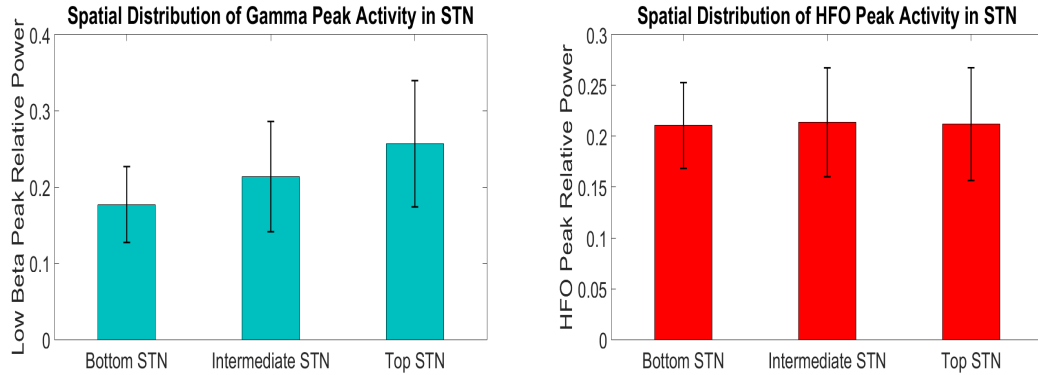


Figure 4.2: Spatial distribution of gamma and “ON” state HFO activity across STN.

0.07 which, with the significance level chosen, means that there are no statistical differences in the distribution of gamma power activity across STN (Fig. 4.2). Even though the distributions seem to be visually different, statistical testing did not confirm this observation, probably due to the small sample size.

“ON” state HFO peaks at 314.25 ± 31.19 were found in 8 patients out of 9. Kruskal-Wallis test with $\alpha = 0.05$ showed a p-value of 0.9119, making it clear that in the dataset the distribution of HFO spectral activity in the medicated state is uniform across the subthalamic nucleus (Fig. 4.2).

4.1.2 Phase-Amplitude Coupling Analysis

4.1.2.1 Mean Vector Length

The analysis of phase-amplitude coupling across bipolar derivations showed the presence of clear nonlinear cross-frequency interactions in unmedicated condition, which

disappeared after effective drug treatment (average coupling maps Fig. 4.3). Accordingly with the results shown in section 4.1.1, the PAC is stronger when the amplitude frequencies are extracted from the top and intermediate STN bipolar derivations, where the highest amount of “OFF” state HFO power was detected. Interestingly, the cross-frequency coupling is shown not only when combining amplitude and phase frequencies that belong to the same bipolar derivation, but also (and with similar strength) when, fixing the location of the amplitude frequencies, the phase frequencies are taken from bipolar pairs all over the STN. This is again coherent with the results shown previously, since the stronger coupling happens in the beta range (as phase frequencies), and it has been demonstrated that the low beta activity was widely distributed in the STN.

The frequency ranges showing coupling were 15-25 Hz for phase frequencies and 200-300 Hz for amplitude frequencies.

Comodulograms relative to a single subject are shown in Fig. 3.1. The PAC amplitude coupling is more localized compared to the average maps.

4.1.2.2 Coherence Value

The considerations expressed in section 4.1.2.1 hold when using the *CV* to compute the phase-amplitude coupling comodulograms and evaluate its spatial distribution (Fig. 4.5). The cross-frequency coupling is stronger when combining the amplitude

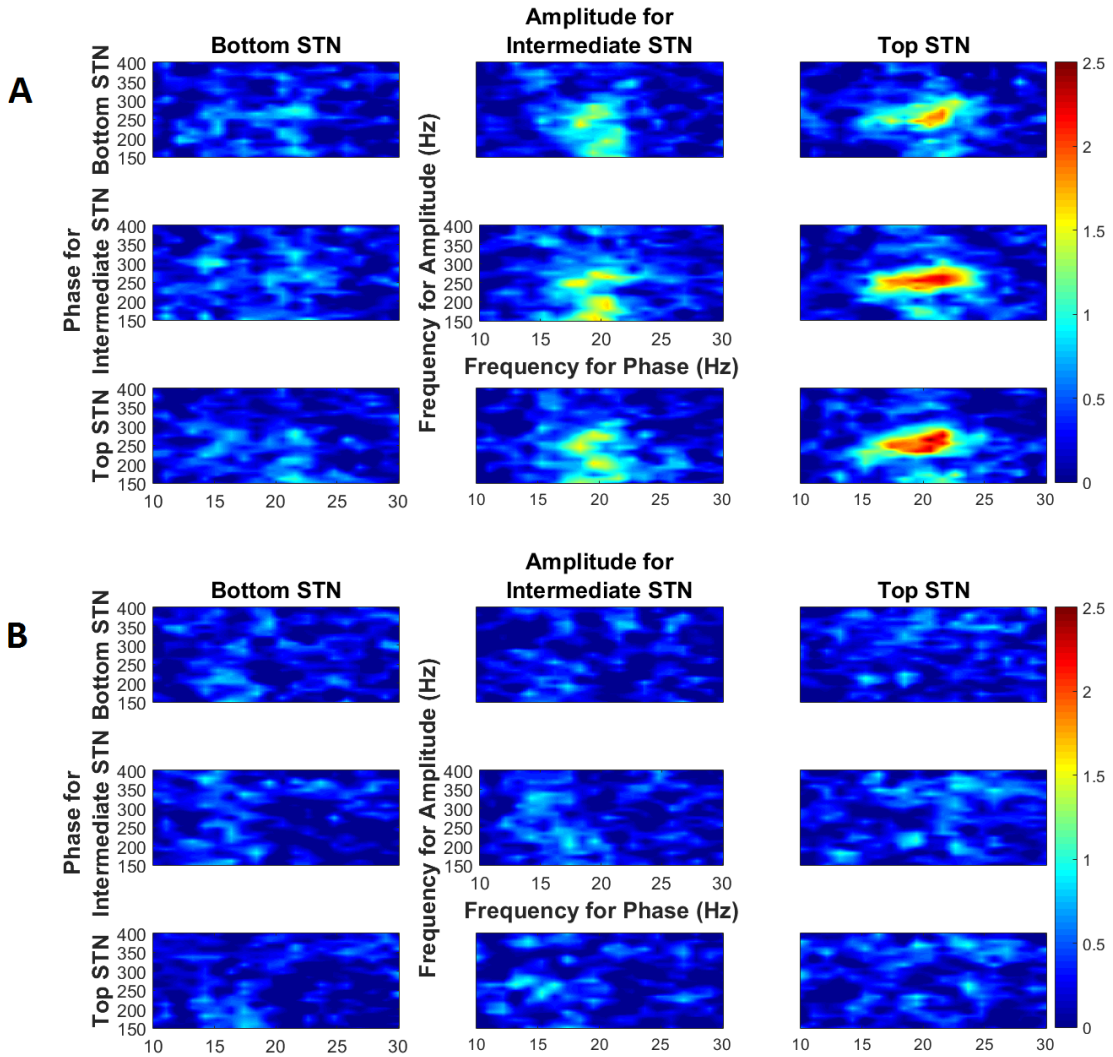


Figure 4.3: Spatial distribution of phase-amplitude coupling in STN in untreated (A) and medicated condition (B) using *MVL*. Hotter color is associated with stronger coupling.

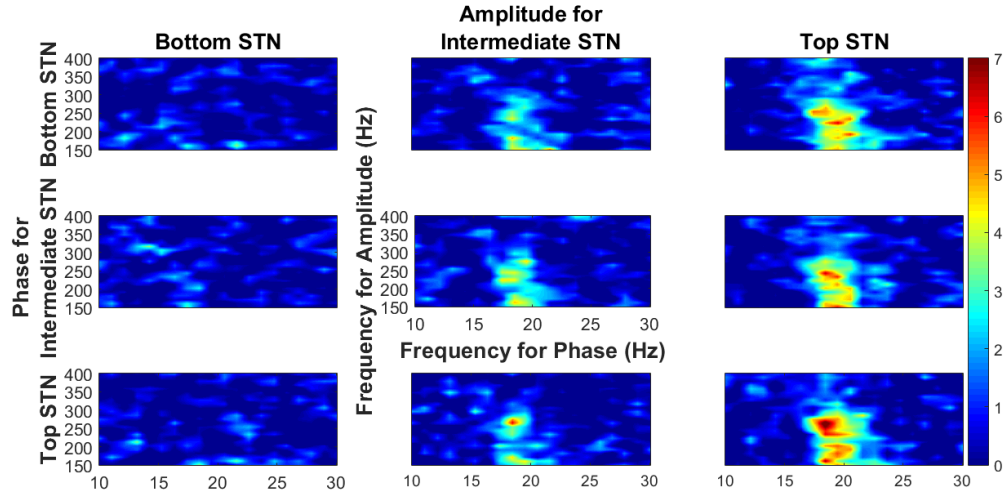


Figure 4.4: Example of spatial distribution of phase-amplitude coupling in “OFF” state for a representative patient. The ranges of phase and amplitude frequencies where PAC occur are more localized compared to the average maps.

frequencies extracted from LFP 2-3 (top STN) with the phase frequencies of all other bipolar pairs.

The frequencies ranges showing coupling were 17-25 Hz for phase frequencies and 200-350 Hz for amplitude frequencies. A qualitative comparison with the comodulograms computed using the *MVL* method shows that the regions with strong coupling in the *CV* maps are smaller but of greater normalized intensity.

4.1.3 Phase-Locking Value

The spatial distribution of comodulograms computed with the phase-locking value showed again the pattern described for the other two cross-frequency coupling measures. In this case, the coupling occurred between 15-25 Hz as phase frequencies and

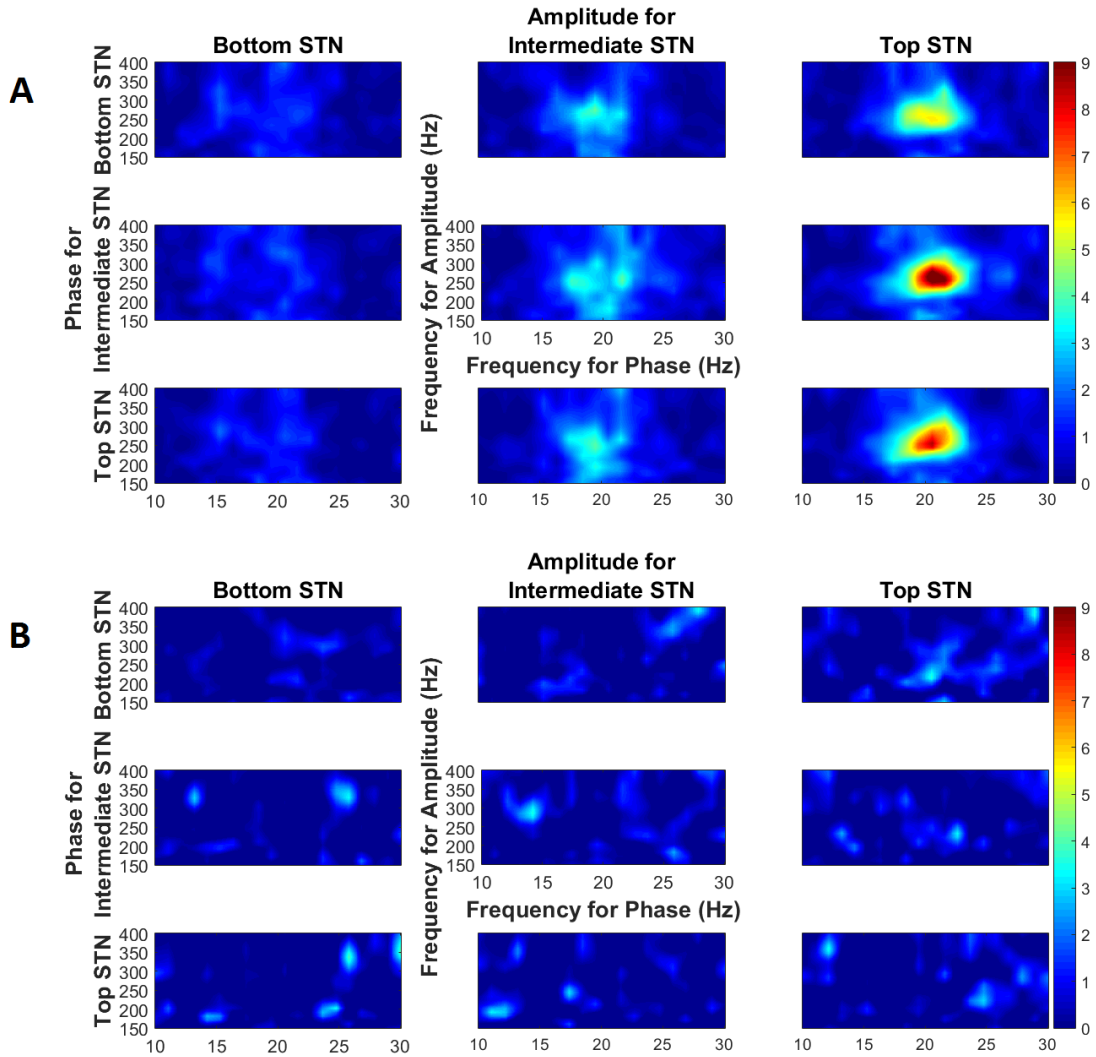


Figure 4.5: Spatial distribution of phase-amplitude coupling in STN in unmedicated (A) and treated condition (B) using *CV* method. Hotter color is associated with stronger coupling.

	LFP 0-1	LFP 1-2	LFP 2-3
Low Beta Peak	0.61	0.49	0.66
HFO	-0.16	-0.26	-0.10

Table 4.1: Correlations of low beta peak power changes with mUPDRS score changes between unmedicated and medicated states. In bold the significant correlations.

225-300 Hz as amplitude frequencies.

4.1.4 Correlation of Power Spectral Changes with Clinical Scores

Percent low beta peak power change between “OFF” and “ON” resting states showed significant correlation with percent mUPDRS score change in the two clinical conditions, while “ON” state HFO power changes did not show significant correlation (Table 4.1 and Fig. 4.7).

4.2 Off-to-On Transition Analysis

Data relative to patient 7 were discarded due to the high amount of artifacts. A significant change in power between unmedicated and medicated conditions was found in all bipolar derivations in 17 out of 27 off-to-on transitions for low beta peak band, in 13 out of 27 for “ON” state HFO, and 8 out of 27 for gamma peak band. Kruskal-Wallis testing showed the presence of significant differences in the timing of power changes in the three bands (p-value $3.88 \cdot 10^{-7}$). Further tests (Mann-Whitney U)

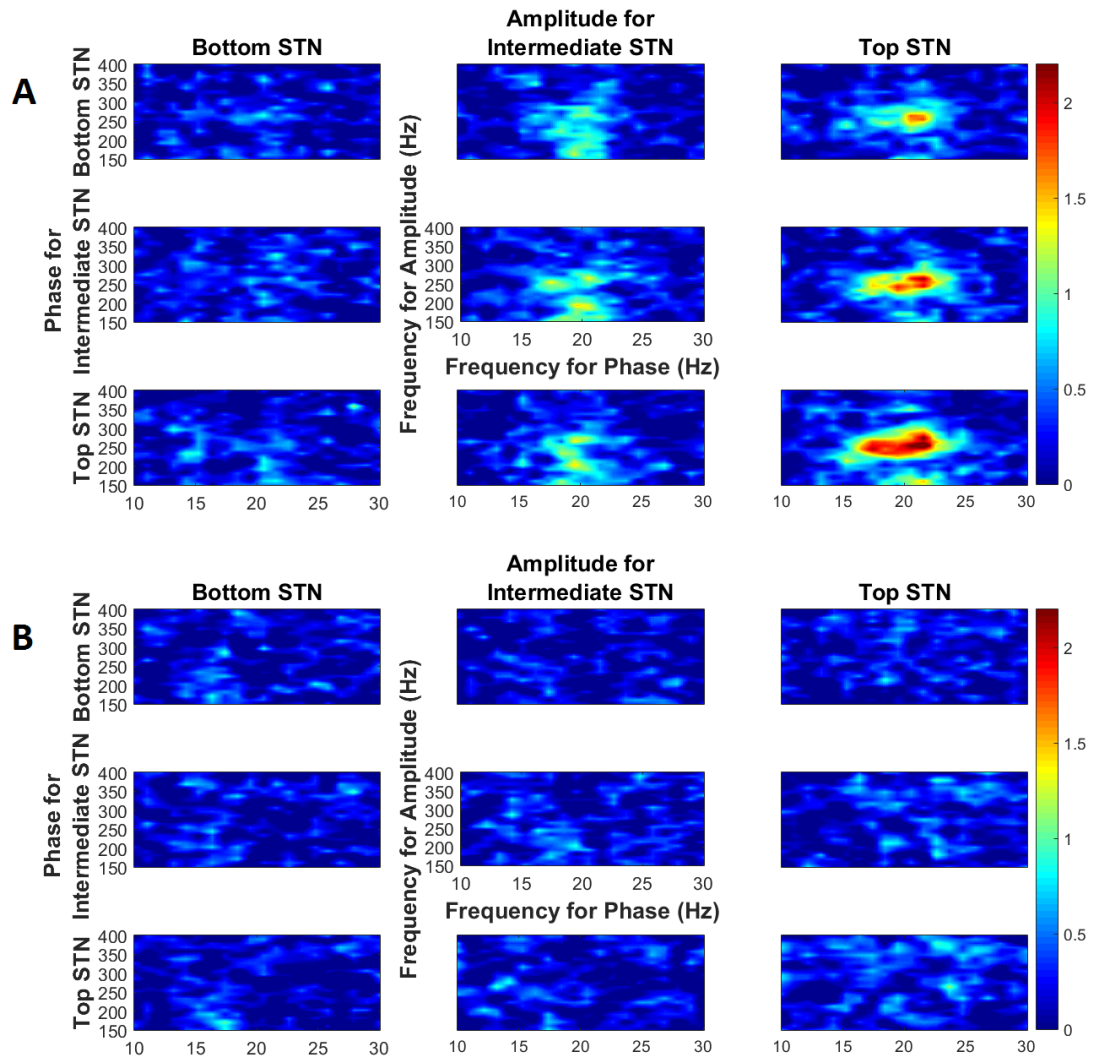


Figure 4.6: Spatial distribution of phase-amplitude coupling in STN in unmedicated (A) and treated condition (B) using *PLV* method. Hotter color is associated with stronger coupling.

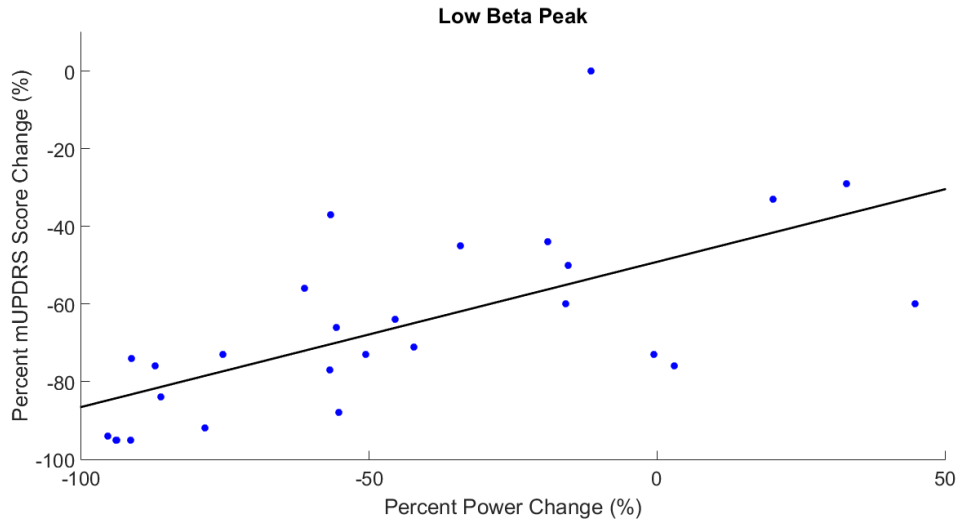


Figure 4.7: Scatter plot showing the correlation of low beta peak power change in LFP 2-3 (top STN) with mUPDRS score change between unmedicated and medicated conditions. The thick line represents the regression line.

	Low Beta VS Gamma	Low Beta VS HFO	Gamma VS HFO
LFP 0-1	$1.45 \cdot 10^{-4}$	$5.21 \cdot 10^{-4}$	> 0.05
LFP 1-2	$1.16 \cdot 10^{-4}$	$4.21 \cdot 10^{-4}$	> 0.05
LFP 2 -3	$1.17 \cdot 10^{-4}$	$2.98 \cdot 10^{-4}$	> 0.05

Table 4.2: P-values of tests comparing the timings of changes between low beta, gamma and “ON” state HFO peak powers.

showed a significant difference in the time of change of low beta peak power compared to the times of change of gamma peak power and “ON” state HFO power, that was consistent among bipolar derivation (Tab. 4.2 and Fig. 4.8 A). On average, the low beta peak power suppression happened 21 minutes before the HFO power rise and 25.9 minutes before the gamma peak power rise.

Fig. 4.8 B shows the power changes in the considered bands following levodopa medication. The time-frequency maps in two representative off-to-on transitions

	LFP 0-1	LFP 1-2	LFP 2-3
Low Beta Peak	-0.48	-0.49	-0.34
HFO	0.35	0.62	0.35

Table 4.3: Correlations of low beta peak power changes with mUPDRS score changes between unmedicated and medicated states. In bold the significant correlations.

depicting the behavior in the higher and lower frequencies are shown in Fig. 4.9.

4.3 Movement Analysis

Data relative to patient 7 were discarded due to the high amount of artifacts and data relative to patient 10 were not considered in the correlation between “ON” state HFO power change and improvement in the task execution because they represented outliers (the power changes were greater than 400%).

4.3.1 Correlation of Power Spectral Changes with Sensory Data

Percent low beta peak power change between “OFF” and “ON” states showed significant correlation with the percent change of number of keyboard presses in the two clinical conditions during task execution. The “ON” state HFO percent power change showed significant correlation only in one bipolar derivation, LFP 1-2 (Tab. 4.3 and Fig. 4.10).

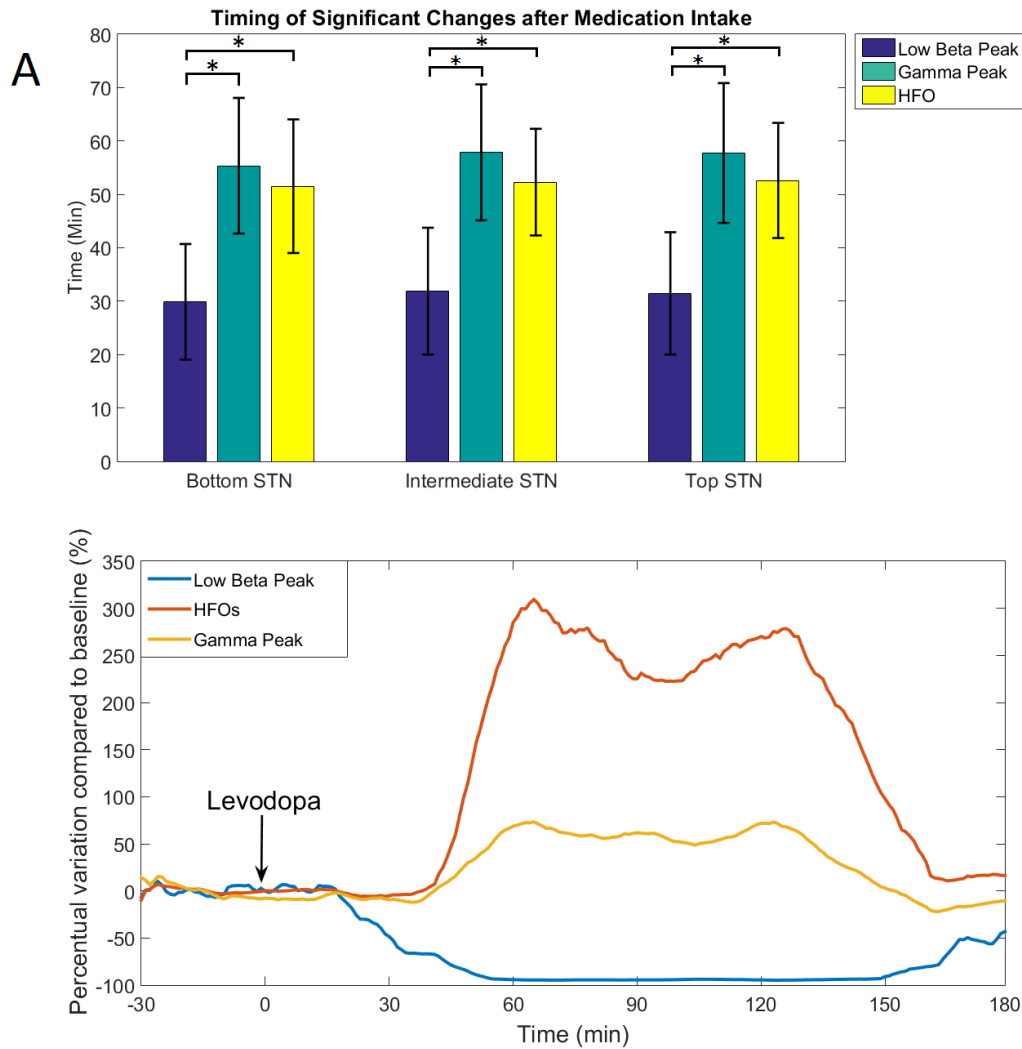


Figure 4.8: A) Timing of significant changes in the low beta, gamma and “ON” HFO peak powers after medication intake (corresponding to time 0). Asterisks represent significant differences in the time of changes between the power band considered. B) Percent power change in the three bands compared to the baseline (average of the power in the corresponding band in the thirty minutes prior to the medication intake) in a representative off-to-on transition obtained extracting LFP data for 210 minutes to show also the wash-out effect of medication in terms of power changes.

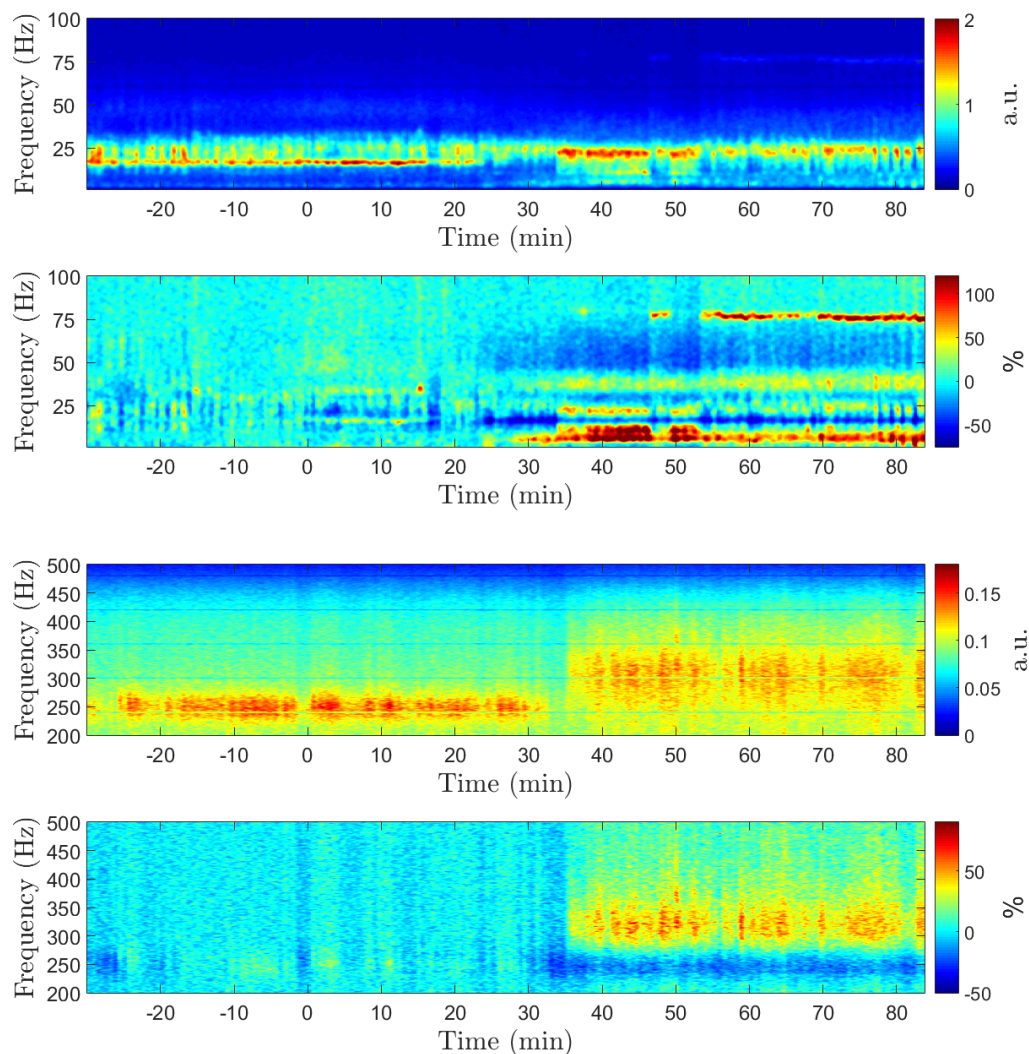


Figure 4.9: A) Representative time-frequency map of a off-to-on transition (medication intake at time 0). At the top, the raw map. At the bottom, the spectra have been computed has percent change compared to the average spectrum of the thirty minutes preceding the levodopa intake. Accordingly to the pattern shown in Fig. 4.8, the power in the low beta range decreases tens of minutes before the gamma power increases. B) Representative time-frequency map of a off-to-on transition (different from the one in A). At the top, the raw map. At the bottom, the spectra have normalized with respect to the period preceding the drug medication intake (time 0). Two distinct HFO activities are shown: “OFF” state HFO at around 250 Hz and “ON” state HFO spread around 350 Hz.

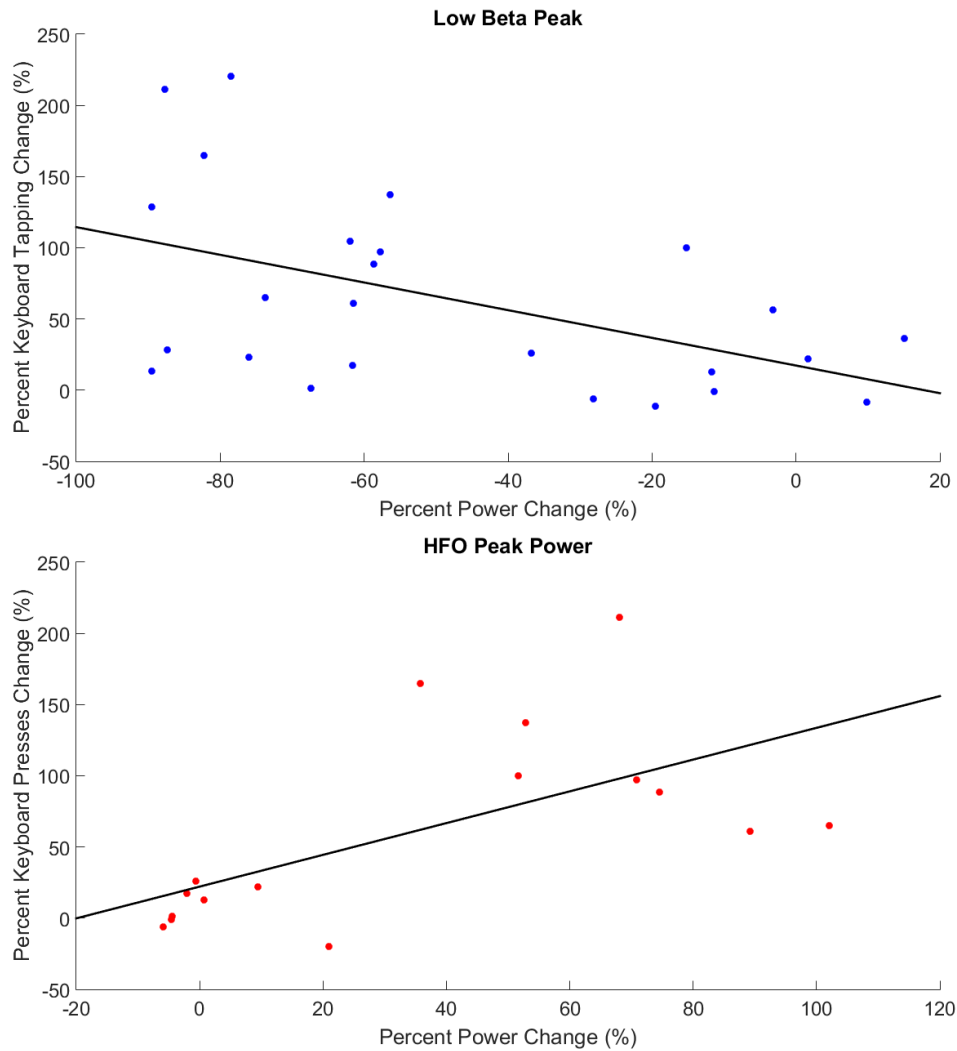


Figure 4.10: Top: scatter plot showing the correlation between the percent low beta peak power change and the percent change in number of keyboard presses during task execution for LFP 1-2. Bottom: scatter plot showing the correlation with percent power change in the “ON” state HFO range for LFP 1-2.

4.3.2 Phase-Amplitude Coupling Analysis

The phase-amplitude coupling did not show modulations in coupling strength during task execution when compared to the resting period present just before the task (Fig. 4.11 A) in the unmedicated condition.

In the medicated condition the coupling does not occur in the resting state and during task execution (Fig.4.11 B).

The spectrograms (Fig. 4.12) showed beta band power desynchronization from resting condition to motor task engagement in both “OFF” and “ON” conditions. Although in the medicated state the power decreases almost completely during task execution, in the untreated state there’s still significant activity which is coherent with the presence of phase-amplitude coupling.

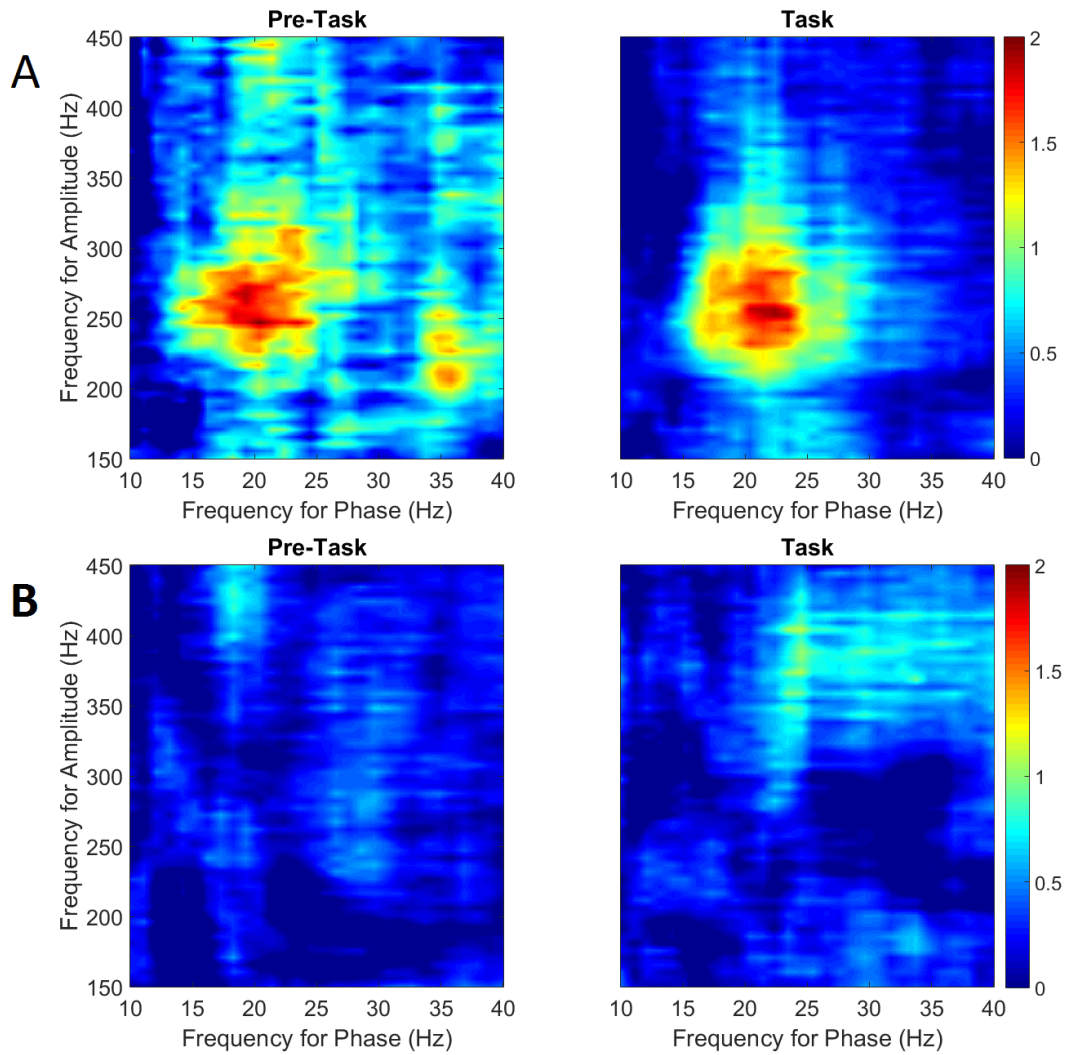


Figure 4.11: Comodulograms showing the strength of PAC before the task initiation and during task execution. The comodulogram relative to the pre-task period is noisier probably because estimated with a shorter data segment (10 s) than the comodulogram computed on the signals recorded during task execution (30 s). A) Untreated condition. B) Medicated condition.

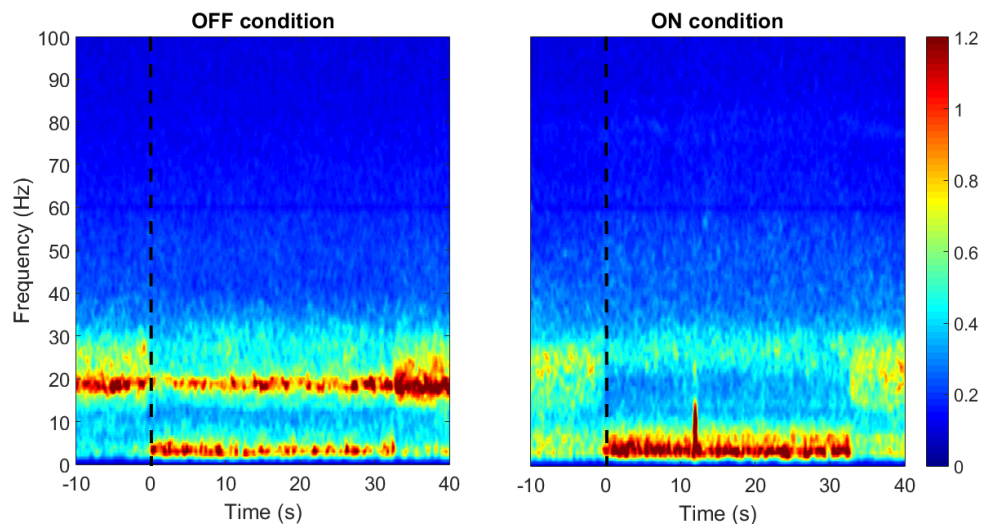


Figure 4.12: Average spectrograms of bipolar derivations showing stronger phase-amplitude coupling in resting condition. The interval from -10 to 0 s is resting prior to task execution, which starts at time 0 for 30 s.

Chapter 5

Discussion and Future Developments

In this work, the frequency content of subthalamic nucleus local field potentials has been analyzed to individuate spatial and timing patterns in spectral power distribution and nonlinear cross-frequency interactions. Classical as well as recently developed methods have been used to investigate the link between neuronal activity recorded at the STN LFP level and Parkinson’s disease pathophysiology.

The distribution of spectral power in the low beta, gamma, and “ON” state HFO bands was found to be widely distributed across STN, suggesting that these rhythms do not encode a unique functionality in the basal ganglia network, but are probably related in a variety of motor and cognitive processes. It was, in fact, recently discovered that perimovement STN beta and gamma bands reactivity is modulated by task complexity [Oswal et al., 2013], showing how motor planning and execution are

intrinsically related with cognitive processing in the basal ganglia circuit. However, it is important to consider that, even though re-referencing monopolar signals into bipolar derivations increases the spatial resolution of the analysis, bipolar derivations collect neuronal activity in a larger volume; this makes the exact source localization difficult. The volume conduction effect has also to be considered, especially in high power rhythms like the beta. Higher frequency rhythms (gamma and HFO, both the ones associated with “ON” and “OFF” clinical conditions) are instead believed to be more local, since they have much less power and they are less affected by volume conduction mechanism, since the tissue behaves generally as low pass filter.

Interestingly, the power of “OFF” state HFO was found to be significantly higher in the superior and middle parts of STN compared to the inferior part. Upper STN is where its motor region is located, so the analysis suggests that HFO rhythms in untreated condition may be specifically related with motor processing, and therefore be involved with the mechanism of generation of motor symptoms in PD. Consistently, studies reported that movement related “OFF” state HFO modulation is correlated with clinical scores [Lopez-Azcarate et al., 2010]. However, a recent study based on intraoperative LFP recordings showed that HFO activity around 250 Hz was localized above the superior entry point of electrode tip in STN, suggesting that this rhythm may not be directly generated in the subthalamic nucleus [Wang et al., 2014].

The first major finding of this work regarded the discovery that low beta peak

power, which is commonly associated with excessive and pathological activity in untreated PD condition, is suppressed many minutes before the increase of power in the HFO and gamma range after medication intake. The reason why this happens is, however, unknown. Pharmacokinetics and pharmacodynamics of the drug administered may be explanatory for the mechanism observed.

Pharmacokinetics refers to the time-dependent concentration of drug in body fluids after the medication administration. It is possible that certain neuronal populations, that are responsible for the generation of lower frequency rhythms, are affected by the medication before other populations whose activity results in high frequency oscillations. However, the time difference between the beta power suppression and HFO power rise was estimated in 21 minutes; this time gap should be further investigated with respect to drug dosage and its pharmacokinetical effect on neurophysiological oscillations.

On the other hand, pharmacodynamics, which refers to the effect caused by the drug concentration in the body fluids, may represent a possible explanation, since the STN is an important structure in the basal ganglia circuit. In fact, network modifications consequent to medication intake may be resulting from complex patterns of local modulations in connected structures, leading to delays in the activation of different neuronal populations. Since subthalamic nucleus receives inputs also from motor cortex, early low beta suppression may also be a direct effect of modulation at

the cortical level due to drug medication. Local high frequency activity may then be generated after beta suppression unlocks firing patterns able to activate the related sources.

Further studies investigating the synchronous activity in multiple structure of basal ganglia network and/or motor cortex are needed to fully address these questions.

The nonlinear cross-frequency coupling analysis obtained combining different sources for phase and amplitude frequency in terms of spatial localization lead to important observations, that are discussed after the methodological considerations.

PAC strength have been estimated using *MVL*, the *CV*, and the *PLV* measures. The *MVL* and *CV* are measures said to be amplitude-dependent, meaning that in some way the gain of the signal (or signals) used for their computation influences the final result. Instead, the *PLV* is amplitude-free since it involves only the use of phases. In previous studies artificial data have been used to compare the performances of the PAC estimators [Tort et al., 2010]; however and in this work they have been applied to real data and qualitatively compared. Amplitude-dependent measure have proved to be strong, especially in the quantification of different coupling strengths, but they're not comparable between different signals when their baseline power varies considerably. The standardization performed with surrogate parameters serves not only as significance testing, but also as a tool to make the PAC measures

more comparable when applied to different signals. Instead, the amplitude-free measures are highly comparable but have shown less discrimination power in terms of PAC strength [Tort et al., 2010].

The phase-amplitude coupling in untreated condition was found to be stronger in the superior and middle STN bipolar LFP derivations, with beta band range as phase frequencies and “OFF” state HFO as amplitude frequencies. This result was consistent with the observation that HFO activity in the unmedicated state was biased towards the superior and middle STN. More interestingly, the PAC maps showed the same topology when combining amplitude frequencies from top or middle STN bipolar LFP with phase frequencies extracted from all bipolar LFP derivations. While it is unlikely that beta activity recorded at the inferior border of STN is directly coupled with HFO rhythms in the superior STN border, it is possible that the excessive beta activity typical of unmedicated PD interacts with other rhythms (maybe not even generated in the STN), causing modifications of the physiological information transfer in the basal ganglia circuit and playing a role in generating the motor symptoms of the disease.

Accordingly to literature, the PAC vanished in medicated condition. This may represent a further proof that segregation of neural oscillations and independence of rhythms represents, to a certain extent, a requirement for the physiological behavior of neural networks [Marceglia et al., 2006]. However, the mechanism of action of

STN PAC is still unclear. One hypothesis [de Hemptinne et al., 2013] suggests that in parkinsonian condition the cortical beta input to the STN is not filtered as should happen in physiological state, leading to a pattern of neuronal discharges where high frequency bursts are tangled with slow beta oscillations, increasing therefore the cross-frequency coupling mechanism.

The movement analysis aimed to correlate spectral power changes during motor task execution across states with objective data represented by the number of alternative key tapping on a common computer keyboard. The result showed correlation in terms of low beta power changes from all bipolar LFP and “ON” state HFO from middle STN bipolar derivation. Since the low beta power change correlated with performance in all STN locations (top, middle, and bottom bipolar LFP) no specific spatial information could be deducted. Instead, positive correlation with HFO power change was found only in LFP 1-2, suggesting that significant modulation in high frequency rhythms power in the corresponding region of STN is involved in motor execution.

Significant phase-amplitude coupling was found both in pre-task rest condition and task execution, suggesting that cross-frequency interaction is not directly involved in motor processes, but rather may represent a background mechanism proper of the basal ganglia network in pathological condition. However, other studies reported a modulation of PAC during motor process [Lopez-Azcarate et al., 2010].

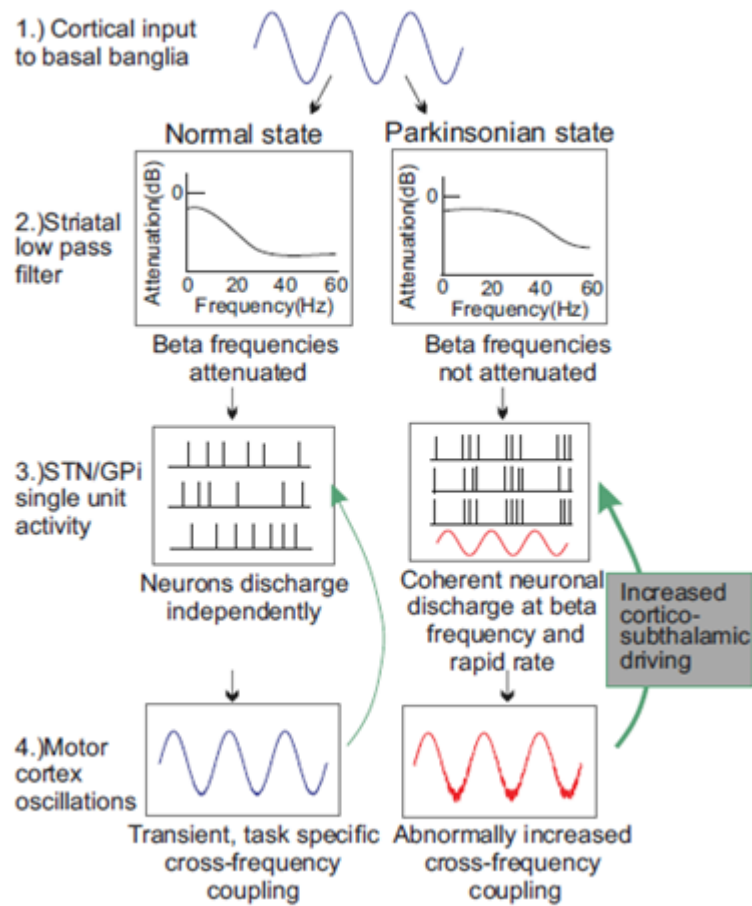


Figure 5.1: Hypothesis for the presence of abnormal phase-amplitude coupling in the parkinsonian state. The cortical beta input to the basal ganglia circuit is filtered in the physiological state while remains present in parkinsonian condition. This may lead to a loss of independence between neuronal discharges at different rates. Reproduced from de Hemptinne et al. [2013].

This discrepancy may result from the observation that in the untreated condition, excessive beta activity was still present during task execution, even if with lower power compared to the rest condition.

There are some limitations related to this work. The most important is represented by the fact that the recordings took place three weeks after the surgical implantation of DBS leads. The surgery provoked cerebral tissue lesions and consequently generation of fibrous capsule, which makes it harder to detect high frequency oscillations from nearby neuronal populations. Also, the electrode placement itself, even if confirmed by post-operative images, may differ inter-subjectively. The group analysis however helps finding common patterns among patients.

The analysis conducted in this work confirmed the potential clinical use of local field potentials, since they provide quantitative information about the condition of the patients. While this work focused on the pathophysiology of Parkinson's Disease, the methodologies used may be implemented in tools for adaptive deep brain stimulation and intraoperative decision support. One of the main uncertainties in the deep brain stimulation surgical protocol is, of course, the correct placement of the macroelectrode lead. Since it has been showed that nonlinear cross-frequency coupling and "OFF" state HFO have spatial patterns, depth-by-depth intraoperative LFP recordings may provide useful information about the localization of the exploratory electrode in the basal ganglia network and, specifically, nearby and inside

the STN. The adaptive deep brain stimulation [Little et al., 2013, Priori et al., 2013] is a closed-loop stimulation protocol which delivers therapeutic stimulation based on a feedback control variables obtained from deep brain recordings. The LFP online analysis could provide features for the control variables allowing smarter stimulation protocols.

Bibliography

- D. Aarsland, K. Bronnick, U. Ehrt, P. P. De Deyn, S. Tekin, M. Emre, and J. L. Cummings. Neuropsychiatric symptoms in patients with Parkinson's disease and dementia: frequency, profile and associated care giver stress. *Journal of Neurology, Neurosurgery, and Psychiatry*, 78(1):36–42, January 2007. ISSN 1468-330X. doi: 10.1136/jnnp.2005.083113.
- A. Abosch, D. Lanctin, I. Onaran, L. Eberly, M. Spaniol, and N. F. Ince. Long-term recordings of local field potentials from implanted deep brain stimulation electrodes. *Neurosurgery*, 71(4):804–814, October 2012. ISSN 1524-4040. doi: 10.1227/NEU.0b013e3182676b91.
- A. Bjorklund and S. B. Dunnett. Dopamine neuron systems in the brain: an update. *Trends in Neurosciences*, 30(5):194–202, May 2007. ISSN 0166-2236. doi: 10.1016/j.tins.2007.03.006.
- J. M. Bronstein, M. Tagliati, and R. L. Alterman. Deep brain stimulation for parkinson disease: An expert consensus and review of key issues. *Archives of Neurology*, 68(2):165–165, February 2011. ISSN 0003-9942. doi: 10.1001/archneurol.2010.260. URL <http://dx.doi.org/10.1001/archneurol.2010.260>.
- D. J. Brooks. Imaging approaches to Parkinson disease. *Journal of Nuclear Medicine: Official Publication, Society of Nuclear Medicine*, 51(4):596–609, April 2010. ISSN 1535-5667. doi: 10.2967/jnumed.108.059998.
- P. Brown. Oscillatory nature of human basal ganglia activity: relationship to the pathophysiology of Parkinson's disease. *Movement Disorders: Official Journal of the Movement Disorder Society*, 18(4):357–363, April 2003. ISSN 0885-3185. doi: 10.1002/mds.10358.
- P. Brown and D. Williams. Basal ganglia local field potential activity: Character and functional significance in the human. *Clinical Neurophysiology*, 116(11):2510–2519, November 2005. ISSN 1388-2457. doi: 10.1016/j.clinph.2005.05.009. URL <http://www.clinph-journal.com/article/S1388245705002142/abstract>.

- P. Brown, A. Oliviero, P. Mazzone, A. Insola, P. Tonali, and V. Lazzaro. Dopamine dependency of oscillations between subthalamic nucleus and pallidum in Parkinson's disease. *The Journal of Neuroscience*, 21(3):1033–1038, February 2001. ISSN 0270-6474, 1529-2401. URL <http://www.jneurosci.org/content/21/3/1033>.
- R. T. Canolty, E. Edwards, S. S. Dalal, M. Soltani, S. S. Nagarajan, H. E. Kirsch, M. S. Berger, N. M. Barbaro, and R. T. Knight. High gamma power is phase-locked to theta oscillations in human neocortex. *Science (New York, N.Y.)*, 313(5793):1626–1628, September 2006. ISSN 1095-9203. doi: 10.1126/science.1128115.
- G. C. Carter, C. Knapp, and A. H. Nuttall. Estimation of the magnitude-squared coherence function via overlapped fast Fourier transform processing. *IEEE Transactions on Audio and Electroacoustics*, 21(4):337–344, August 1973. ISSN 0018-9278. doi: 10.1109/TAU.1973.1162496.
- A. Castrioto, A. M. Lozano, Y. Poon, A. E. Lang, M. Fallis, and E. Moro. Ten-year outcome of subthalamic stimulation in Parkinson disease: a blinded evaluation. *Archives of Neurology*, 68(12):1550–1556, December 2011. ISSN 1538-3687. doi: 10.1001/archneurol.2011.182.
- C. C. Chen, A. Pogosyan, L. U. Zrinzo, S. Tisch, P. Limousin, K. Ashkan, T. Yousry, M. I. Hariz, and P. Brown. Intra-operative recordings of local field potentials can help localize the subthalamic nucleus in Parkinson's disease surgery. *Experimental Neurology*, 198(1):214–221, March 2006. ISSN 0014-4886. doi: 10.1016/j.expneurol.2005.11.019.
- M. X. Cohen. Assessing transient cross-frequency coupling in EEG data. *Journal of Neuroscience Methods*, 168(2):494–499, March 2008. ISSN 0165-0270. doi: 10.1016/j.jneumeth.2007.10.012.
- L. Lee Colgin, T. Denninger, M. Fyhn, T.l Hafting, T. Bonnevie, O. Jensen, M. Moser, and E. I. Moser. Frequency of gamma oscillations routes flow of information in the hippocampus. *Nature*, 462(7271):353–357, November 2009. ISSN 0028-0836. doi: 10.1038/nature08573. URL <http://www.nature.com/nature/journal/v462/n7271/abs/nature08573.html>.
- F. Darvas and A. O. Hebb. Task specific inter-hemispheric coupling in human subthalamic nuclei. *Frontiers in Human Neuroscience*, 8:701, 2014. doi: 10.3389/fnhum.2014.00701. URL <http://journal.frontiersin.org/article/10.3389/fnhum.2014.00701/full>.
- C. A. Davie. A review of Parkinson's disease. *British Medical Bulletin*, 86:109–127, 2008. ISSN 1471-8391. doi: 10.1093/bmb/ldn013.

- C. de Hemptinne, E. S. Ryapolova-Webb, E. L. Air, P. A. Garcia, K. J. Miller, J. G. Ojemann, J. L. Ostrem, N. B. Galifianakis, and P. A. Starr. Exaggerated phase-amplitude coupling in the primary motor cortex in Parkinson disease. *Proceedings of the National Academy of Sciences of the United States of America*, 110(12): 4780–4785, March 2013. ISSN 0027-8424. doi: 10.1073/pnas.1214546110. URL <http://www.ncbi.nlm.nih.gov/pmc/articles/PMC3606991/>.
- L. de Lau and M. Breteler. Epidemiology of Parkinson's disease. *The Lancet Neurology*, 5(6):525–535, June 2006. ISSN 1474-4422. doi: 10.1016/S1474-4422(06)70471-9. URL <http://www.sciencedirect.com/science/article/pii/S1474442206704719>.
- G. Deuschl, C. Schade-Brittinger, P. Krack, J. Volkmann, H. Schafer, K. Botzel, C. Daniels, A. Deutschlander, U. Dillmann, W. Eisner, D. Gruber, W. Hamel, J. Herzog, R. Hilker, S. Klebe, M. Kloss, J. Koy, M. Krause, A. Kupsch, D. Lorenz, S. Lorenzl, H. M. Mehdorn, J. R. Moringlane, W. Oertel, M. O. Pinsker, H. Reichmann, A. Reuss, G. Schneider, A. Schnitzler, U. Steude, V. Sturm, L. Timmermann, V. Tronnier, T. Trottenberg, L. Wojtecki, E. Wolf, W. Poewe, and J. Voges. A randomized trial of deep-brain stimulation for Parkinson's disease. *New England Journal of Medicine*, 355(9):896–908, August 2006. ISSN 0028-4793. doi: 10.1056/NEJMoa060281. URL <http://dx.doi.org/10.1056/NEJMoa060281>.
- D. W. Dickson, H. Braak, J. E. Duda, C. Duyckaerts, T. Gasser, G. M. Halliday, J. Hardy, J. B. Leverenz, K. Del Tredici, Z. K. Wszolek, and I. Litvan. Neuropathological assessment of Parkinson's disease: refining the diagnostic criteria. *The Lancet. Neurology*, 8(12):1150–1157, December 2009. ISSN 1474-4465. doi: 10.1016/S1474-4422(09)70238-8.
- L. J. Findley. The economic impact of Parkinson's disease. *Parkinsonism & Related Disorders*, 13, Supplement:S8–S12, September 2007. ISSN 1353-8020. doi: 10.1016/j.parkreldis.2007.06.003. URL <http://www.sciencedirect.com/science/article/pii/S1353802007001058>.
- G. Foffani, A. Priori, M. Egidi, P. Rampini, F. Tamma, E. Caputo, K. A. Moxon, S. Cerutti, and S. Barbieri. 300-Hz subthalamic oscillations in Parkinson's disease. *Brain: A Journal of Neurology*, 126(Pt 10):2153–2163, October 2003. ISSN 0006-8950. doi: 10.1093/brain/awg229.
- A. Galvan and T. Wichmann. Pathophysiology of parkinsonism. *Clinical Neurophysiology: Official Journal of the International Federation of Clinical Neurophysiology*, 119(7):1459–1474, July 2008. ISSN 1388-2457. doi: 10.1016/j.clinph.2008.03.017.

- F. Gustafsson. Determining the initial states in forward-backward filtering. *Trans. Sig. Proc.*, 44(4):988–992, April 1996. ISSN 1053-587X. doi: 10.1109/78.492552. URL <http://dx.doi.org/10.1109/78.492552>.
- N. F. Ince, A. Gupte, T. Wichmann, J. Ashe, T. Henry, M. Bebler, L. Eberly, and A. Abosch. Selection of optimal programming contacts based on local field potential recordings from subthalamic nucleus in patients with Parkinson’s disease. *Neurosurgery*, 67(2):390–397, August 2010. ISSN 1524-4040. doi: 10.1227/01.NEU.0000372091.64824.63.
- J. Jankovic. Parkinson’s disease: clinical features and diagnosis. *Journal of Neurology, Neurosurgery & Psychiatry*, 79(4):368–376, April 2008. ISSN , 1468-330X. doi: 10.1136/jnnp.2007.131045. URL <http://jnnp.bmj.com/content/79/4/368>.
- J. Jankovic and L. G. Aguilar. Current approaches to the treatment of Parkinson’s disease. *Neuropsychiatric Disease and Treatment*, 4(4):743–757, August 2008. ISSN 1176-6328. URL <http://www.ncbi.nlm.nih.gov/pmc/articles/PMC2536542/>.
- M. Johansson. The Hilbert transform. *Mathematics Masters Thesis. Voxjo University*, 1999.
- A. A. Kuhn, D. Williams, A. Kupsch, P. Limousin, M. Hariz, G. Schneider, K. Yarrow, and P. Brown. Event-related beta desynchronization in human subthalamic nucleus correlates with motor performance. *Brain: A Journal of Neurology*, 127(Pt 4):735–746, April 2004. ISSN 0006-8950. doi: 10.1093/brain/awh106.
- A. A. Kuhn, A. Kupsch, G. Schneider, and P. Brown. Reduction in subthalamic 8-35 Hz oscillatory activity correlates with clinical improvement in Parkinson’s disease. *The European Journal of Neuroscience*, 23(7):1956–1960, April 2006. ISSN 0953-816X. doi: 10.1111/j.1460-9568.2006.04717.x.
- S. Lesage and A. Brice. Parkinson’s disease: from monogenic forms to genetic susceptibility factors. *Human Molecular Genetics*, 18(R1):R48–R59, April 2009. ISSN 0964-6906, 1460-2083. doi: 10.1093/hmg/ddp012. URL <http://hmg.oxfordjournals.org/content/18/R1/R48>.
- S. Little, A. Pogosyan, S. Neal, B. Zavala, L. Zrinzo, M. Hariz, T. Foltynie, P. Limousin, K. Ashkan, J. FitzGerald, A. L. Green, T. Z. Aziz, and P. Brown. Adaptive deep brain stimulation in advanced Parkinson disease. *Annals of Neurology*, 74(3):449–457, September 2013. ISSN 1531-8249. doi: 10.1002/ana.23951.
- J. Lopez-Azcarate, M.I Tainta, M. C. Rodriguez-Oroz, M. Valencia, R. Gonzalez, J. Guridi, J. Iriarte, J. A. Obeso, J. Artieda, and M. Alegre. Coupling between

- beta and high-frequency activity in the human subthalamic nucleus may be a pathophysiological mechanism in Parkinson's disease. *The Journal of Neuroscience: The Official Journal of the Society for Neuroscience*, 30(19):6667–6677, May 2010. ISSN 1529-2401. doi: 10.1523/JNEUROSCI.5459-09.2010.
- S. Marceglia, G. Foffani, A. M. Bianchi, G. Baselli, F. Tamma, M. Egidi, and A. Priori. Dopamine-dependent non-linear correlation between subthalamic rhythms in Parkinson's disease. *The Journal of Physiology*, 571(Pt 3):579–591, March 2006. ISSN 0022-3751. doi: 10.1113/jphysiol.2005.100271.
- S. McClelland. A cost analysis of intraoperative microelectrode recording during subthalamic stimulation for Parkinson's disease. *Movement Disorders: Official Journal of the Movement Disorder Society*, 26(8):1422–1427, July 2011. ISSN 1531-8257. doi: 10.1002/mds.23787.
- S. K. Mitra. *Digital Signal Processing: A Computer-Based Approach*. McGraw-Hill School Education Group, 2nd edition, 2001. ISBN 0-07-252261-5.
- F. Mormann, J. Fell, N. Axmacher, B. Weber, K. Lehnertz, C. E. Elger, and G. Fernandez. Phase/amplitude reset and theta-gamma interaction in the human medial temporal lobe during a continuous word recognition memory task. *Hippocampus*, 15(7):890–900, 2005. ISSN 1050-9631. doi: 10.1002/hipo.20117.
- National Collaborating Centre for Chronic Conditions, UK. *Parkinson's Disease: National Clinical Guideline for Diagnosis and Management in Primary and Secondary Care*. National Institute for Health and Clinical Excellence: Guidance. Royal College of Physicians (UK), London, 2006. ISBN 1860162835. URL <http://www.ncbi.nlm.nih.gov/books/NBK48513/>.
- A. J. Noyce, J. P. Bestwick, L. Silveira-Moriyama, C. H. Hawkes, G. Giovannoni, A. J. Lees, and A. Schrag. Meta-analysis of early nonmotor features and risk factors for Parkinson disease. *Annals of Neurology*, 72(6): 893–901, December 2012. ISSN 1531-8249. doi: 10.1002/ana.23687. URL <http://onlinelibrary.wiley.com/doi/10.1002/ana.23687/abstract>.
- J. A. Obeso, M. C. Rodriguez-Oroz, B. Benitez-Temino, F. J. Blesa, J. Guridi, C. Marin, and M. Rodriguez. Functional organization of the basal ganglia: Therapeutic implications for Parkinson's disease. *Movement Disorders*, 23(S3): S548–S559, January 2008. ISSN 1531-8257. doi: 10.1002/mds.22062. URL <http://onlinelibrary.wiley.com/doi/10.1002/mds.22062/abstract>.

- W. G. Ondo, K. Dat Vuong, H. Khan, F. Atassi, C. Kwak, and J. Jankovic. Daytime sleepiness and other sleep disorders in Parkinson's disease. *Neurology*, 57(8):1392–1396, October 2001. ISSN 0028-3878.
- A. V. Oppenheim, R. W. Schaffer, and J. R. Buck. *Discrete-time Signal Processing (2nd Ed.)*. Prentice-Hall, Inc., Upper Saddle River, NJ, USA, 1999. ISBN 0-13-754920-2.
- A. Oswal, V. Litvak, C. Brucke, J. Huebl, G. Schneider, A. A. Kuhn, and P. Brown. Cognitive factors modulate activity within the human subthalamic nucleus during voluntary movement in Parkinson's disease. *The Journal of Neuroscience: The Official Journal of the Society for Neuroscience*, 33(40):15815–15826, October 2013. ISSN 1529-2401. doi: 10.1523/JNEUROSCI.1790-13.2013.
- T. E. Ozkurt, M. Butz, M. Homburger, S. Elben, J. Vesper, L. Wojtecki, and A. Schnitzler. High frequency oscillations in the subthalamic nucleus: A neurophysiological marker of the motor state in Parkinson's disease. *Experimental Neurology*, 229(2):324–331, June 2011. ISSN 0014-4886. doi: 10.1016/j.expneurol.2011.02.015. URL <http://www.sciencedirect.com/science/article/pii/S001448861100063X>.
- J. Parkinson. An essay on the shaking palsy. 1817. *The Journal of Neuropsychiatry and Clinical Neurosciences*, 14(2):223–236; discussion 222, 2002. ISSN 0895-0172.
- W. D. Penny, E. Duzel, K. J. Miller, and J. G. Ojemann. Testing for nested oscillation. *Journal of Neuroscience Methods*, 174(1):50–61, September 2008. ISSN 0165-0270. doi: 10.1016/j.jneumeth.2008.06.035.
- A. Priori, G. Foffani, L. Rossi, and S. Marceglia. Adaptive deep brain stimulation (aDBS) controlled by local field potential oscillations. *Experimental Neurology*, 245:77–86, July 2013. ISSN 0014-4886. doi: 10.1016/j.expneurol.2012.09.013. URL <http://www.sciencedirect.com/science/article/pii/S0014488612003755>.
- V. A. Sironi. Origin and evolution of deep brain stimulation. *Frontiers in Integrative Neuroscience*, 5, August 2011. ISSN 1662-5145. doi: 10.3389/fnint.2011.00042. URL <http://www.ncbi.nlm.nih.gov/pmc/articles/PMC3157831/>.
- Y. Smith, T. Wichmann, S. A. Factor, and M. R. DeLong. Parkinson's disease therapeutics: new developments and challenges since the introduction of levodopa. *Neuropsychopharmacology*, 37(1):213–246, January 2012. ISSN 0893-133X. doi: 10.1038/npp.2011.212. URL <http://www.nature.com/npp/journal/v37/n1/full/npp2011212a.html>.

- P. A. Starr, J. L. Vitek, and R. A. Bakay. Ablative surgery and deep brain stimulation for Parkinson's disease. *Neurosurgery*, 43(5):989–1013; discussion 1013–1015, November 1998. ISSN 0148-396X.
- P. A. Starr, A. J. Martin, J. L. Ostrem, P. Talke, N. Levesque, and P. S. Larson. Subthalamic nucleus deep brain stimulator placement using high-field interventional magnetic resonance imaging and a skull-mounted aiming device: technique and application accuracy. *Journal of Neurosurgery*, 112(3):479–490, March 2010. ISSN 1933-0693. doi: 10.3171/2009.6.JNS081161.
- A. Stocco, C. Lebiere, and J. R. Anderson. Conditional routing of information to the cortex: A model of the basal ganglia's role in cognitive coordination. *Psychological Review*, 117(2):541–574, 2010. ISSN 1939-1471(Electronic);0033-295X(Print). doi: 10.1037/a0019077.
- A. Stuart, K. Ord, and S. Arnold. *Wiley: Kendall's Advanced Theory of Statistics, Volume 2A, Classical Inference and the Linear Model, 6th Edition*. 2008. URL <http://eu.wiley.com/WileyCDA/WileyTitle/productCd-0470689242.html>.
- I. Telkes, N. F. Ince, I. Onaran, and A. Abosch. Localization of subthalamic nucleus borders using macroelectrode local field potential recordings. *Conference proceedings: Annual International Conference of the IEEE Engineering in Medicine and Biology Society. IEEE Engineering in Medicine and Biology Society. Annual Conference*, 2014:2621–2624, 2014. ISSN 1557-170X. doi: 10.1109/EMBC.2014.6944160.
- A. B. L. Tort, R. Komorowski, H. Eichenbaum, and N. Kopell. Measuring phase-amplitude coupling between neuronal oscillations of different frequencies. *Journal of Neurophysiology*, 104(2):1195–1210, August 2010. ISSN 0022-3077. doi: 10.1152/jn.00106.2010. URL <http://www.ncbi.nlm.nih.gov/pmc/articles/PMC2941206/>.
- G. Van Maele-Fabry, P. Hoet, F. Vilain, and D. Lison. Occupational exposure to pesticides and Parkinson's disease: a systematic review and meta-analysis of cohort studies. *Environment International*, 46:30–43, October 2012. ISSN 1873-6750. doi: 10.1016/j.envint.2012.05.004.
- J. Volkmann, J. Herzog, F. Kopper, and G. Deuschl. Introduction to the programming of deep brain stimulators. *Movement Disorders: Official Journal of the Movement Disorder Society*, 17 Suppl 3:S181–187, 2002. ISSN 0885-3185.
- B. Voytek, R. T. Canolty, A. Shestyuk, N. E. Crone, J. Parvizi, and R. T. Knight. Shifts in gamma phase-amplitude coupling frequency from theta to

- alpha over posterior cortex during visual tasks. *Frontiers in Human Neuroscience*, 4, October 2010. ISSN 1662-5161. doi: 10.3389/fnhum.2010.00191. URL <http://www.ncbi.nlm.nih.gov/pmc/articles/PMC2972699/>.
- J. Wang, J. Hirschmann, S. Elben, C. J. Hartmann, J. Vesper, L. Wojtecki, and A. Schnitzler. High-frequency oscillations in Parkinson's disease: spatial distribution and clinical relevance. *Movement Disorders: Official Journal of the Movement Disorder Society*, 29(10):1265–1272, September 2014. ISSN 1531-8257. doi: 10.1002/mds.25962.
- F. M. Weaver, K. Follett, M. Stern, K. Hur, C. Harris, W. J. Marks, J. Rothlind, O. Sagher, D. Reda, C. S. Moy, R. Pahwa, K. Burchiel, P. Hogarth, E. C. Lai, J. E. Duda, K. Holloway, A. Samii, S. Horn, J. Bronstein, G. Stoner, J. Heemskerk, G. D. Huang, and CSP 468 Study Group. Bilateral deep brain stimulation vs best medical therapy for patients with advanced Parkinson disease: a randomized controlled trial. *JAMA*, 301(1):63–73, January 2009. ISSN 1538-3598. doi: 10.1001/jama.2008.929.
- A. Williams, S. Gill, T. Varma, C. Jenkinson, N. Quinn, R. Mitchell, R. Scott, N. Ives, C. Rick, J. Daniels, S. Patel, and K. Wheatley. Deep brain stimulation plus best medical therapy versus best medical therapy alone for advanced Parkinson's disease (PD SURG trial): a randomised, open-label trial. *Lancet Neurology*, 9(6): 581–591, June 2010. ISSN 1474-4422. doi: 10.1016/S1474-4422(10)70093-4. URL <http://www.ncbi.nlm.nih.gov/pmc/articles/PMC2874872/>.
- R. Williams. Alim-Louis Benabid: stimulation and serendipity. *The Lancet Neurology*, 9(12):1152, December 2010. ISSN 1474-4465. doi: 10.1016/S1474-4422(10)70291-X.
- S. C. Yao, A. D. Hart, and M. J. Terzella. An evidence-based osteopathic approach to Parkinson disease. *Osteopathic Family Physician*, 5(3):96–101, May 2013. ISSN 1877-573X. doi: 10.1016/j.osfp.2013.01.003. URL <http://www.sciencedirect.com/science/article/pii/S1877573X13000154>.
- J. Yelnik. Functional anatomy of the basal ganglia. *Movement Disorders: Official Journal of the Movement Disorder Society*, 17 Suppl 3:S15–21, 2002. ISSN 0885-3185.